REVIEW

10th Anniversary Article

ADVANCED
ENERGY
MATERIALS

www.advenergymat.d

Check for updates

Host Materials Anchoring Polysulfides in Li–S Batteries Reviewed

Lei Zhou, Dmitri L. Danilov, Rüdiger-A. Eichel, and Peter H. L. Notten*

Lithium–sulfur batteries (Li–S) have become a viable alternative to future energy storage devices. The electrochemical reaction based on lithium and sulfur promises an extraordinary theoretical energy density, which is far higher than current commercialized Li-ion batteries. However, the principal disadvantage impeding the success of Li–S batteries lies in the severe leakage and migration of soluble lithium polysulfide intermediates out of cathodes upon cycling. The loss of active sulfur species incurs significant capacity decay and poor battery lifespans. Considerable efforts have been devoted to developing various sulfur host materials that can effectively anchor lithium polysulfides. Herein, a comprehensive review is presented of recent advances in sulfur host materials. On the basis of the electrochemistry of Li–S batteries, the strategies for anchoring polysulfides are systematically categorized into physical confinement and chemical bonding. The structural merits of various sulfur host materials are highlighted, and the interaction mechanisms with sulfur species are discussed in detail, which provides valuable insights into the rational design and engineering of advanced sulfur host materials facilitating the commercialization of Li–S batteries. Future challenges and promising research prospects for sulfur host materials are proposed at the end of the review.

L. Zhou, Dr. D. L. Danilov, Prof. P. H. L. Notten
Eindhoven University of Technology
P.O. Box 513, Eindhoven 5600 MB, The Netherlands
E-mail: p.h.l.notten@tue.nl
L. Zhou, Dr. D. L. Danilov, Prof. R.-A. Eichel, Prof. P. H. L. Notten
Institute of Energy and Climate Research
Fundamental Electrochemistry (IEK-9)
Forschungszentrum Jülich
Jülich D-52425, Germany
Prof. R.-A. Eichel
Institute of Physical Chemistry
RWTH Aachen University
Aachen D-52074, Germany
Prof. P. H. L. Notten
Centre for Clean Energy Technology
University of Technology Sydney
Broadway, Sydney, NSW 2007, Australia

The ORCID identification number(s) for the author(s) of this article can be found under https://doi.org/10.1002/aenm.202001304.

1. Introduction

Electrical energy conversion and storage is becoming one of the increasingly major concerns in future low carbon society. The depletion of fossil fuels and oils, as well as the revival of electric vehicles, has motivated scientists to develop sustainable electrical energy storage systems.[1–6] Over the past three decades, rechargeable lithium-ion (Li-ion) batteries have gained in popularity due to their large energy storage, low self-discharge, and stable cycling performance, significantly advancing the development of energy storage technologies.[7–9] However, current commercialized Li-ion batteries using conventional insertion cathode materials, such as $LiCoO_2$ and $LiFePO_4$, have reached an energy density of around 300 Wh kg^{-1}, which is expected not to lead to a considerable improvement in the near future owing to battery technologies and their theoretical limits. According to the commercialization goal of the United States Advanced Battery Consortium (USABC), such an energy density cannot accomplish a 500 km travel range based on a single charge. The exploration of novel battery systems, showing a higher energy density and longer cycle life, would be a viable alternative to conventional Li-ion systems.

First proposed in the early 1960s, lithium–sulfur (Li–S) batteries have received a great deal of attention.[10–13] Owing to the overwhelming theoretical specific energy of 2600 Wh kg^{-1} and impressive specific capacity of 1675 mAh g^{-1}, respectively, Li–S batteries hold a promising opportunity to achieve a quantum leap in energy storage, addressing current challenges. Since then, Li–S batteries have been recognized as an attractive option among the most potential energy storage devices for practical applications. More importantly, sulfur is naturally abundant, cost-effective, and eco-friendly, thus boosting the potential for commercialization of Li–S batteries.

Despite these prominent merits in energy density and cost, several problems have restricted the development of Li–S batteries for commercialization.[14–16] The first issue is that elemental sulfur and its final discharge species Li_2S_n ($1 \leq n \leq 2$) are poor conductors, leading to large electrochemical polarizations and battery impedances. Another obstacle is diffusion and migration of sulfur intermediates into the electrolyte upon charging and discharging. These long-chain lithium polysulfide

intermediates can be transported to the anodes, react with metallic lithium, and form short-chain lithium polysulfides. This so-called shuttle effect incurs severe losses of electroactive substances in cathodes. The third problem lies in the volumetric variation of sulfur cathodes upon cycling. The lithiation and delithiation process pulverizes the cathode and detaches the active mass from conductive substrates. Among those problems, the dissolution of lithium polysulfides into the electrolyte is most notorious and intractable. It severely decreases the utilization of sulfur cathodes, resulting in fast capacity degradation, low coulombic efficiency, and eventual battery failure.

Over the past few years, considerable endeavors to alleviate the detrimental shuttle issue have been devoted, including cathode functionalization,[17–22] separator modification,[23–26] and electrolyte tailoring.[27–29] The design and engineering of sulfur host materials confining active sulfur intermediates have been proven to be a successful approach to improving the capacity and cycling stability of sulfur cathodes. Various sulfur host materials possessing desirable structures have been developed to confine sulfur species through spatial inhibition and chemical anchoring.[30–32] Despite numerous perspectives to solve the shuttle issue, very few reviews have been published, systematically discussing the various anchoring strategies for polysulfides to improve the performance of Li–S batteries.

This review specifically focuses on various sulfur host materials that are able to anchor polysulfides in Li–S batteries. By interpreting the underlying anchoring mechanisms of polysulfides, the review is expected to provide a comprehensive and detailed insight into the function and role of sulfur host materials. The operation and reaction mechanism of Li–S batteries are first elucidated. Furthermore, the anchoring strategies of host materials toward sulfur species are systematically discussed on the basis of physical confinement and chemical bonding. Then three classes of sulfur host materials, that is, nanostructured carbon, polymers, and metal compounds, are presented to highlight the breakthroughs in sulfur cathodes. Finally, perspectives on future challenges and promising directions of sulfur hosts are proposed, providing more insight into the design and engineering of cathode materials, which may consequently boost the future development of advanced Li–S batteries. Since this review aims for sulfur host materials, modified separators and interlayers will not be discussed here.

2. Electrochemistry of Li–S Batteries

As illustrated in **Figure 1**a, the configuration of Li–S batteries involves a metallic lithium anode and an elemental sulfur cathode immersed in an organic electrolyte. Elemental sulfur reacts with lithium converting to lithium sulfide (Li_2S) during discharging and Li_2S decomposes into Li and S during charging. The overall electrochemical charge transfer reaction at the cathode can be represented by Equation (1).

$$S_8 + 16\,Li^+ + 16\,e^- \rightarrow 8\,Li_2S \qquad (1)$$

This two-electron (per S atom) redox process offers a considerable theoretical capacity of sulfur cathodes, which is almost ten times higher than that of the present commercial Li-ion
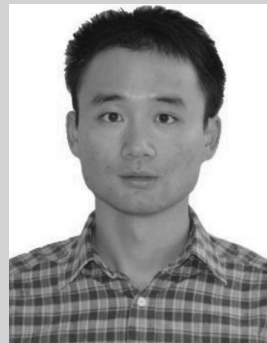
Lei Zhou is pursuing his Ph.D. degree under the supervision of Prof. Peter H. L. Notten at Eindhoven University of Technology (TU/e), the Netherlands. Currently, he is conducting his research at Forschungszentrum Jülich (Germany). His research interests focus on the design and development of effective strategies for high-performance Li–S batteries.

Dmitri L. Danilov, Ph.D., has a background in physics and mathematics and obtained his M.Sc. at the Saint-Petersburg University in 1993. In 2003, he got Ph.D. degree from the University of Tilburg. In 2002, he joined Eurandom institute in Eindhoven University of Technology, being involved in various national and international research projects. His current research interests include mathematical modeling of complex electrochemical systems, including Li-ion and NiMH batteries, ageing and degradation processes, thin-film batteries, and advanced characterization methods. Starting 2017, he joined IEK-9 in the Forschungszentrum Jülich.

Peter H. L. Notten joined Philips Research Laboratories (Eindhoven, The Netherlands) from 1975 to 2010. He received his Ph.D. degree from Eindhoven University in 1989. Since then, he focused on energy storage research, including hydrogen and lithium storage materials, new battery technologies, modeling electrochemical systems, and design of battery-management algorithms. In 2000, he was appointed as professor at TU/e where he heads the group Energy Materials and Devices. In 2014, he has been appointed as International Adjunct Faculty at Amrita University, Coimbatore (India), as group leader at Forschungszentrum Jülich (Germany), and in 2018 as honorary professor at University of Technology Sydney.

cathode materials.[33] In comparison with conventional metal oxide cathode materials undergoing insertion reactions with lithium, sulfur involves numerous structural changes and

ADVANCED
SCIENCE NEWS
www.advancedsciencenews.com

ADVANCED
ENERGY
MATERIALS
www.advenergymat.de
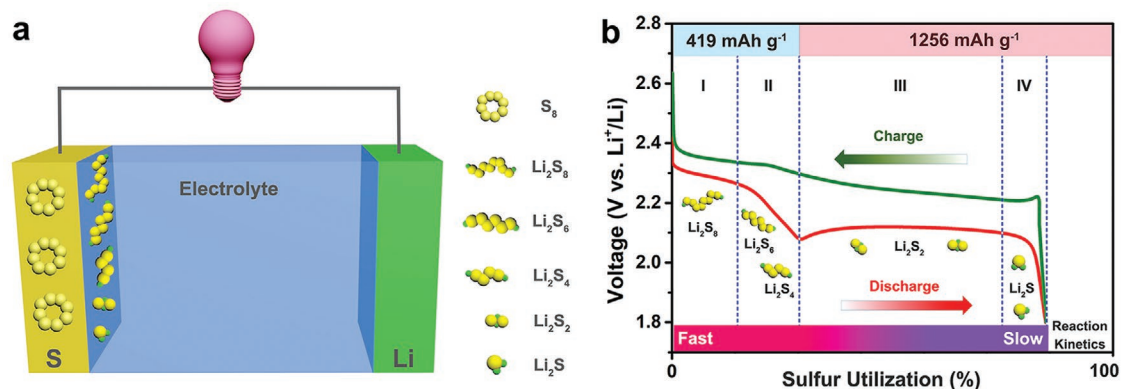
Figure 1. a) Schematic representation and b) typical charging and discharging voltage profile of Li–S batteries, also indicating the various intermediate sulfur species.

complicated reactions due to the multistep electrochemical process occurring upon cycling. The soluble lithium polysulfide intermediates (Li_2S_n, $4 \leq n \leq 8$) and insoluble Li_2S/Li_2S_2 discharge products have a major impact on the electrochemistry of Li–S batteries.[34,35]

A typical charge (green curve) and discharge voltage (red curve) profile of a Li–S battery is shown in Figure 1b. On the basis of the phase transitions of sulfur species, four stages can be distinguished in the discharge process:

Stage I: The reduction from solid sulfur into highly soluble long-chain Li_2S_8, corresponding to a solid–liquid two-phase reaction in Equation (2).[36]

$$S_8 + 2Li^+ + 2e^- \rightarrow Li_2S_8 \tag{2}$$

A small sloping plateau emerges during discharging at a relatively high voltage of approximately 2.3 V. Due to the continuous dissolution of Li_2S_8 into the electrolyte, the cathode becomes porous, resulting in the volumetric contraction of the cathode.

Stage II: A two-step reduction process of Li_2S_8 into soluble Li_2S_4, involving a liquid–liquid single-phase reaction, according to Equations (3) and (4).

$$3Li_2S_8 + 2Li^+ + 2e^- \rightarrow 4Li_2S_6 \tag{3}$$

$$2Li_2S_6 + 2Li^+ + 2e^- \rightarrow 3Li_2S_4 \tag{4}$$

During this stage, the concentration and viscosity of soluble polysulfides gradually rise. A small voltage peak emerges at the end of this discharge stage, which results from a higher overpotential caused by the high electrolyte viscosity due to polysulfide dissolution.[37] Stages I and II contribute to the one fourth (419 mAh g^{-1}) of the overall theoretical specific capacity, corresponding to the acceptance of 0.5 electron per sulfur atom.[38]

Stage III: Soluble Li_2S_4 is reduced to insoluble Li_2S_2 and Li_2S species. This stage involves liquid–solid conversions in Equations (5) and (6), resulting in gradually decreased redox kinetics.

$$Li_2S_4 + 2Li^+ + 2e^- \rightarrow 2Li_2S_2 \tag{5}$$

$$Li_2S_4 + 6Li^+ + 6e^- \rightarrow 4Li_2S \tag{6}$$
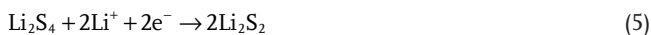
These reduction reactions take place simultaneously and compete with each other at the long lower voltage plateau of about 2.1 V.

Stage IV: The last stage relates to the further reduction of Li_2S_2 to Li_2S, which suffers high polarization and slow kinetics due to the solid–solid transformation reaction, according to Equation (7).

$$Li_2S_2 + 2Li^+ + 2e^- \rightarrow 2Li_2S \tag{7}$$

Note that Stage IV considerably depends on Stage III, in which the competition reactions occur. The sloping plateau, characteristic for Stage IV, becomes short or even disappears when the dominant reaction in Stage III is Equation (6). Stages III and IV contribute to three fourths (1256 mAh g^{-1}) of the overall theoretical specific capacity, corresponding to the acceptance of additional 1.5 electrons per sulfur atom.[39]

Upon the reversible charging process, the solid Li_2S and Li_2S_2 species are oxidized to various soluble polysulfides, which are finally converted into elemental sulfur (green voltage curve in Figure 1b). Another peak appears during the initial stage of the solid–liquid phase transition from Li_2S_2 and Li_2S into soluble polysulfides. This potential barrier mainly arises from the phase nucleation of polysulfides.[40]

Overall, from the electrochemical reaction of Li–S batteries discussed above, the dissolution and diffusion of polysulfides have a substantially detrimental effect on the electrochemical performance of Li–S batteries. Practically, due to the shelf-discharge of cathodes and the shuttle effect of polysulfides, sulfur cathodes therefore suffer heavy capacity degradation. Various strategies to effectively anchor polysulfides within the cathode have proven to be successful for the design of high-performance Li–S batteries.

3. Strategies for Anchoring Polysulfides

The design and fabrication of various sulfur host materials that can encapsulate and anchor polysulfides have been extensively reported. Specifically, the current investigations can mainly be classified into two strategies: physical confinement and chemical binding. Here, systematic and comprehensive analyses and

discussions on physical confinement and chemical binding for Li–S batteries are presented in the following context.

3.1. Physical Confinement

Physical confinement is a common and facile strategy to anchor polysulfides, which aims to spatially confine polysulfides inside sulfur cathodes. The focus of this strategy lies in the structural design of sulfur host materials. Generally, an ideal sulfur host should be able to become an efficient physical barrier that impedes polysulfide migration into the electrolyte. Based on this principle, the structure of sulfur hosts can mainly be divided into two classes: 1) porous structures and 2) shelled/layered structures.

The diffusion of soluble polysulfides can be physically confined either by porous materials or by external barrier coatings. Materials which either are porous or can be readily tailored into shelled/layered structures are perceived as efficient sulfur host materials. Among these, carbon-based materials, possessing a large specific surface area, tunable structures, and excellent conductivity, have been considered as one of the ideal candidates to physically confine polysulfides.[41–43] Various carbon-based materials, including porous carbon, graphene, and carbon nanotubes (CNTs), have been extensively employed as sulfur hosts to enhance the electrical conductivity of electrodes as well as to inhibit the diffusion of polysulfides outside the cathodes.

3.1.1. Porous Structures

Due to the porosity and large specific surface area, porous structures are able to effectively accommodate sulfur particles and confine sulfur species into the porous configurations. Consequently, a higher sulfur loading can be achieved and the volume variation during the cycling process can additionally be mitigated. The pore walls act as physical barriers and the charge transfer reaction of the encapsulated sulfur occurs within the pores, preventing the diffusion of polysulfides. The initial research using mesoporous carbon materials in sulfur cathodes was conducted by Wang et al.[44,45] The authors employed active carbon with a main pore size of 2.5 nm to mix with sulfur. During the thermal treatment, sulfur converted into liquid and moved into the mesopores of the active carbon. Owing to the physical confinement of polysulfides into the mesopores, the initial specific capacity of the composite cathodes reached 800 mAh g^{-1}. A stable capacity of about 440 mAh g^{-1} was maintained with high sulfur utilization of 90% upon cycling. From that moment on, various porous structures, such as porous carbon,[46,47] porous carbon fibers (PCFs),[48,49] and porous organic polymers,[50] have been proposed to confine sulfur species.

Porous carbon-based structures can be fabricated from various precursors. Using a hard template from self-stacked water-soluble NaCl and Na$_2$S crystals, Li et al. synthesized 3D porous graphitic carbon (PGC).[51] As shown in **Figure 2**a, the authors initially fabricated a 3D glucose-coated hybrid material by freeze-drying. Then, a thermal treatment transformed the glucose into PGC. Sulfur nanoparticles were in situ formed in PGC due to the reaction between Na$_2$S and Fe(NO$_3$)$_3$. The prepared sulfur composite cathode, designated as 3D S@PGC, achieved tunable sulfur contents with a maximum of 90 wt% by altering the ratio of Na$_2$S and glucose. This in situ approach resulted in the covalent bonding of sulfur at the surface of PGC. Due to these covalent bonds, hierarchically porous networks, and homogeneous sulfur nanoparticles, the 3D S@PGC composite cathodes exhibited substantially enhanced cycle life and excellent rate capabilities.

Metal–organic frameworks (MOFs) have been considered as promising precursors to fabricate carbon materials with tunable porous morphologies. Xi et al. selected four kinds of zinc metal-centered MOFs to produce hierarchically porous carbon structures since zinc was readily eliminated as metallic vapor during high-temperature pyrolysis.[55] Four MOFs were pyrolyzed under Ar atmosphere to produce hierarchically porous carbons. The authors demonstrated that the porosity of the pyrolyzed MOFs depended linearly on the Zn/C ratio of the precursors. As sulfur host materials, their pore volumes and pore size distribution had distinct effects on the initial storage capacities and cycling stabilities of Li–S batteries. Micropores benefited a prolonged cycle life by effectively confining polysulfides, while mesopores enabled a higher initial capacity by facilitating the Li$^+$ transfer.

Inorganic compounds can also be tailored to porous structures as sulfur hosts. Sun et al. synthesized a porous VN nanoribbon/graphene (VN/G) hybrid with high conductivity (Figure 2b).[52] Two steps were conducted to synthesize this porous VN/G composite material. First, a hydrothermal method converted graphene oxide (GO) and NH$_4$VO$_3$ precursors into a vanadium oxide/graphene (VO$_x$/G) hydrogel. This process resulted in the in situ formation of VO$_x$ on GO and the simultaneous formation of a 3D foam. Then the VO$_x$/G hydrogel was immersed in deionized water followed by freeze-drying to form a VO$_x$/G macrostructure. The freestanding VN/G composite material was obtained after annealing in an NH$_3$ atmosphere. The Li$_2$S$_6$ catholyte was directly added to the VN/G host. The 3D free-standing graphene network facilitated the charge transfer and benefited the electrolyte absorption. The VN nanoribbons contained a large number of mesopores, allowing fast ionic transportation and strong adsorption of polysulfides. As a result, the VN/G cathode exhibited a high initial capacity of 1471 mAh g^{-1} at 0.2 C and mitigated polarization (Figure 2c).

3.1.2. Shelled/Layered Structures

Coating a shell or layer on the surface of sulfur particles can also impede their diffusion spatially. These shelled/layered structures can adequately suppress the undesirable shuttle effect. Sulfur cathodes with core–shell structures show superior electrochemical performance, where the sulfur core is coated with shells composed of carbon or other homogenous materials. For example, Wu et al. developed a unique coating structure via the layer-by-layer (LBL) assembly. As illustrated in Figure 2d, the authors employed graphene sheets (GS) as the outer shell and polyelectrolyte multilayers (PEMs) as an inner shell to encapsulate the hollow carbon sphere/sulfur
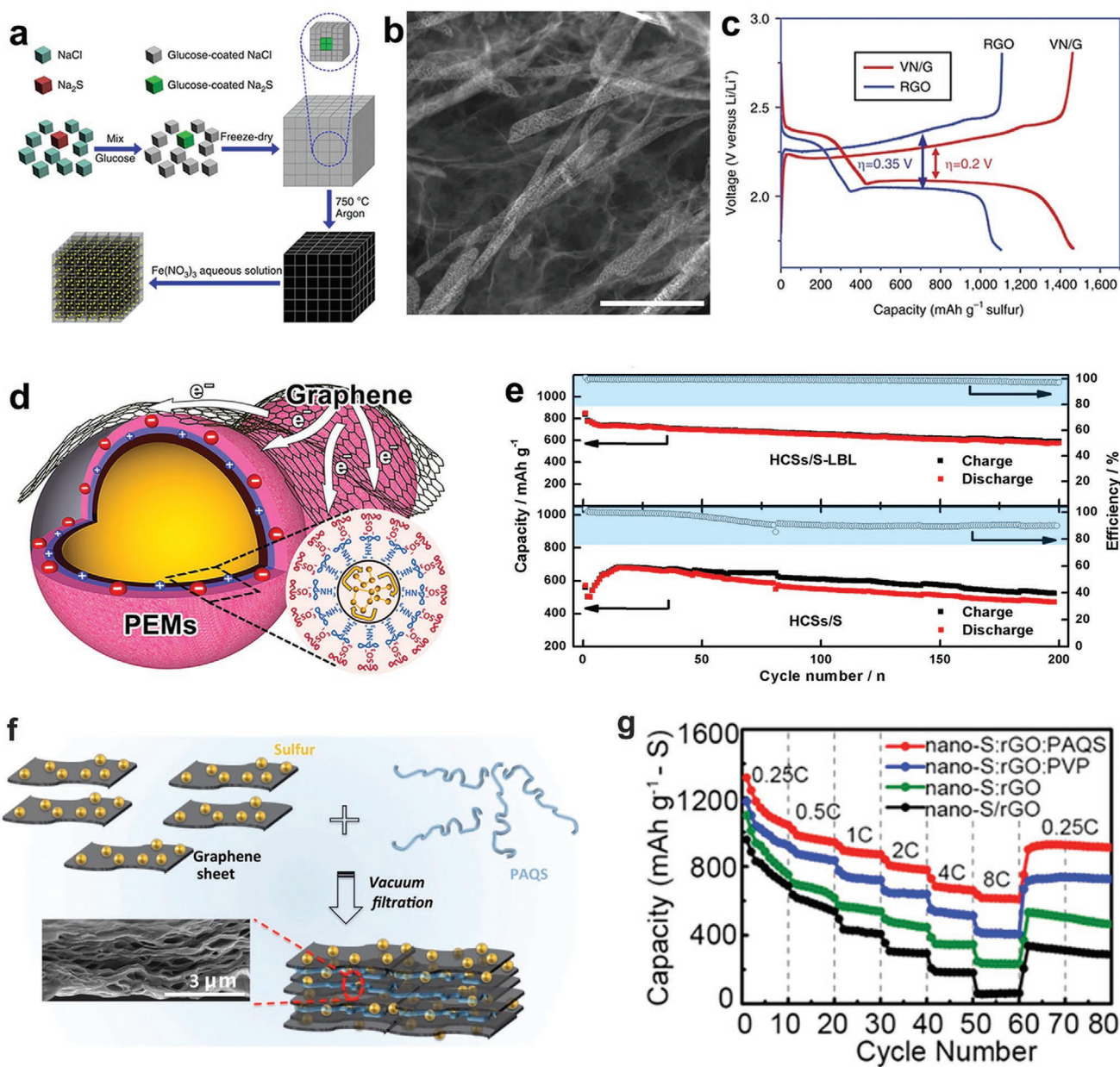
Figure 2. a) Schematic representation of in situ preparation of 3D S@PGC. b) STEM image of VN/G (scale bar: 500 nm). c) Voltage profile of an VN/G electrode at 0.2 C. d) LBL film coated HCS/S composites. e) Cycle life performance and coulombic efficiency of HCS/S-LBL at 1 A g^{-1}. f) Schematic illustration and g) rate performance of a nano-S:rGO:PAQS thin film cathode. (a) Reproduced with permission.[51] Copyright 2016, Springer Nature. (b,c) Reproduced with permission.[52] Copyright 2017, Springer Nature. (d,e) Reproduced with permission.[53] Copyright 2016, American Chemical Society. (f,g) Reproduced with permission.[54] Copyright 2015, American Chemical Society.

composites (HCS/S).[53] The LBL shells have multiple advantages. The inner PEMs restrained the movement of polysulfides via electrostatic repulsion. The outer GS stabilized the PEMs and accelerated the charge transfer by providing sufficient electron pathways. The beneficial effects of the LBL shells contributed to the HCS/S-LBL cathode with an enhanced storage capacity of over 200 cycles at 1 A g^{-1} (Figure 2e). Other types of core–shell structures, including the inorganic compound shells[56,57] and multiple shells,[32,58] have also been proven to effectively confine polysulfides.

However, the lithiation of sulfur cores is accompanied by a large volume expansion, which causes the protective shells to crack and fracture. The design of sulfur yolk–shell structures can be a good alternative.[59,60] The major advantage of the yolk–shell structures lies in the presence of the gap between yolks and shells. The additional voids allow the large volumetric variation of sulfur during cycling, thus enabling the integral shell structures. Based on this strategy, a sulfur–polyaniline (S-Pani) yolk–shell nanoarchitecture has been designed as sulfur cathodes for Li–S batteries by Zhou et al.[61] A facile fabrication

**ADVANCED
SCIENCE NEWS**
www.advancedsciencenews.com

**ADVANCED
ENERGY
MATERIALS**
www.advenergymat.de

approach was employed to obtain S-Pani yolk–shell composites. Uniform sulfur nanoparticles were initially synthesized by a chemical reaction. Subsequently, polyaniline was coated on sulfur nanoparticles to achieve an S-Pani core–shell composite. Thermal treatment at 180 °C under argon resulted in the in situ vulcanization of polyaniline, forming the S-Pani yolk–shell structures. In contrast to the S-Pani core–shell composites, the yolk–shell counterpart exhibited significantly enhanced cycling stabilities.

Coating a barrier layer on sulfur cathodes is another structural design to inhibit the diffusion of polysulfides upon cycling. By this method, a tiny amount of coating can significantly enhance the active sulfur utilization. Using atomic layer deposition (ALD), Yu et al. deposited TiO$_2$ layers on nitrogen-doped graphene/sulfur electrodes adding only negligible additional weight.[62] The deposited TiO$_2$ layers immobilized the soluble polysulfide species and prevented a severe loss of sulfur upon cycling. The resulting sulfur cathodes exhibited improved cycling stability. In addition, the deposition of Al$_2$O$_3$ coatings has also been proven effective to confine polysulfides.[63,64]

Sulfur can also be encapsulated within the layers of 2D materials. 2D materials with a large specific area can intrinsically act as the barrier layer to confine sulfur particles. Moreover, these layers can also provide excellent conductive pathways for charge transfer. A case in point is the sulfur cathodes designed by Chen et al.[54] The authors combined reduced graphene oxide (rGO) with poly(anthraquinonyl sulfide) (PAQS) to assemble a freestanding composite thin film as sulfur cathodes. As shown in Figure 2f, a sulfur-amine chemical process enabled nanoscale sulfur particles to grow in rGO suspensions (S@rGO). Then, the addition of PAQS gave rise to the adsorptive interaction with S@rGO. Vacuum filtration achieved the assembly of freestanding stacked films (S:rGO:PAQS). In this structure, rGO restricted the shuttle effect of polysulfides and alleviated the volume variation of sulfur cathodes. PAQS provided favorable ionic conduction pathways and also inhibited the polysulfide shuttling. The resulting sulfur composite cathodes maintained a steady storage capacity of 615 mAh g^{-1} at 8 C (Figure 2g). Besides, 2D inorganic compounds that are composed of nanosheets[65,66] and nanoflakes[67,68] can serve as an effective barrier layer to confine active sulfur species.

In conclusion, both porous and shelled/layered structures can function as effective sulfur host materials. Their large surface area enables efficient physical confinement, and therefore sulfur particles are spatially restricted into the cathode. Various of these developed host materials are carefully analyzed and summarized in this review with the focus on the advantages of physical confinement of polysulfides. The comprehensive and systematic discussion is beneficial for the reader to gain a better understanding of the design of the various available sulfur host materials.

3.2. Chemical Bonding

Considering the polarity of polysulfides, it is desirable to employ materials that can form strong chemical bonding with polysulfides as sulfur hosts.[69] The strong chemical interaction between sulfur host materials and polysulfides can substantially enhance the anchoring of polysulfides, hence inhibiting their movement and diffusion into the electrolyte. Generally, the chemical bonding between sulfur hosts and polysulfides can be achieved by four approaches: 1) polar–polar interactions; 2) Lewis acid–base interactions; 3) redox interactions; 4) covalent binding interactions. In order to attain optimum chemical bonding, materials should be designed in such a way to provide sufficient bonding sites, which are able to generate chemical interactions with polysulfides. Therefore, structures with a large specific surface area and pore volume are considered to be ideal sulfur host materials. Various materials, including metal oxides, heteroatom doped carbon, and MOFs have been investigated to explore their chemical binding with polysulfides, as will be outlined below.

3.2.1. Polar–Polar Interactions

The asymmetry of polysulfides endows them with polarity, so polar materials can anchor polar polysulfides by polar–polar interactions. Materials with strong polarity have the potential as good sulfur hosts. Due to the intrinsic polarity, metal compounds can be directly applied as host material. There have been many studies that demonstrate their superiority in confining polysulfides.[11,70] On the other hand, some of the metal compounds exhibit relatively poor conductivity, which is detrimental to the redox kinetics of sulfur cathodes. Highly conductive carbon materials are therefore often added to improve Li–S batteries.

By modifying the carbon surface with heteroatoms (e.g., oxygen and nitrogen), non-polar carbon materials can be converted to polar materials. These heteroatoms can chemically anchor polysulfides by forming polar interactions. Concerning the abundant oxygen-containing polar groups of GO, Ji et al. initially demonstrated that the functional groups on GO exhibited enhanced chemical bonding to sulfur via theoretical calculation and X-ray absorption spectroscopy.[71] Doping not only increases the polarity of carbon-based materials but also enhances the conductivity. Many studies have confirmed that nitrogen,[72,73] phosphorus,[74] and multiple doping elements[75,76] create abundant active sites at carbon, effectively enabling chemical anchoring of sulfur species. These doped carbon precursors can be graphene, CNTs, porous carbon, and carbon nanospheres. Although some of the research did not definitely indicate polar–polar interactions, the corresponding theoretical calculations and experimental analyses revealed the presence of electron transfer between polar carbon hosts and sulfur species.[71,77]

Metal oxides have been widely reported to confine polysulfides by polar–polar interactions. The strong polarity allows them to form metal–sulfur bonds or oxygen–lithium bonds. The Nazar group initially employed Magnéli phase (Ti$_4$O$_7$) to chemically bind polysulfides.[78] Ti$_4$O$_7$ containing polar O-Ti-O units has a strong affinity for polysulfides (**Figure 3**a). Combining the visual adsorption investigations with X-ray photoelectron spectroscopic (XPS) and X-ray absorption near-edge structure (XANES) studies, the authors confirmed the strong metal oxide–polysulfide chemical interactions. As a result, Ti$_4$O$_7$/S cathodes achieved a durable cycling stability for 500 cycles at
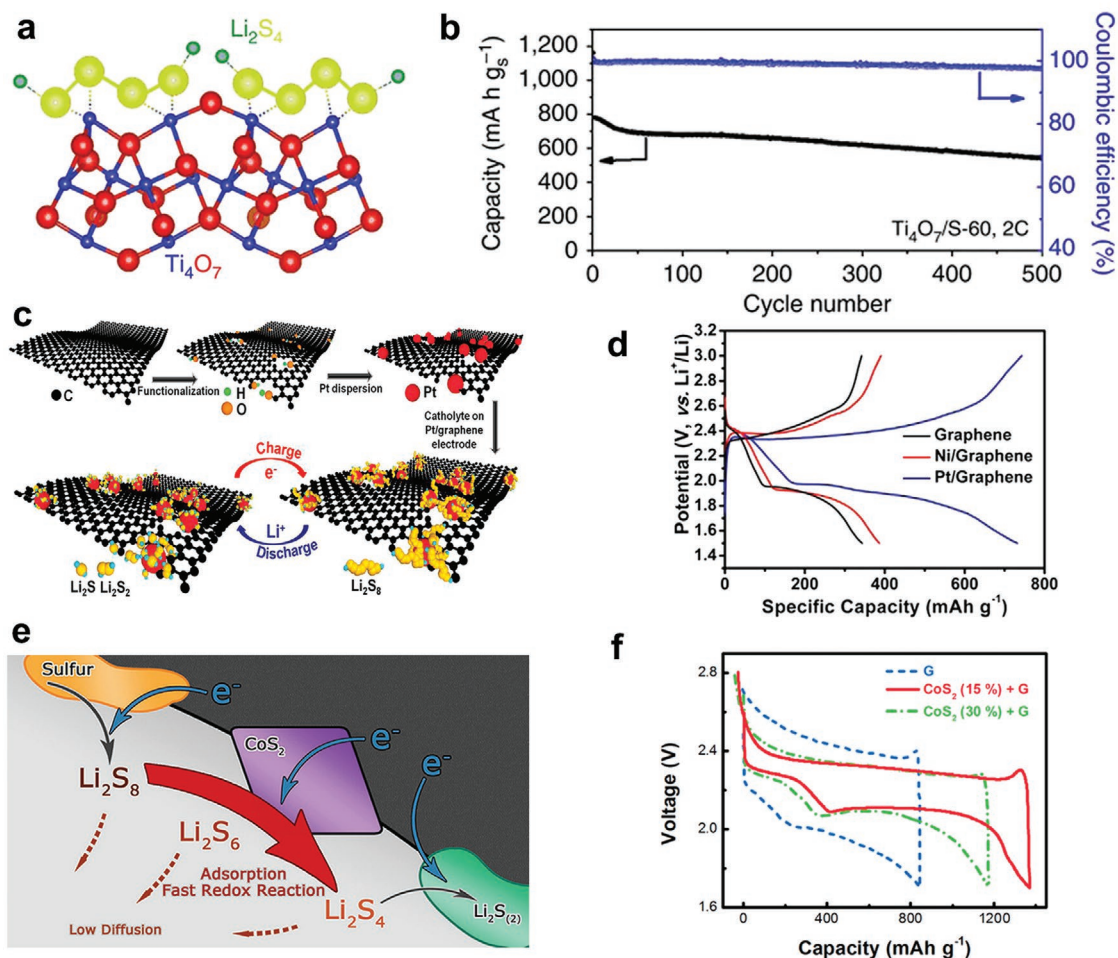
Figure 3. a) Schematic illustration of electron density transfer between Li_2S_4 and Ti_4O_7. b) Cycle life performance of a Ti_4O_7/S-60 electrode at 2 C. c) Synthesis of electrocatalyst-anchored graphene nanocomposite and its interaction with polysulfides. d) Voltage profiles of pristine and electrocatalyst-anchored graphene electrodes. e) Schematic illustration of the adsorption and accelerated redox reaction of polysulfides by CoS_2. f) Voltage profiles of S/G cathodes with and without CoS_2. (a,b) Reproduced with permission.[78] Copyright 2014, Springer Nature. (c,d) Reproduced with permission.[86] Copyright 2015, American Chemical Society. (e,f) Reproduced with permission.[30] Copyright 2016, American Chemical Society.

2 C (Figure 3b). Other oxides including TiO_2, Co_3O_4, and Fe_3O_4 have been developed to anchor polysulfides.[58,79,80] Their high polarity can generate strong polar–polar interactions with polysulfides. Also, many studies have employed sulfides, such as Co_9S_8, MoS_2, and TiS_2 to chemically bond polysulfides.[81–83] The charge transfer and configuration distortion caused by polar–polar interactions were validated by both theoretical calculations and experimental results. Besides, some polar nitrides and carbides have also been demonstrated to form polar–polar interactions with polysulfides.[84,85]

3.2.2. Lewis Acid–Base Interactions

Since polysulfide anions own occupied orbitals with lone electron pairs, they can be considered as a Lewis base. Lewis acids, containing unoccupied orbitals, can accept the lone pair of electrons of Lewis bases to form coordinate bonds. Therefore, a chemical species with the property of a Lewis acid is capable of anchoring polysulfides by Lewis acid–base interactions. It has been demonstrated that the metal ions in MOFs and MXenes can accept a lone pair of electrons from polysulfides. As sulfur hosts, MOFs and MXenes can therefore significantly suppress the dissolution of polysulfides from the cathode.

Zheng et al. initially investigated the Lewis acid–base interactions between MOFs and polysulfide anions in detail.[87] A new Ni-based MOF host (Ni-MOF) was synthesized to impregnate sulfur. Electrochemical studies revealed that the Ni-MOF/S cathode exhibited considerably increased cycling stability than other MOF/S cathodes. The authors expected that apart from the pore effects of MOFs, other factors might also affect the behavior of sulfur cathodes.

First-principles calculations were initially introduced to analyze the interactions between Li_2S_x ($2 \leq x \leq 8$) and Ni-MOF. The calculated binding energies increased with the chain length of polysulfides. Accordingly, the Ni 2p XPS spectra of MOF/S shifted to lower binding energies, confirming the interaction between nickel cations and polysulfide anions. The authors further synthesized Co-MOF by substituting nickel with cobalt to study the interaction mechanisms between polysulfide anions

and metal cations. Compared to Ni-MOF/S, the Co-MOF/S cathode indicated an inferior cycling performance and lower binding energies between Co-MOF and polysulfides, which means a weaker coordination between the cobalt cations and polysulfide anions. These results were consistent with the Irving–Williams Series, in which the stability constant of the Ni(II) complex is higher than that of the Co(II) counterpart.

From then on, various MOFs with open metal sites have been reported as Lewis acid to anchor polysulfides. The Lewis acid–base interactions between MXenes and polysulfide anions were first proposed by Nazar et al.[88] The authors found the surface Ti atoms of Ti_2C had unoccupied orbitals to bind with polysulfide anions forming strong Ti—S bonds. This interaction resulted in the suppression of the polysulfide diffusion. A more detailed discussion on MXenes as Lewis acid will proceed in the section of metal compound hosts.

3.2.3. Redox Interactions

When an electrode material is above the redox potential window of polysulfides, the polysulfides can be oxidized to generate thiosulfate/polythionate species anchored at the material surface. This reaction significantly inhibits the loss of polysulfides and boosts the electrochemical performance of sulfur cathodes. This novel anchoring mechanism was initially proposed by the Nazar group.[89] MnO_2 nanosheets were chosen as the prototype to investigate their interactions with polysulfides. Based on XPS analyses, they proposed that the insoluble thiosulfate species are responsible for mediating the polysulfide conversion in a two-step redox process. Polysulfides initially produced at the discharging stage reacted with MnO_2 to form thiosulfate groups. With the reaction proceeding, the fresh polysulfides then reacted with the thiosulfate groups to generate polythionate complexes and shorter-chain polysulfides. The relatively poor solubility of the polythionate complex considerably suppressed the shuttle issue of polysulfides. This conversion proceeded gradually until the discharging process was finished. Meanwhile, MnO_2 was reduced to Mn^{2+}. The resulting S/MnO_2 cathode with 75 wt% sulfur loading delivered a 0.036% capacity fading per cycle during 2000 cycles at 2 C. Their further studies demonstrated that this mechanism could also be responsible for the superior cell performance with GO hosts. In their follow-up work, Nazar et al. concluded that materials having a redox potential window of 2.4–3.05 V (e.g., VO_2) were able to trigger this reaction mechanism to chemically anchor polysulfides.[90] Besides, they also revealed that the formation of thiosulfate was responsible for the interaction between titanium-based MXene phases and polysulfides.[91] The terminal hydroxyl groups of MXenes reacted with polysulfides to form thiosulfate species. Together with the resulting Ti—S bonding based on Lewis acid–base interactions, these dual anchoring effects substantially inhibited the loss of sulfur species, leading to the increased cycle life of sulfur cathodes.

In view of the complex multistep reactions and sluggish redox kinetics, accelerating the conversion of sulfur species is beneficial to the mitigation of polysulfide losses. Electrocatalysis may play a major role in regulating the redox conversion rate. Many reports have demonstrated that host materials have catalytic properties, accelerating the conversion of soluble polysulfides, the deposition of solid lithium sulfides, and the oxidation of Li_2S during charging and discharging. The electrocatalysis of the polysulfide transformation was initially proposed by Al Salem et al.[86] These authors chose graphene to support Pt nanoparticles to increase the surface areas and the number of catalytic sites, as schematically shown in Figure 3c. The superior catalytic effect of Pt/graphene composites significantly reduced the overpotential of the oxidation and reduction peaks observed in cyclic voltammetry (CV) compared to pristine graphene. Moreover, the enhanced exchange current densities during (dis)charging clearly showed that Pt/graphene accelerated the conversion reactions of polysulfides. Benefiting from these merits, Pt/graphene cathodes revealed a 40% increase in capacity over pristine graphene (Figure 3d). The XPS spectra also confirmed the existence of Pt^{2+} species during discharging, indicating the redox interactions with polysulfides. A decrease in Pt^{2+} intensity during charging further revealed the reversibility of the redox interactions. Electrocatalysis therefore offers new routes to anchor and effectively convert sulfur species, leading to a better performance of Li–S batteries.

The anchoring and conversion approaches have further been developed by Yuan et al. They incorporated sulfiphilic CoS_2 into carbon/sulfur cathodes to promote the redox reactions of polysulfides (Figure 3e).[30] Owing to the strong chemical affinity with polysulfides, CoS_2 effectively increased the sulfur utilization. This has been confirmed by the CV of symmetrical Li_2S_6 cells, in which the current densities significantly increased with a rise in the CoS_2 weight ratio. The enhanced current density resulted from the accelerated reaction kinetics of polysulfides. Consequently, a CoS_2/graphene composite host with 15% CoS_2 weight ratio (CoS_2 (15%) + G) exhibited an optimal capacity of 1368 mAh g^{-1} (Figure 3f).

During the charging process, catalyzing the oxidation of solid Li_2S can mitigate the reaction overpotential and thus contribute to better redox kinetics. The Cui group found a series of metal sulfides showing catalytic effects for the decomposition of Li_2S to sulfur upon charging.[92] The decomposition process was perceived as one Li_2S molecule converting into one LiS cluster and one Li^+. They concluded that the decomposition of Li_2S correlated with the binding of sulfur atoms in sulfides to isolated lithium ions. The strong interactions gave rise to lower overpotentials, which was the principal reason for a reduced decomposition barrier, while the weak interactions of carbon materials toward lithium ions incurred a high activation energy barrier.

3.2.4. Covalent Binding Interactions

Sulfur covalently binding at the surface of carbon and polymer materials is an effective approach to eliminate the dissolution of soluble polysulfides during cycling. In this case, sulfur exists in the form of short sulfur chains to form covalent bonds with carbon atoms, for example, C—S and C=S. Various carbons and polymers can covalently bind with sulfur by sulfurization at elevated temperatures. The resulting sulfurized compounds are promising cathode materials.[93] Because of covalent binding interactions, sulfur is fully anchored at the host material, achieving a solid-to-solid transformation between covalent

sulfur chains and lithium sulfides during the discharging and charging process. The covalently bound sulfur produces a distinctly different electrochemical characteristic of Li–S batteries. Traditional composites, integrating sulfur and hosts, present two cathodic peaks and two discharge plateaus in their CV and voltage profiles, respectively. This reaction process results from the conversion of sulfur to polysulfides and solid lithium sulfides. In contrast, sulfurized compounds typically exhibit solely one cathodic CV peak and one sloping discharge plateau at 1.9 V, indicating a solid-to-solid phase transformation.[94,95] Moreover, because of the complete elimination of polysulfides upon cycling, carbonate electrolytes can be beneficially applied in combination with sulfurized compounds.

The content of sulfur in sulfurized compounds depends on the types of host material and sulfurization temperature. Hosts with abundant surface functional groups, such as hydroxyl and carbonyl, are capable of reacting with sulfur forming covalently bound sulfur. Surface functionalized carbon and polymers, like polyacrylonitrile (PAN) and polyaniline, are desirable precursors for sulfurization. The sulfurization temperature varies from the boiling point of sulfur up to 600 °C. For example, Frey et al. synthesized a sulfurized material from polymethyl methacrylate (PMMA) and PAN via facile thermal conversion.[96] A 550 °C heating treatment for 3 h resulted in sulfur covalently bound to PAN. The obtained sulfurized PAN (SPAN) exhibited a high sulfur content of 46 wt%. Generally, a high sulfurization temperature contributes to a shorter sulfur chain, implying a lower sulfur content and specific storage capacity. On the other hand, the sulfur distribution will be more homogeneous, so an improved cycling stability can be expected. Overall, the present sulfur content in sulfurized compounds is not as high as in sulfur/host composites. By covalent binding interactions, the dissolution issue of polysulfides can be fully suppressed. Sulfurized compounds provide therefore an interesting alternative to construct reliable Li–S batteries.

Generally, the four interactions discussed above do not exist separately between host materials and sulfur species. A sulfur host may have multiple interactions. For example, MXenes anchor polysulfides through both Lewis acid–base and redox interactions. Based on different characterization methods and detailed analyses, it has been concluded that one sulfur host may offer distinct interaction mechanisms. Despite the insufficient understanding, it has been firmly demonstrated that these interactions improve the polysulfide anchoring effectively and consequently boost the utilization of sulfur species, which leads to a significant improvement of the electrochemical performance of sulfur cathodes. The concluded four interactions cover the main mechanisms of chemical bonding to polysulfides. Together with the two host structures for physical confinement, a systematic and comprehensive perspective on strategies for anchoring polysulfides is therefore offered, which provides a better insight and outlook on sulfur host materials.

4. Nanostructured Carbon Hosts

Nanostructured carbon materials have been considered to be effective sulfur hosts because of the good mechanical stability, excellent conductivity, natural abundance, and high specific surface area. Polysulfides are prone to be confined within the carbon matrix to inhibit their diffusion into the electrolyte, resulting in enhanced electrochemical performance of sulfur cathodes. Nanostructured carbon materials employed as sulfur hosts can be divided into five categories: 1) porous carbon; 2) graphene; 3) carbon nanotubes and fibers; 4) heteroatom-doped carbon; 5) carbon nitride.

4.1. Porous Carbon

Porous carbon materials generally can be used as a framework to host active sulfur species, where polysulfides are mainly encapsulated in the pores. Owing to the excellent conductivity, large specific surface area, and adequate pore volume, porous carbon can substantially improve the conductivity of sulfur cathodes. Also, the porous structure effectively anchors polysulfides and accommodates the volume variation of cathodes upon cycling.[97–99] According to the variation in pore size, porous carbon is mainly categorized into three different types, where the pore diameter (d) is leading: 1) microporous carbon ($d < 2$ nm); 2) mesoporous carbon (2 nm $< d <$ 50 nm); and 3) macroporous carbon ($d > 50$ nm). Many efforts have been devoted to developing porous carbon materials with various morphologies and structures as sulfur host in recent years.[51,100–102]

4.1.1. Microporous Carbon

Microporous carbon (MPC) structures are widely perceived as a good sulfur host that can homogenously anchor sulfur intermediates. Considering the reduced dimension of micropores, sulfur molecules tend to be anchored into the carbon matrix in the form of small $S_{2–4}$ molecules instead of the larger S_8 molecules.[103–105] This leads to a deviating discharging profile which is significantly different from that of the reduction of S_8 molecules into dissolved polysulfides. The sulfur shuttle problem can therefore be avoided. Tailoring S_8 into small allotropes, Xin et al. realized a new strategy to confine metastable $S_{2–4}$ molecules (S_2, S_3, and S_4) into the internal voids of a conductive MPC matrix.[103] Multi-walled CNTs coated with a MPC layer were designed for sulfur accommodation. As shown in **Figure 4**a, the obtained CNT@MPC revealed a coaxial structure with a CNT core and a MPC sheath. The micropore size of MPC was about 0.5 nm. Since the size of large $S_{5–8}$ molecules exceeded that of MPC, only small chain-like $S_{2–4}$ molecules smaller than 0.5 nm can be accommodated in the micropores of MPC. The voltage profile of S/(CNT@MPC) in Figure 4b shows a single long sloping discharge plateau at about 1.7 V. The confined small $S_{2–4}$ molecules avoid the detrimental conversion between S_8 and S_4^{2-} upon (dis)charging, and limit the overall process to a direct solid–solid reaction, according to Equation (8).

$$S_{2–4} + Li^+ + e^- \leftrightarrow Li_2S \qquad (8)$$

In another report, microporous carbon with subnano-internal voids was synthesized as a sulfur host, where
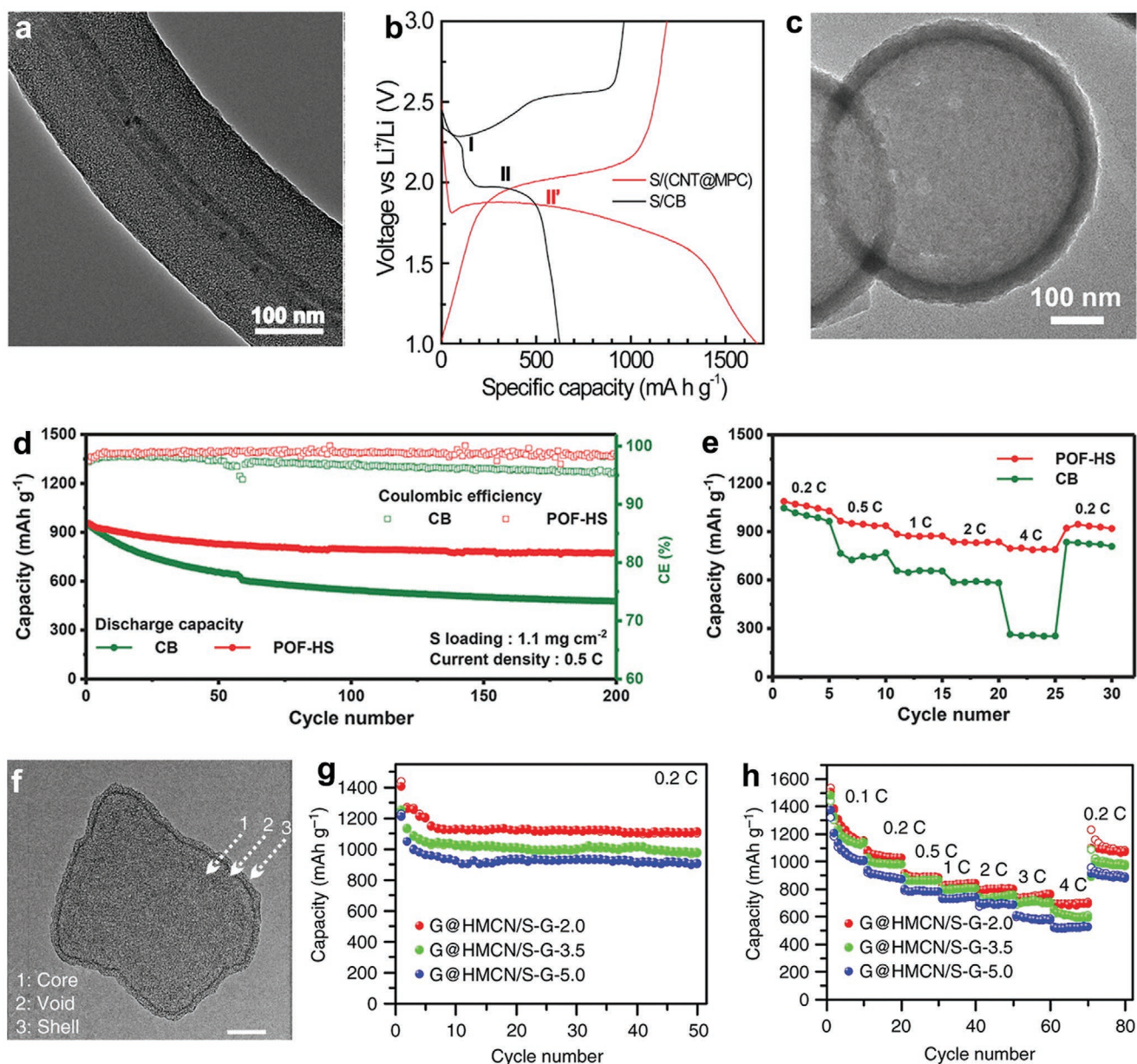
Figure 4. a) TEM image of a CNT@MPC nanocable. b) Voltage profile of S/(CNT@MPC) at 0.1 C. c) TEM image of POF-HS with the typical hollow spherical morphology. d) Cycling performance and e) rate performance of POF-HS/S. f) TEM image of G@HMCN (scale bar: 50 nm). g) Voltage profiles and h) rate performance of G@HMCN/S-G cathodes with various sulfur loading. (a,b) Reproduced with permission.[103] Copyright 2012, American Chemical Society. (c–e) Reproduced with permission.[106] Copyright 2018, Wiley-VCH. (f–h) Reproduced with permission.[107] Copyright 2017, Springer Nature.

short-chain S_2 species were successfully confined inside the pores.[104] The subnano-entrapped S_2 cathodes revealed a unique electrochemical mechanism which may correspond to the coupling between the charge-sharing $C/2S^{2-}$ matrix and Li ions, according to Equation (9).

$$C/S_2 + 4e^- + 4Li^+ \leftrightarrow C/2S^{2-}/4\left(Li^+\right) \tag{9}$$
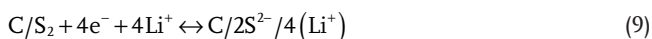
In a carbonate electrolyte, a novel solid electrolyte interphase (SEI) comprising thiocarbonates was formed during the initial cycle at the composite cathode surface. Both the subnano-confinement and the SEI, covering the surface, effectively

prevented the shuttling of S_2 species. The SEI-coated C/S cathode showed a high storage capacity even after 4000 cycles with very low capacity losses. Furthermore, Zhu et al. employed a novel ultra-microporous carbon (UMC) to encapsulate small $S_{2–4}$ molecules.[105] The UMC was designed and prepared from polyvinylidenefluoride (PVDF) by a facile pyrolysis process. The micropores with a homogeneous size of 0.55 nm enabled UMC to exclusively trap smaller $S_{2–4}$ molecules. Therefore, the corresponding discharge process only showed the direct reduction of $S_{2–4}$ to Li_2S. The shuttle effect caused by dissolved polysulfides was fundamentally avoided. The merits of UMC hosts were demonstrated by the prolonged cycling stability, in which

**ADVANCED
SCIENCE NEWS**

www.advancedsciencenews.com

**ADVANCED
ENERGY
MATERIALS**

www.advenergymat.de

only about 0.03% capacity loss per cycle occurred in the first 1000 cycles at 1 C-rate.

Conclusively, the electrochemical performance of sulfur molecules encapsulated in micropores has been significantly changed due to the pore size effect of the host material. However, the intrinsic drawback of low sulfur loading still restricts the widespread application of microporous carbon materials. The low sulfur content loaded inside the micropores inevitably results in rather low energy densities of complete Li–S batteries, impeding further practical applications of microporous carbon host materials.

4.1.2. Mesoporous Carbon

To accommodate as much as sulfur in host materials, various mesoporous carbon materials have been extensively developed. A series of breakthroughs have been achieved by the Nazar group. They encapsulated sulfur into a highly ordered mesoporous carbon (CMK-3) host with channel voids of 3 to 4 nm.[17] The synthesized CMK-3 host was composed of a combination of hollow carbon rods of 6.5 nm thickness separated by channel voids in 3 to 4 nm width. The mixture of elemental sulfur and CMK-3 was heated at 155 °C; consequently, the liquid sulfur could easily diffuse into the mesopores making use of capillary forces. A 70 wt% sulfur content was achieved with the as-prepared composite cathode, leading to a favorable capacity of 1005 mAh g^{-1} in the first cycle. A further modification was conducted with a polyethylene glycol (PEG) coating. The PEG-modified composite cathode revealed an increase in initial capacity of 1320 mAh g^{-1}. The confinement of sulfur species inside the mesopores ensured fast reaction kinetics and the cathode capacity could be adequately exploited. From then on, many mesoporous carbon host materials have been developed to anchor the sulfur species and significantly boosted the advancement of the use of sulfur cathodes.

In subsequent investigations, Schuster et al. synthesized unique nanoscale spherical-ordered mesoporous carbons (OMC) with extremely high bimodal porosities.[108] The spherical OMC revealed a homogeneous particle size with a diameter of about 300 nm. The applied silica etching process generated hierarchical mesopores 6 and 3.1 nm in size. The resulting composite cathodes with 49.7 wt% sulfur content combined an initial capacity of 1200 mAh g^{-1} at 1 C with a favorable cycle life. Analyzing nanosize and bulk carbon, the authors concluded that the nanoscale morphology of mesoporous carbon was responsible for the excellent electrochemical properties of Li–S cells.

Park et al. synthesized ordered mesoporous carbon nanosheets (OMCNS) with honeycomb-like structures to load sulfur.[109] An acidic etching process of the self-assembled carbon nanosheets and iron oxide hybrid produced the 2D OMCNS. OMCNS displayed homogeneous 20 nm long mesoporous tight-packed cells between which gaps existed of about 4 nm wide. The ordered mesoporous cubes with numerous voids mitigated the volumetric expansion of the cathode material and also anchored the polysulfides upon cycling, thereby effectively suppressing the shuttle effect and offering a stable cycle life performance. The OMCNS-S cathodes combine an initial storage capacity of 1238 mAh g^{-1} at 0.1 C

with an impressive capacity fading of only 0.081% per cycle maintained for 500 cycles.

Due to the complex fabrication process of the mesoporous carbon materials, their large-scale application for Li–S batteries is, however, heavily hampered. The synthesis of mesoporous carbons involves a series of complex steps, such as a high-temperature process, pretreatment, and etching of templates. This approach makes the practical production of these materials rather cost-ineffective.

4.1.3. Hollow Carbon

Hollow carbons have a macropore structure and adequate internal cavities, which can maximize the energy density of Li–S batteries. Hollow carbon materials have therefore been widely investigated as sulfur hosts. Early research on hollow carbon tends to employ the pure carbon structure to confine sulfur. Recently, combining other elements or components with hollow carbon has become a common approach. These introduced components not only enhance the conductivity of cathodes but also benefit polysulfide adsorption.

Considering the advantages of the highly controllable morphology of organic frameworks, Li et al. prepared porphyrin organic framework hollow spheres (POF-HS) using polystyrene (PS) microspheres as template.[106] The as-synthesized POF-HS exhibited a hollow spherical morphology with inner diameter and thickness of 500 and 40 nm, respectively (Figure 4c). Due to the favorable polarity and hollow structures, POF-HS adequately alleviated the polysulfide shuttling via the dual functions of physical confinement and chemical adsorption. The POF-HS/S electrode combined a steady capacity of 773 mAh g^{-1} after 200 cycles with a stable coulombic efficiency of close to 100% (Figure 4d), implying a substantial inhibition of polysulfide shuttling. The excellent reaction kinetics of the composite cathode was also demonstrated at high rates. A favorable storage capacity of 800 mAh g^{-1} was attained at 4.0 C (Figure 4e).

More recently, Zhong et al. reported a novel porous carbon with macrocellular structures.[46] The authors were inspired by the instantaneous puffing to produce popcorn. The rice was directly puffed into a highly porous macrocellular structure by an in situ pressure-releasing approach. Specifically, the pristine rice with a dense structure was loaded into a heated pressure vessel. Under the internal vapor pressure, the rice starch became unstable and gradually expanded. The inner starch had a volume enlargement of about 20 times when the outer pressure was released by opening the sealed vessel. The puffed rice derived carbon (PRC) was achieved through facile carbonization. The prepared PRC possessed a 3D microcellular porosity generated by interconnected secondary carbon sheets with a large pore size of 100 µm. Ni nanoparticles were further embedded in the PRC. A PRC/Ni composite was achieved with both high conductivity and a large surface area. The designed PRC/Ni/S cathode exhibited a high reversible capacity of 1257 mAh g^{-1} at 0.2 C and achieved a 65% capacity retention after 500 cycles. It was concluded that the excellent properties resulted from the improved conductivity and increased polysulfide adsorption of the PRC/Ni structure.

ADVANCED
SCIENCE NEWS

www.advancedsciencenews.com

ADVANCED
ENERGY
MATERIALS

www.advenergymat.de

4.1.4. Hierarchical Porous Carbon

Hierarchical porous carbon, combining different types of pore sizes, such as micropores, mesopores, and even macropores, has also drawn extensive attention. Pores with different sizes have distinct roles in the electrochemical performance. Macroporous structures are typically used to accommodate and encapsulate enough sulfur to obtain Li–S batteries with desirable energy densities. Mesoporous structures are also beneficial to electrolyte access for good charge transfer kinetics. Resulting from their specific spatial confinement and an abundance of adsorption sites, micropores can confine sulfur species and mitigate the shuttle effect. The design and fabrication of sulfur hosts, combining various pore structures, will therefore contribute to desirable sulfur cathodes.

Various approaches have recently been proposed to design hierarchical porous carbon for improving Li–S batteries.[47,102,110,111] For instance, Pei et al. designed a unique 2D yolk–shell carbon nanostructure to build a self-supporting cathode.[107] This yolk–shell nanostructure consisted of highly dispersible graphene encapsulated in hollow mesoporous carbon nanosheets (G@HMCN). As illustrated in Figure 4f, G@HMCN revealed a clear void space between the core and the shell. A free-standing and flexible G@HMCN/S-G hybrid paper cathode was obtained by vacuum filtration of the aqueous dispersion containing G@HMCN/S and graphene. The authors investigated three G@HMCN/S-G cathodes with different sulfur loading (2.0, 3.5, and 5.0 mg cm^{-2}). From the cycling performance shown in Figure 4g, all of them revealed high sulfur utilization at 0.2 C. Also, three G@HMCN/S-G cathodes exhibited good rate capability even up to 4 C (Figure 4h). Moreover, a higher sulfur loading was reached at 10 mg cm^{-2}, giving rise to an increase in areal storage capacity to 11.4 mAh cm^{-2}. This research demonstrated that self-supporting structures can effectively mitigate capacity degradation and offer insights into the application of Li–S batteries with high energy density.

4.2. Graphene

Graphene, composed of a few layers of graphite atoms, is a 2D carbon material with fascinating electrical and mechanical characteristics. The excellent conductivity and large specific surface area make graphene a highly promising sulfur host material.[112] Various methods have been developed to synthesize and modify graphene and its derivatives to improve the electrical conductivity and confinement of polysulfides.

In order to localize active sulfur species at the cathode side, Zhou et al. designed a novel sulfur cathode where pure sulfur was sandwiched between two graphene layers.[113] The active sulfur material was coated with a graphene membrane at one side, which was used as a current collector. A commercial separator was covering another graphene membrane. The sulfur composite electrode wrapped by these two graphene membranes enabled fast charge transfer pathways, mitigated the volumetric expansion of sulfur, and alleviated the shuttle issue. This sandwich electrode structure contributed to Li–S batteries with higher energy density. Recently, Li–S batteries with high volumetric energy densities were achieved by Li
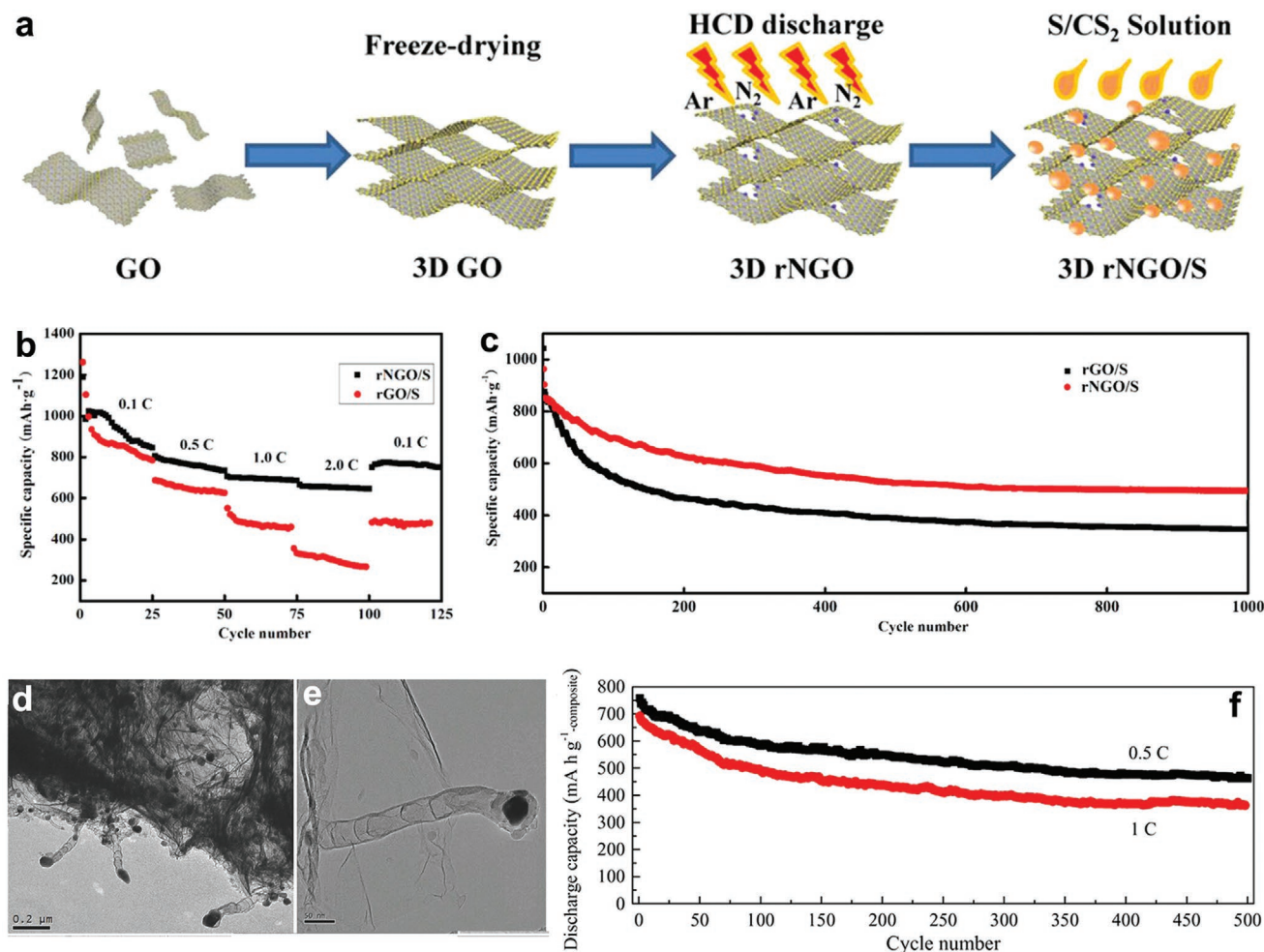
et al., using dense graphene monolith (GM) to host the Li$_2$S$_6$ catholyte.[114] The authors produced "ink-bottle-like" (IB) pores in GM through a phosphoric acidic activation process. The final IBGM structure was obtained by capillary evaporation-induced drying (CEID). Because of the narrow neck and wide-body pore configuration, polysulfides were readily confined in IBGM. Consequently, a composite cathode loading of 5.6 mg cm^{-2} sulfur (54% loading) revealed a high volumetric capacity of 653 mAh cm^{-3}. Furthermore, a 100 µm thick cathode exhibited an extraordinary volumetric energy density of up to 408 Wh L^{-1}.

The functionalization of graphene gives rise to a change in molecular structure, which not only enhances the affinity of polysulfides but also accelerates the charge transfer kinetics. For example, by employing a template-free thermally induced expansion approach, Song et al. prepared nitrogen-doped graphene (NG) sheets with highly crumpled structures, which displayed a large surface area and a considerably high pore volume.[115] The interweaving of the NG sheets offered many nitrogen-containing active sites, which allowed strong polysulfide adsorption and high sulfur content in the NG host. The obtained NG-S composite cathode with 80 wt% sulfur loading showed an initial storage capacity of 1227 mAh g^{-1} and durable cycling stability. Meanwhile, cathodes with 5 mg cm^{-2} sulfur loading showed an areal storage capacity of 5 mAh cm^{-2}. The abundant porosities, interwoven structures, and favorable polysulfide adsorption resulting from the NG sheets, contributed to the excellent electrochemical performance.

Duan et al. synthesized N-doped graphene (rNGO) with a 3D porous framework structure via an in situ hollow cathode discharge plasma (HCD) approach.[116] As illustrated in **Figure 5**a, a GO suspension was freeze-dried to generate uniform 3D GO frameworks. With an argon and nitrogen flow treatment, these frameworks underwent synchronous reduction and N-doping by HCD, resulting in high-quality 3D rNGO. The rNGO/S composite was obtained by infiltrating the S/CS$_2$ solution into rNGO. Compared to the rGO/S composite cathode, rNGO/S exhibited better rate capability at various current densities (Figure 5b). Moreover, rNGO/S maintained a higher capacity retention than rGO/S at 1 C, achieving a steady capacity of 578 mAh g^{-1} after 1000 cycles (Figure 5c). This rNGO framework increased the charge transfer kinetics and offered highly effective interactions between nitrogen atoms and polysulfides, which minimized the polysulfide shuttling in the rNGO/S composite cathode.

Reduced graphene oxide (rGO) can offer sufficient electrode conductivity and maintain certain polarity that facilitated to confine polysulfides. Therefore, it has been considered as good sulfur hosts. Wang et al. proposed a facile approach employing amino-functionalized rGO to covalently stabilize active sulfur species.[118] Ethylenediamine (EDA) was chosen for functionalization since it offered a strong affinity of lithium sulfides and effectively prevented the loss of active mass. Density functional theory (DFT) calculations revealed high binding energies of EDA-functionalized rGO (EFG) toward lithium sulfides. The synthesized EFG-S cathode combined a steady capacity retention of up to 80% at 0.5 C within 350 cycles with excellent rate capabilities.

The combination of rGO and graphene foam (GF) has been reported by Hu et al. as sulfur host.[119] Highly conductive GF

**ADVANCED
SCIENCE NEWS**
www.advancedsciencenews.com

**ADVANCED
ENERGY
MATERIALS**
www.advenergymat.de

Figure 5. a) Schematic illustration of the fabrication of rNGO/S. b) Rate capability and c) cycling performance of rNGO/S composite cathodes. d,e) TEM images of the GN-CNT matrix. f) Prolonged cycling performance of S/GN-CNT composites. (a–c) Reproduced with permission.[116] Copyright 2019, Wiley-VCH. (d–f) Reproduced with permission.[117] Copyright 2017, Wiley-VCH.

prepared via chemical vapor deposition (CVD) acted as a substrate to assemble conductive rGO aerogels. The as-obtained 3D GF-rGO hybrid material revealed a hierarchically interconnected structure, which successfully increased the contents and areal sulfur loading in the cathode. The hierarchical network helped retain the electrolyte and effectively alleviated the volume variation of sulfur cathodes during cycling. Benefiting from the integrated merits of favorable conductivity and high host porosity, the high loading GF-rGO/S cathodes exhibited a high areal capacity of more than 10 mAh cm^{-2} with good capacity retention of over 350 cycles. Another research involved hydrothermally reduced graphene oxide (rGO) as a conductive matrix to efficiently wrap submicrometer sized sulfur particles.[120] Thiosulfate was reduced by concentrated HCl to form sulfur particles homogeneously distributed on rGO with the addition of polyvinylpyrrolidone (PVP). Evaluated as sulfur cathodes, this composite electrode displayed a reversible capacity of over 900 mAh g^{-1} at 0.2 C and more than 650 mAh g^{-1} after 100 cycles.

Graphene combined with other types of carbons, for example, CNTs, is also a promising approach to form effective

host materials for sulfur composite cathodes.[121–124] Zhang et al. employed a facile pyrolysis approach to integrate graphene nanosheets (GN) with CNTs to a unique 3D GN-CNT matrix.[117] CNTs were in situ grown on GN and revealed strong covalent bonding to GN. As shown in Figure 5d, even with the ultrasonic treatment, CNTs still adhere well to GN. The grown CNTs revealed an external and inner diameter of 38 and 32 nm, respectively (Figure 5e). The CNT density and length could be easily regulated. This 3D GN-CNT matrix had two advantages: 1) The open and porous structure offered rapid charge transfer pathways and accelerated electrolyte penetration; 2) abundant nitrogen, oxygen dopants, and cobalt nanoparticles, existing in the GN-CNT matrix, were beneficial to the immobilization of active sulfur species via chemical interaction. The resulting S/GN-CNT composite cathodes exhibited effective sulfur utilization and high capacity for more than 500 cycles. Both at 0.5 and 1 C, the cathodes revealed only a slow capacity fading (Figure 5f).

Another similar research was presented by Yang et al. Nitrogen-doped CNTs (NCNTs) were in situ grown on graphene via a nickel-catalyzed thermolysis method, synthesizing

**ADVANCED
SCIENCE NEWS**
www.advancedsciencenews.com

**ADVANCED
ENERGY
MATERIALS**
www.advenergymat.de

a NCNT-G composite.[125] The grown NCNTs indicated good chemical bonding to graphene, in which NCNTs were regularly distributed. The graphene sheets facilitated an efficient charge transfer network. In addition, the highly doped NCNTs enhanced the chemical anchoring of polysulfides. The NCNTs in combination with graphene inhibited the polysulfide shuttle effect and guaranteed a high sulfur utilization. The obtained NCNT-G/S electrode showed a highly steady storage capacity of 1484 mAh g^{-1} at 0.1 C. Even at 1 C, it still maintained 400 cycles with a capacity fading as low as 0.06% per cycle.

4.3. Carbon Nanotubes and Nanofibers

Due to their high aspect ratio and excellent conductivity, CNTs and carbon nanofibers (CNFs) can provide a high surface area for anchoring active sulfur species and create better conductive networks in the electrodes. The 1D configuration substantially enhances the electron conduction between current collectors and sulfur species. In addition, their outstanding mechanical properties are capable of mitigating the volume variation of sulfur cathodes upon cycling. These merits allow them to design and fabricate highly flexible and freestanding sulfur composite cathodes.

4.3.1. Carbon Nanotubes

Integrating CNTs with sulfur as cathodes has been considered as a promising method for better Li–S batteries.[126–128] A typical approach is to heat the mixture of sublimed sulfur and CNTs under optimized conditions, preparing sulfur composite cathodes. However, the mixing and heating method has an implicit drawback for CNTs. The inhomogeneous dispersion of sulfur particles might incur low utilization of cathode materials and inferior cycling stability.

Inspired by the sulfur solubility in CS_2, Guo et al. proposed a novel approach to impregnate disordered CNTs (DCNTs) with sulfur.[129] The dissolved sulfur in CS_2 was uniformly impregnated into the DCNT arrays. The sulfur-impregnated DCNTs (SDCNTs) were subsequently heated in a vacuum-sealed quartz tube at optimized temperatures. This method had two advantages: 1) the high-temperature heating facilitated the vaporized sulfur incorporation into DCNTs, in which the liquid electrolyte penetration was prevented; 2) S_8 molecules were broken into smaller S_6 or S_2 molecules, enabling the formation of sulfur–carbon bonds. A new charging–discharging mechanism emerged, which did not involve anymore the soluble polysulfide intermediates from the Li–S_8 reaction. The voltage curves of SDCNT obtained with the high-temperature treatment revealed that both the conversion of sulfur to S_6^{2-} and the reduction of S_6^{2-} to S_4^{2-} have almost disappeared. The CV observation also indicated a new charge transfer mechanism as represented by a new cathodic peak. The heat treatment had a critical impact on the electrochemistry of SDCNT cathodes. A 500 °C heating allowed the SDCNT cathodes to show a high capacity retention of up to 72.9% over 100 cycles at 0.25 C.
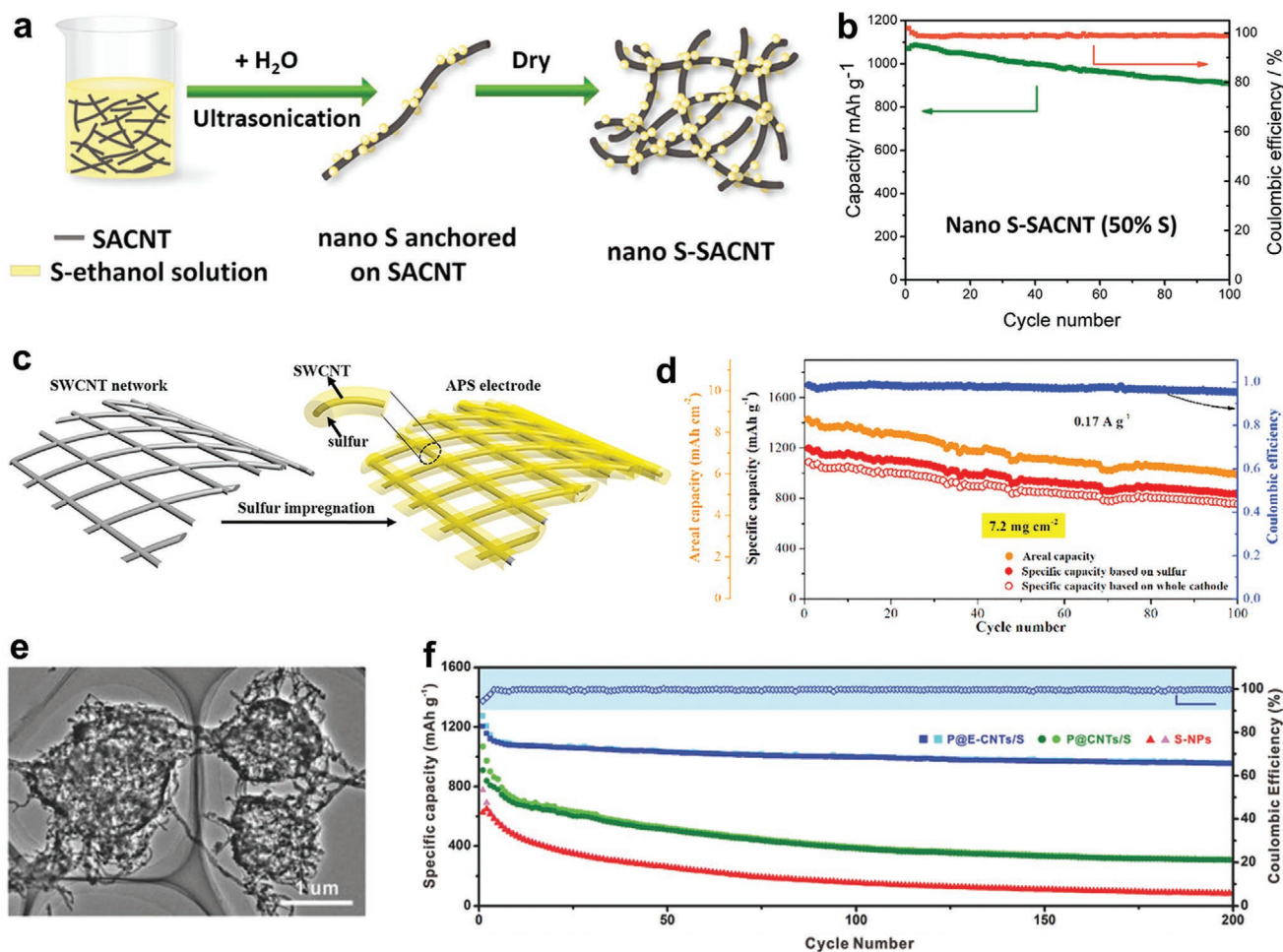
Given the excellent conductivity of CNTs, it is expected to achieve high-rate sulfur cathodes. A super-aligned CNT (SACNT)

matrix has been employed to anchor sulfur nanocrystals.[130] The SACNT exhibited a large aspect ratio of about 10^4 and intense intermolecular interactions between tubes and bundles. As illustrated in **Figure 6**a, the SACNT bundles were impregnated with a sulfur–ethanol solution. The ultrasonic dispersion induced swelling of these bundles to a continuous 3D network with highly open and porous structures. With the dropwise addition of deionized water, sulfur nanoparticles deposited uniformly on SACNT, forming a nano S-SACNT composite as a flexible and binder-free electrode after drying. Such nano S-SACNT electrodes delivered a capacity of 1071 mAh g^{-1} in the first cycle at 1 C. The corresponding capacity retention was as high as 85% over 100 cycles with nearly 100% coulombic efficiency (Figure 6b). Compared to the rigid sulfur host materials, the flexible nano SACNT enabled a more accessible network for adequate electrolyte infiltration and fast charge transfer, giving rise to the excellent electrochemical performance. The 85% capacity retention at a high current density enabled Li–S batteries with high power density.

An increase in sulfur content of the electrodes is obviously beneficial for the energy density. Aligned CNTs have therefore been employed as sulfur host by Cheng et al.[133] The authors developed a scalable, facile, and one-step ball milling strategy to fabricate the CNT/sulfur composite cathodes. Sulfur was well confined in the aligned CNTs with interconnected conductive networks. Such a strategy considerably increased the tap density of composite cathodes, implying enhanced specific capacity and energy density. The composite cathode reached 90 wt% sulfur loading with a high tap density, delivering favorable storage capacities based on the whole electrode mass. The significantly increased sulfur content was proven to be a promising alternative for aligned CNTs to practical applications. A facile bottom-up strategy has been proposed by the Zhang group to design a hierarchically freestanding CNT-S paper cathode.[134] Specifically, 15 nm wide multi-walled CNTs (MWCNTs) 10–50 μm long were chosen to host sulfur because of the short-range conductivity. Moreover, the authors also used vertically aligned CNTs (VACNTs), more than 1000 μm long, to provide long-range conductivity. The hierarchically conductive CNT networks were able to reach ultrahigh sulfur-loading up to 17.3 mg cm^{-2} through piling three CNT-S papers. This stacked cathode revealed an areal capacity of 15.1 mAh cm^{-2}. The bottom-up electrode design offered a good alternative to efficiently load active sulfur species for practical applications.

More recently, based on theoretical considerations, Fang et al. indicated that CNTs with smaller diameter revealed a high conductivity efficiency because of the shorter electron transfer distance. The authors designed a lightweight single-wall CNT (SWCNT) network with interconnected structures to host sulfur.[131] This freestanding network achieved flexible film cathodes composed of almost pure sulfur (APS), in which the sulfur content was as high as 95 wt% (Figure 6c). The interwoven SWCNT network contributed to accelerated pathways for charge transport and also allowed polysulfides confined within the cathode. Consequently, the areal sulfur loading of electrodes substantially increased to 7.2 mg cm^{-2} through a simple stacking. A high areal storage capacity of nearly 9 mAh cm^{-2} was attained with a favorable cycle life (Figure 6d).

Functional modifications of CNTs are attractive strategies to boost the utilization of sulfur. CNTs with amine

**ADVANCED
SCIENCE NEWS**

www.advancedsciencenews.com

**ADVANCED
ENERGY
MATERIALS**

www.advenergymat.de

Figure 6. a) Schematic representation of the synthesis of nano S-SACNT composites. b) Cycling performance of S-SACNT at 1 C. c) SWCNT network of an APS electrode. d) Cycling performance of 3-stacked SWCNT electrode. e) TEM image of P@E-CNT/S. f) Cycling performance of P@E-CNT/S at 0.2 C. (a,b) Reproduced with permission.[130] Copyright 2014, American Chemical Society. (c,d) Reproduced with permission.[131] Copyright 2017, Elsevier. (e,f) Reproduced with permission.[132] Copyright 2018, Wiley-VCH.

functionalization have been demonstrated to effectively promote the polysulfide immobilization. For instance, Ma et al. designed and synthesized a hybrid sulfur host consisting of CNTs covalently linked to polyethylenimine (PEI) polymers with abundant amine groups.[135] As determined by DFT analyses and spectroscopic measurements, the amine groups in the PEI chain revealed strong and covalent-like bonds with polysulfides. The authors further analyzed the polysulfide dissolution kinetics in the tetraglyme solvent by measuring the time-dependent concentration. CNT-PEI substantially decreased the dissolution rate of polysulfides into the electrolyte. Associated with the interconnected conductive CNT substrate, the composite cathodes with 70 wt% sulfur maintained a capacity of 750 mAh g^{-1} after 300 cycles at 0.5 C.

Another aminated carbon nanotubes network for sulfur host had also been employed recently. Yan et al. used EDA to modify CNT networks and then covered these with polyaniline, forming a 3D ferroconcrete-like architecture (P@E-CNT).[132] The prepared P@E-CNT/S composite preserved the initial morphology (Figure 6e). The EDA moieties were very effective to anchor the

polar discharge products at nonpolar carbon, hence efficiently preventing polysulfides from dissolving into the electrolyte. The polyaniline layers provided a favorable blocking effect on restraining polysulfides within cathodes. The authors analyzed the chemical adsorption of E-CNT toward sulfur species by DFT calculations. E-CNT revealed a strong binding energy of 1.95 eV toward Li_2S with the smallest steric hindrance, which was much stronger than pristine CNTs. The resulting P@E-CNT/S cathode exhibited a capacity of 1215 mAh g^{-1} in the first cycle at 0.2 C. A reversible storage capacity up to 975 mAh g^{-1} was attained after 200 cycles (Figure 6f). Overall, modifying nonpolar CNTs with polar components to chemically anchor sulfur species offers a desirable approach to improve Li–S batteries.

4.3.2. Carbon Nanofibers

The morphology and conductivity of CNFs are similar to those of CNTs, while CNFs possess a significantly larger diameter. Therefore, CNFs with hollow structures possess larger inner

**ADVANCED
SCIENCE NEWS**
www.advancedsciencenews.com

**ADVANCED
ENERGY
MATERIALS**
www.advenergymat.de

space to accommodate sulfur, which is beneficial to the polysulfide confinement.

Research on CNFs as a sulfur host has been reported to boost the performance of Li–S batteries.[49,136,137] For instance, the early exploration by Cui and co-workers was to encapsulate sulfur in hollow carbon nanofiber (HCF) arrays.[138] Synthesized by thermal carbonization of polystyrene on anodic aluminum oxide (AAO) templates, CNFs with high aspect ratio provided a high-quality matrix for anchoring polysulfides. Sulfur was effectively confined in the interior of CNFs, limiting the direct exposure to the electrolyte only through the two open ends. The developed HCF-encapsulated sulfur cathodes achieved high capacities for more than 150 cycles at 0.2 C. In their follow-up study, hollow CNFs modified with an amphiphilic surface were introduced to improve the cycling performance.[139] The amphiphilic surface rendered strong chemical bonding between polar polysulfides and the nonpolar carbon, effectively stabilizing the discharge products. This modification strategy enabled sulfur cathodes a capacity up to 1180 mAh g^{-1} at 0.2 C and maintained an 80% storage capacity after 300 cycles at 0.5 C.

Due to the open end morphology of CNFs, the electrolyte is inevitably in contact with active sulfur species during cycling, leading to dissolution and diffusion of polysulfides out of the cathode. Designing HCFs with closed ends would therefore be an interesting solution for this drawback. Zhang et al. reported a sulfur host of HCFs with closed ends and dynamically adjustable pore sizes.[140] By etching the SiO$_2$ layer at the surface of HCFs, the carbon network gradually stacked together and the initial mesopores in the walls were retracted to micropores. Such dynamically adjustable pore sizes eliminated the excessive exposure of sulfur species to the electrolyte, and the closed structure further blocked the polysulfide dissolution from both ends. The as-prepared S@HCF cathodes exhibited an adequate sulfur utilization of up to 98%, excellent rate capabilities at high current densities, and a high capacity of 847 mAh·g^{-1} at 2.0 C after 300 cycles with a low capacity fading of 0.055% per cycle.

The insulating nature of sulfur impedes the rate capability of sulfur cathodes. Several studies have developed CNFs with various structures to enhance the rate performance. For example, the Manthiram group synthesized multichannel carbon nanofibers (MCNF) by simple single-nozzle co-electrospinning and a KOH activation reaction (**Figure 7**a).[141] The obtained MCNF, comprising parallel mesoporous channels with interconnected microporous structures, was demonstrated to be a favorable sulfur reservoir (Figure 7b). By the KOH activation process, the produced MCNF (a-MCNF) revealed nanoscale pores and oxygen-containing groups, further enhancing the anchoring of sulfur at the CNFs. The S-a-MCNF composite cathode was loaded with 2.2 mg cm^{-2} sulfur and showed outstanding rate capabilities. Even at 5 C, an 847 mAh g^{-1} storage capacity was still attained (Figure 7c). The improvement of the rate capability was attributed to two elements: 1) mesoporous multi-channels facilitated the electrolyte to penetrate the CNFs and shortened the charge transfer pathways; 2) sulfur species were well dispersed in the micropores with the assistance of the oxygen-containing groups, resulting in firm adsorption of sulfur particles onto the CNFs.

In order to achieve a high areal capacity for practical applications, Yun et al. reported an interwoven CNF matrix as sulfur host to anchor the polysulfides.[142] Polyacrylonitrile was chosen as the precursor to produce the electrospun CNFs. The interwoven CNF structures created cross-junctions via interconnected networks. As shown in Figure 7d, sulfur particles were intertwined between the nanofibers by impregnating the heat-treated CNF sheets with 1-methyl-2-pyrrolidone and the sublimed sulfur mixture. This simple design achieved tunable sulfur loading in CNFs. On the basis of the viscosity of polysulfides, the entanglement of interwoven CNF matrices effectively adsorbed polysulfides via cohesive forces. The obtained CNF-S cathodes loaded with 4.4, 6.0, and 10.5 mg cm^{-2} exhibited favorable storage capacities and cycling stabilities (Figure 7e,f). Another example involves the preparation of hierarchically porous carbon nanofiber (HPCNF) via a simple electrospinning approach to achieve a freestanding cathode with high sulfur loading.[144] The HPCNF structure possessed macropores surrounded by micro/mesopores near the edges. The macropores accommodated a large number of sulfur species and the denser micro/mesoporous structures impeded the sulfur losses during cycling. The hierarchical architecture allowed sulfur loading of more than 12 mg cm^{-2} and significantly utilized sulfur species up to 80% with an 11.3 mAh cm^{-2} areal capacity.

Because of the nonpolar nature, CNFs have relatively weak chemical interaction with polar polysulfides. Increasing the polarity of CNFs is a promising approach to chemically anchor sulfur species. This can be achieved by doping or composition to modify the CNFs.[145,146] For instance, Li et al. integrated nickel nanoparticles with N-doped porous CNFs as sulfur host.[137] The synthesized composite host efficiently encapsulated sulfur in the network. The porous structures benefited the spatial confinement of polysulfides and shortened the charge transport pathways. Moreover, the Ni nanoparticles and nitrogen doping enhanced the chemical anchoring of polysulfides, causing favorable redox kinetics. The composite cathodes exhibited good capacities with low polarization at various current densities. At 0.2 C, a high capacity up to 1320 mAh·g^{-1} was attained.

Other approaches include the combination of the merits of CNFs and CNTs to reach advanced sulfur hosts.[147,148] For instance, Zhang et al. integrated porous CNFs with CNTs to fabricate free-standing PCNF/CNT films.[149] Such a carbon structure presented a 3D interconnected network, offering a high sulfur loading, good electrolyte penetration, and the mitigation of volume variation of cathodes. The nitrogen and oxygen doping further improved the chemical anchoring of polysulfides. The resulting S/PCNF/CNT film cathodes revealed favorable cycling stabilities and rate capabilities with 3.9 mg cm^{-2} sulfur loading. Moreover, a multi-layer stacked electrode reached a 12 mg cm^{-2} sulfur loading, exhibiting an areal capacity of nearly 11 mAh cm^{-2} after 50 cycles.

4.4. Heteroatom-Doped Carbon

Nanostructured carbon with heteroatom doping can anchor sulfur species by chemical bonding, which will boost the suppression of the shuttle effect. Heteroatom doping has been introduced to various carbon precursors, such as graphene,[115,150] CNTs,[73,151] and porous carbon.[152] Among them,
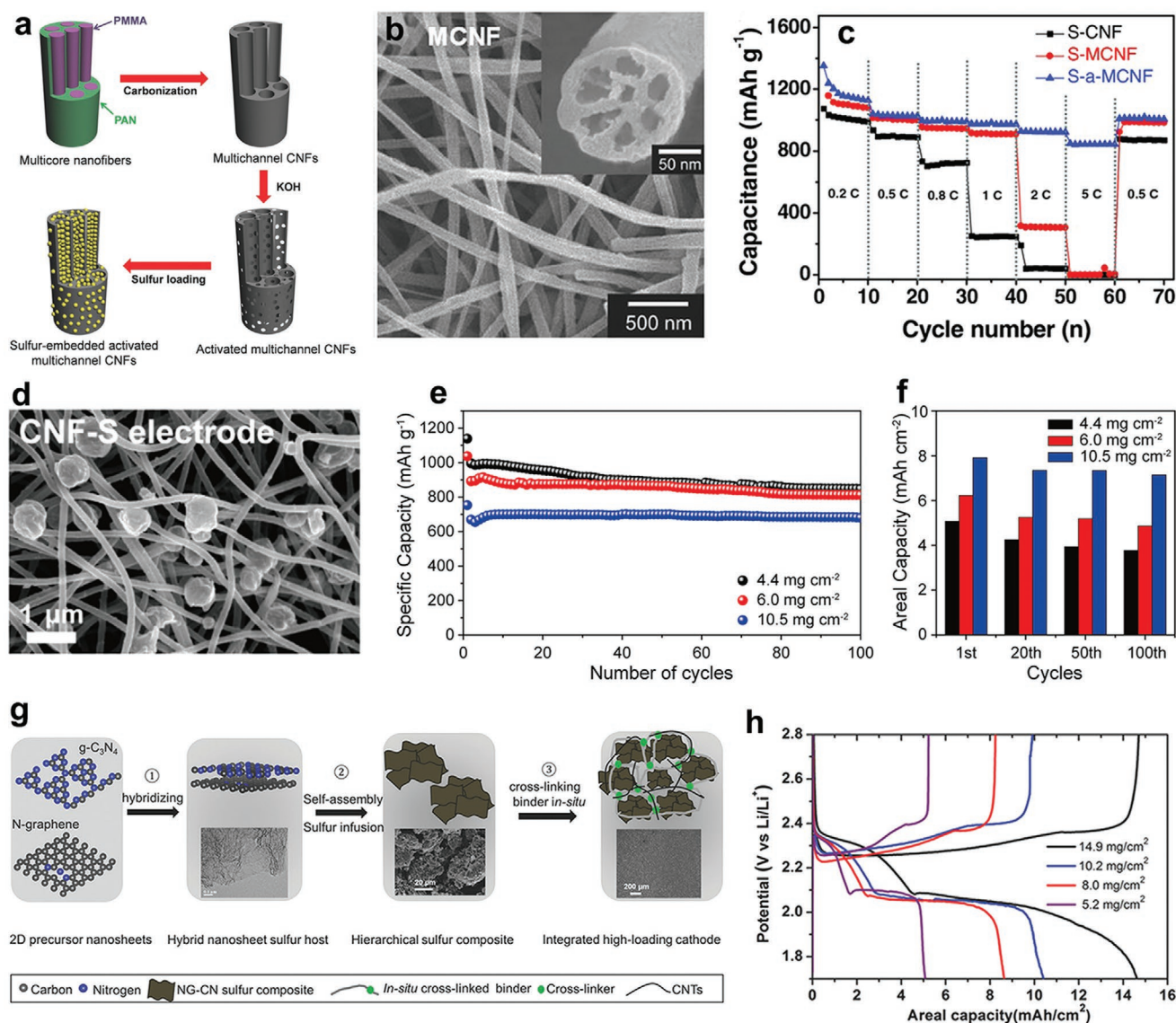
Figure 7. a) Illustration of the fabrication of S-a-MCNF. b) Low and enlarged cross-sectional (inset) SEM images of MCNF; the inset shows the microporous shell. c) Rate capabilities of S-a-MCNF. d) SEM image of CNF-S electrodes. e) Cycling performance and f) areal capacities of CNF-S electrodes with various sulfur loading. g) Concept of coupling hierarchical sulfur composite with in situ cross-linked binder to fabricate stable high-loading cathodes. h) Voltage profiles of a NG-CN/CMC-CA sulfur cathode with various sulfur loadings at 0.5 mA cm⁻². (a–c) Reproduced with permission.[141] Copyright 2017, Wiley-VCH. (d–f) Reproduced with permission.[142] Copyright 2018, American Chemical Society. (g,h) Reproduced with permission.[143] Copyright 2016, Wiley-VCH.

nitrogen doping has been proven as a promising approach. For example, a novel nitrogen and oxygen dual-doped nonporous carbonaceous material (NONPCM) was synthesized by Mi et al. to improve sulfur cathodes.[153] The polar NONPCM possessed abundant active sites to chemically confine sulfur species. XPS analyses and DFT calculations revealed that the presence of Li-N bonds significantly inhibited the polysulfide dissolution and enhanced the utilization of sulfur species. NONPCM loaded with 70 wt% sulfur exhibited a stable capacity up to 540 mAh g⁻¹ at nearly 1 C after 300 cycles. Lu et al. designed a new dodecylamine micelle-induced nitrogen-doped carbon comb (NCC) as sulfur host.[154] This nitrogen-doped NCC substantially increased the conductivity of cathodes and introduced

the chemical anchoring toward polysulfides, effectively suppressing the losses of sulfur species upon cycling. As a result, NCC with a high loading of sulfur achieved an impressive cycling lifespan and rate performance. Besides, Chen et al. grew ZIF in situ on graphene nanosheets and then converted these into nitrogen-doped porous carbon (NPC/G) by carbonization.[72] The doped nitrogen enabled the successful immobilization of polysulfides by chemical adsorption. The composite cathode achieved 1372 mAh g⁻¹ in capacity at a moderate current.

Apart from nitrogen doping, phosphorus,[76,155] boron,[151,156] and sulfur doping[150,157,158] are also advantageous to the polysulfide confinement. Wang et al. proposed a facile approach to fabricate double-shelled N and P codoped carbon spheres

**ADVANCED
SCIENCE NEWS**
www.advancedsciencenews.com

**ADVANCED
ENERGY
MATERIALS**
www.advenergymat.de

(NPDSCS), which showed good trapping for polysulfides via strong chemical affinity.[75] XPS analyses of NPDSCS-S composite cathodes revealed the formation of P—S and P—Li bonds after cycling. DFT calculations demonstrated that the binding energies of polysulfides significantly increased with the introduction of P-doping. These results validated the strong chemical interactions between NPDSCS and polysulfides. At 0.1 C, a 1326 mAh g^{-1} capacity was achieved based on an NPDSCS cathode loading of 72.4 wt% sulfur. A boron-doped porous carbon sphere/graphene hybrid (BPCS-G) was developed by Ai et al.[159] With a high boron dopant content up to 6.51 wt%, BPCS-G exhibited favorable polysulfide adsorption. The effectiveness of chemical binding polysulfides with BPCS-G was confirmed by DFT calculations. Consequently, the corresponding BPCS-G/S cathode combined a high capacity at 0.02 C with a prolonged cycling life at 0.5 C over 500 cycles with 0.05% capacity fading per cycle.

4.5. Carbon Nitride

Carbon nitride (C$_3$N$_4$) is a type of compound composed of continuous tri-s-triazine or triazine building blocks with a high ratio of nitrogen to carbon. C$_3$N$_4$ compounds have been extensively developed and investigated for energy storage and catalysis.[160] Due to the abundant polar functional groups, C$_3$N$_4$ can offer a number of anchoring sites (e.g., pyridinic N) to confine polysulfides by chemical interactions. On the other hand, the poor conductivity of C$_3$N$_4$ is detrimental to the charge transfer kinetics of sulfur cathodes. Integrating other highly conductive materials with C$_3$N$_4$ is a favorable approach to improve the utilization of sulfur species. The Nazar group initially demonstrated that a light-weight nanoporous graphitic C$_3$N$_4$ (g-C$_3$N$_4$) had superior polysulfide adsorptivity.[161] As sulfur host, g-C$_3$N$_4$ ensured an ultralow capacity loss of 0.04% per cycle during long-term cycling (1500 cycles) at 0.5 C.

In their follow-up research, they employed alternately stacked g-C$_3$N$_4$ and graphene to construct a stable cathode with high sulfur content.[143] As shown in Figure 7g, a hybridization process formed an integrated sulfur host. Sulfur was then loaded into the host via self-assembly and sulfur diffusion. With a cross-linked elastomeric binder carboxymethyl cellulose (CMC), a crack-free and compact electrode with 14.9 mg cm^{-2} sulfur loading has been obtained by traditional slurry processing. Such an integrated sulfur host enabled desirable conductivity and polysulfide anchoring, which was verified by DFT calculations and potentiostatic titration. The cross-linked CMC binder was beneficial to particle adhesion and electron transport. This comprehensive strategy enabled the electrode with an ultralow electrolyte/sulfur ratio of 3.5:1 (μL:mg). An initial areal capacity of nearly 15 mAh cm^{-2} was attained (Figure 7h). The combination of a superior graphene conductivity network and chemical adsorption of g-C$_3$N$_4$ toward polysulfides played a major role in the performance enhancement of these sulfur cathodes.

In addition to the strong affinity with polysulfides, C$_3$N$_4$ also showed a favorable influence on the charge transfer kinetics. On the basis of theoretical calculations, Liang et al. confirmed the presence of electrostatically induced strong interaction between polysulfides and polymeric C$_3$N$_4$ (p-C$_3$N$_4$).[162] They

fabricated a p-C$_3$N$_4$/graphene hybrid material to directly host the Li$_2$S$_6$ catholyte. Compared to pure graphene, p-C$_3$N$_4$/graphene contributed to good polysulfide redox stability and considerably good charge transfer kinetics. Such an effect was ascribed to the strong affinity of p-C$_3$N$_4$, which changed the steric and bonding configurations of polysulfides.

Gong et al. proposed a self-assembly method to prepare a nanocomposite composed of 3D porous C$_3$N$_4$ nanosheets and rGO (PCN@rGO).[163] The PCN has numerous polar sites, allowing chemical immobilization of polysulfides, and rGO facilitated fast electron transfer. The resulting sulfur composite electrode delivered a capacity of about 1000 mAh g^{-1} at 0.5 C, which was more or less stable up till 800 cycles. Another work involving the integration of g-C$_3$N$_4$ and porous graphene was presented by Wang and co-workers.[164] The authors introduced g-C$_3$N$_4$ into a 3D hierarchically porous graphene structure. The formed g-C$_3$N$_4$ nanosheets in the graphene network catalyzed fast polysulfide conversion, effectively enhancing the sulfur utilization. Further integration of C$_3$N$_4$ with graphene or CNTs has also been developed.[165,166]

Considering the intrinsic advantages and current achievements, nanostructured carbon host materials have tremendous potential for practical applications in Li–S batteries. On the basis of these advances, nanostructured carbon host materials used in Li–S batteries are listed in **Table 1**, presenting the latest studies of host structures and battery performance parameters for comparison.

5. Polymer Hosts

Polymers have long been considered as promising sulfur host materials, since they have the following advantages for sulfur cathodes: 1) favorable conductivity benefits the charge transfer kinetics of sulfur cathodes; 2) abundant functional groups can chemically confine active sulfur species; 3) mechanical flexibility affords the volume variation of sulfur cathodes during cycling; 4) facile synthesis conditions allow fast incorporation of sulfur. A number of studies demonstrated that polymer–sulfur composites were formed by various approaches such as coating, encapsulation, and vulcanization.

The Cui group has conducted thorough research into polymer coatings to improve sulfur cathodes.[167–169] They investigated sulfur cathodes fabricated from different polymer-coated hollow sulfur nanospheres. The results revealed that the polymer shells were able to physically confine polysulfides. The chemically bound Li$_x$S ($1 \leq x \leq 2$) to the heteroatoms from polymers substantially boosted the cycle life of sulfur cathodes. Lim et al. employed a facile surface-induced cross-linking polymerization strategy to coat a polymer on sulfur cathodes.[170] The cross-linked polymer layer was chemically anchored to the sulfur electrode by coordinated Cu ions. Such an electrode maintained an interesting storage capacity of nearly 700 mAh g^{-1} for 100 cycles at high currents.

Jia et al. synthesized Fe-doped macroporous conjugated polymers with Fe-doping as sulfur host.[171] As illustrated in **Figure 8**a, poly(3-hexylthiophene) (P3HT) was in situ grown on RGO sheets. Then, a gelation process in p-xylene followed by freeze-drying formed macroporous conjugated polymers

**ADVANCED
SCIENCE NEWS**

www.advancedsciencenews.com

**ADVANCED
ENERGY
MATERIALS**

www.advenergymat.de

Table 1. Summary of performance parameters for nanostructured carbon host materials used in Li–S batteries.

| Host material	Sulfur content [wt%][a]	Sulfur loading [mg cm⁻²]	Voltage range [V]	Rate [C][b]	Cycle number	Initial capacity [mAh g⁻¹]	Retained capacity [mAh g⁻¹]	Ref.
CNT@MPC	32	1.0	1.0–3.0	0.1	200	1670	1142	[103]
UMC	32	1.0	1.0–3.0	1.0	100	≈1000[c]	510	[105]
2D OMCNS	49	1.1–1.2	1.7–2.8	0.5	500	N/A	505	[109]
POF-HS	52.2	1.1	1.8–2.8	0.5	200	955	773	[106]
PRC/Ni	60.9	2.0	1.7–2.8	0.2	500	1257	813	[46]
Carbon microspheres	48	0.3–0.5	1.7–2.8	2.0	2000	728	449	[102]
G@HMCN	73	5.0	1.7–2.8	1.0	500	900	719	[107]
IBGM	43.2	5.6	1.5–3.0	0.5	500	714	379	[114]
rNGO	56	1.2	1.5–3.0	1.0	1000	≈970[c]	578	[116]
GF-rGO	83	9.8	1.5–2.8	0.2	350	1000	645	[119]
rGO-PVP	68	1.3–1.6	1.7–2.6	0.2	100	1021	631	[120]
GO-CNT	70	4.0	1.7–2.6	0.1	500	≈650[c]	500	[124]
GN-CNT	53.5	1.3–1.6	1.7–2.8	0.5	500	758[d]	464[d]	[117]
NCNT-G	49	1.4–1.8	1.5–3.0	1.0	400	835	635	[125]
CNT paper	54	6.3	1.7–2.8	0.05	150	995	700	[134]
SWCNT	95	7.2	1.8–2.8	0.17 (A g⁻¹)	100	≈1200[c]	≈850[e]	[131]
E-CNT	57.6	2.0	1.4–2.8	0.2	200	1215	975	[132]
a-MCNF	64	4.6	1.8–2.8	0.5	200	990	753	[141]
CNF	79	10.5	1.6–2.9	0.1	100	753	680	[142]
HPCNF	56	12.1	1.7–2.8	0.2	100	943	N/A	[144]
PCNF/CNT	62	12	1.7–2.8	0.6 (mA cm⁻²)	50	1126	≈900[e]	[149]
N-doped CNTs embedded with Co nanoparticles	64	1.84	1.7–2.8	1.0	400	N/A	700	[73]
NPDSCS	58	5.8	1.5–3.0	1.0	500	952	814	[75]
Co-embedded N, P-doped porous carbon	56	0.8-1.0	1.7–2.8	5.0	400	480	411	[152]
NONPCM	52.5	1.39	1.5–3.0	1.6 (A g⁻¹)	300	654	540	[153]
BPCS-G	49	1.0–1.3	1.8–2.8	0.5	500	740	555	[159]
NG/g-C₃N₄ hybrid	65.5	2.0	1.7–2.8	0.5	100	≈1100[c]	N/A	[143]
PCN@rGO	55	4.0	1.7–2.8	0.1	200	1025	720	[163]
rGO/g-C₃N₄/CNT	56.6	4.2	1.7–2.8	0.2	300	1017	712	[166]

[a] Sulfur content in cathodes; [b] 1 C ≈ 1675 mA g⁻¹; [c] Initial; [d] Capacity with respect to composites; [e] Retained capacity estimated from the figure as the specific value was not given in the reference.

(RGO-g-P3HT). The macroporous RGO-g-P3HT hosts possessed a high pore volume up to 34 cm³ g⁻¹ with tunable porosities, ensuring excellent encapsulation of sulfur. DFT calculations demonstrated the enhanced interaction between the P3HT frameworks and polysulfides with the incorporation of Fe (Figure 8b). The sulfur composite cathode with Fe-doping exhibited enhanced capacities and cycling stabilities, indicating that Fe-doping accelerated the charge transfer kinetics of sulfur cathodes and hence inhibited the shuttle problem of polysulfides.

The main-chain imidazolium-based ionic polymer (ImIP) has also been introduced as sulfur host materials by Cheng et al.[174] It was demonstrated to be efficient for anchoring polysulfides. Due to the electrostatic interactions between polysulfides and ImIP, the polysulfide shuttling was

significantly inhibited and the charge transport was also accelerated. Such a novel anchoring approach of polysulfides allowed sulfur cathodes with good reversible capacities and durable cycle life.

By means of vulcanization, Park and co-workers synthesized sulfur-rich polymers with 3D interconnected networks as cathode active materials.[175] The authors proposed a soft template preparation, starting from porous trithiocyanuric acid (TTCA) crystals. The TTCA template was initially vulcanized at 160 °C in a sealed vessel to encapsulate sulfur in the pores. A thermal treatment at 245 °C resulted in the sulfur ring opening and subsequent polymerization at the thiol surfaces, generating 3D interconnected sulfur-rich polymers. This vulcanization approach was facile to synthesize organosulfur compounds with tunable morphology. The cathodes with sulfur-rich
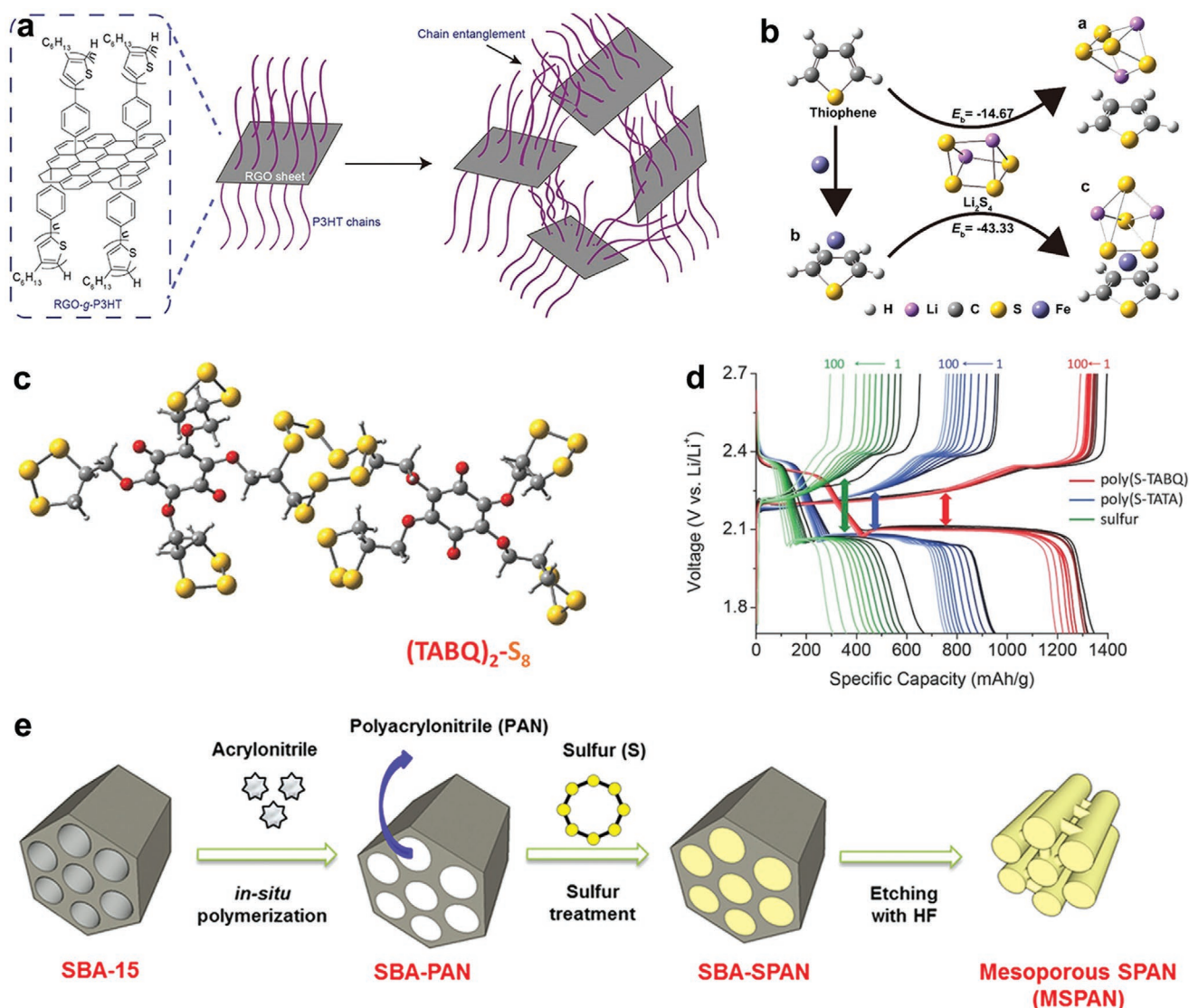
Figure 8. a) Chemical structure of an RGO-g-P3HT sheet and schematic representation of the gelation via physical cross-linking between P3HT chains. b) Enhanced binding by Fe atoms between polysulfides and P3HT frameworks. c) Conformations of TABQ dimers with optimized geometries. d) Voltage profiles of the cells based on poly(S-TABQ). e) Illustration of the fabrication for MSPAN composites. (a,b) Reproduced with permission.[171] Copyright 2019, American Chemical Society. (c,d) Reproduced with permission.[172] Copyright 2018, Wiley-VCH. (e) Reproduced with permission.[173] Copyright 2017, American Chemical Society.

polymers achieved a high storage capacity of 850 mAh g^{-1} with 83% capacity retention after 450 cycles. A strong rate capability was attained at 5 C with a reversible capacity of up to 730 mAh g^{-1}. The enhanced performance was obtained from the complete anchoring of polysulfide intermediates onto the vulcanized polymers and the fast charge transport facilitated by the amine groups of TTCA frameworks. In their follow-up research, sulfur-rich polymers synthesized from different functional linkers were reported.[172] The authors prepared these sulfur-rich polymers from four ligands with quinone and triazine structures. The results revealed that the tetra(allyloxy)-1,4-benzoquinone (TABQ) ligand (Figure 8c) allowed the sulfur cathode to significantly increase the conductivity by about 450 times. Furthermore, the corresponding redox kinetics also enhanced twofold. Benefiting from these improvements, the

prepared poly(S-TABQ) cathodes exhibited an excellent capacity of 1346 mAh g^{-1} in the first cycle and maintained steady for over 100 cycles at 0.1 C (Figure 8d). Even at an ultrahigh 10 C-rate, poly(S-TABQ) still reached 833 mAh g^{-1} in capacity. The introduction of TABQ resulted in a homogeneous sulfur distribution and facilitated charge transport in the sulfur-rich polymers frameworks. Associated with the polar anchoring of TABQ, poly(S-TABQ) attained a considerable increase in electrochemical performance.

Vulcanization or sulfurization results in the covalent binding of sulfur onto the polymer surface via C—S bonds, which might change the (dis)charging mechanism of sulfur cathodes. Some of the studies confirmed that sulfurized polymers by the high-temperature process showed only a single sloping voltage plateau near 2 V with a significant voltage hysteresis.[95,176,177]

**ADVANCED
SCIENCE NEWS**

www.advancedsciencenews.com

**ADVANCED
ENERGY
MATERIALS**

www.advenergymat.de

This is mainly because short sulfur chains are generated at high temperatures, eliminating the conversion from S_8 molecules to soluble long-chain polysulfide intermediates during cycling. For instance, Liu et al. employed SBA-15 with ordered mesoporous structures as a template to prepare mesoporous sulfurized polyacrylonitrile (MSPAN).[173] As schematically shown in Figure 8e, an in situ polymerization process produced the SBA-PAN composite. Followed by direct sulfurization, sulfur was incorporated into PAN. The resulting MSPAN composite was achieved by the HF etching to remove the SBA-15 template. MSPAN with highly ordered mesopores revealed a large surface area, hence improving the electrolyte impregnation and charge transport. MSPAN cathodes displayed a distinct reaction mechanism in the CV curves, only revealing a broad cathodic peak below 2.0 V. This CV result indicates that no polysulfides were produced since active sulfur species mainly existed in the form of S_3 or S_2 chains covalently bound to the PAN backbone. Besides, Tsao et al. coated sulfur by aniline polymerization.[178] The obtained sulfur@polyaniline (S@P) then convert into vulcanized polymers (S@h-P) via a facile thermal treatment. S@h-P exhibited cross-linked networks with abundant covalently bound sulfur. Due to the complete elimination of the polysulfide shuttling, the S@h-P cathode exhibited satisfactory cycling stabilities and desirable rate performance.

Overall, polymers applied as host materials can confine sulfur species via three different approaches: 1) similar to carbon-based materials, the facile tuning of structures allows polymers as desirable barriers to physically block polysulfides; 2) the presence of abundant surface groups further enhances the polysulfide anchoring via chemical anchoring; 3) the covalent bonding of polymers gives rise to a distinct anchoring mechanism of sulfur species from other confinement approaches. The intrinsic merits of polymer materials considerably broaden the design and understanding of sulfur host electrodes. A summary of performance parameters for polymer host materials used in Li–S batteries is listed in **Table 2**.

6. Metal Compound Hosts

Various polar metal compounds possess strong chemical interactions with polysulfides. Compared with non-polar carbon, such polar host materials reveal much stronger chemical anchoring of polysulfides. They can mitigate the polysulfide loss and improve sulfur utilization. On the other hand, the poor conductivity of some metal compounds restricts the rate capability of these sulfur cathodes. Metal compounds are therefore often combined with highly conductive carbon materials.

6.1. Metal Oxides

Extensive investigations have been carried out to explore the chemical anchoring of metal oxides toward polysulfides. Metal oxides have a strong polar surface due to the presence of oxygen anions. As a result of the abundant polar active sites for the polysulfide adsorption, polar metal oxide hosts substantially promote the electrochemistry of sulfur cathodes.

6.1.1. Titanium-Based Oxides

The use of titanium dioxide (TiO_2) as sulfur host has been extensively reported. The early work has been investigated by Seh et al., employing TiO_2 as shells to alleviate the cathode volume swelling caused by the lithiation process.[179] The authors covered a sulfur core with TiO_2 layers to form a yolk–shell structure, which successfully maintained the integral shell upon cycling for inhibiting the polysulfide dissolution. Various TiO_2 morphologies have been developed to confine polysulfides, such as spheres, nanotubes, and nanosheets.

Using the electrospinning technique with subsequent heat treatment, Qian et al. prepared mesoporous TiO_2 nanotubes (MTDNTs) as sulfur hosts.[180] The MTDNTs with anatase

Table 2. Summary of performance parameters for polymer host materials used in Li–S batteries.

Host material	Sulfur content [wt%][a]	Sulfur loading [mg cm^{-2}]	Voltage range [V]	Rate [C][b]	Cycle number	Initial capacity [mAh g^{-1}]	Retained capacity [mAh g^{-1}]	Ref.
PEDOT:PSS-coated CMK-3	43	1.0	1.7–2.6	0.2	150	1140	600	[167]
PVP	49	1.0	1.5–2.6	0.5	1000	≈750[c]	535	[168]
Chemically anchored polymer	50	N/A	1.8–2.6	2.0	100	N/A	665	[170]
RGO-g-P3HT	49	1.0	1.5–3.0	0.1	100	1103	780	[171]
ImIP	38.4	4.2	1.5–3.0	1.06 (mA cm^{-2})	120	1131	914	[174]
TTCA	45	0.8	1.7–2.7	0.5	300	1050[c]	886	[175]
TABQ	45	1.2-2.5	1.7–2.7	0.1	400	1346	911	[172]
TABQ	45	1.2-2.5	1.7–2.7	1.0	500	1077	772	[172]
carbonized PAN	36	3.0	1.5–3.0	0.5	100	1500	735	[177]
MSPAN	37	2.45	1.0–3.0	2.0	900	717	610	[173]
Polyaniline	N/A	N/A	1.0–3.0	1.0 (A g^{-1})	300	≈500[c]	312	[178]

[a]Sulfur content in cathodes; [b]1 C ≈ 1675 mA g^{-1}; [c]Initial capacity estimated from the figure as the specific value was not given in the reference.
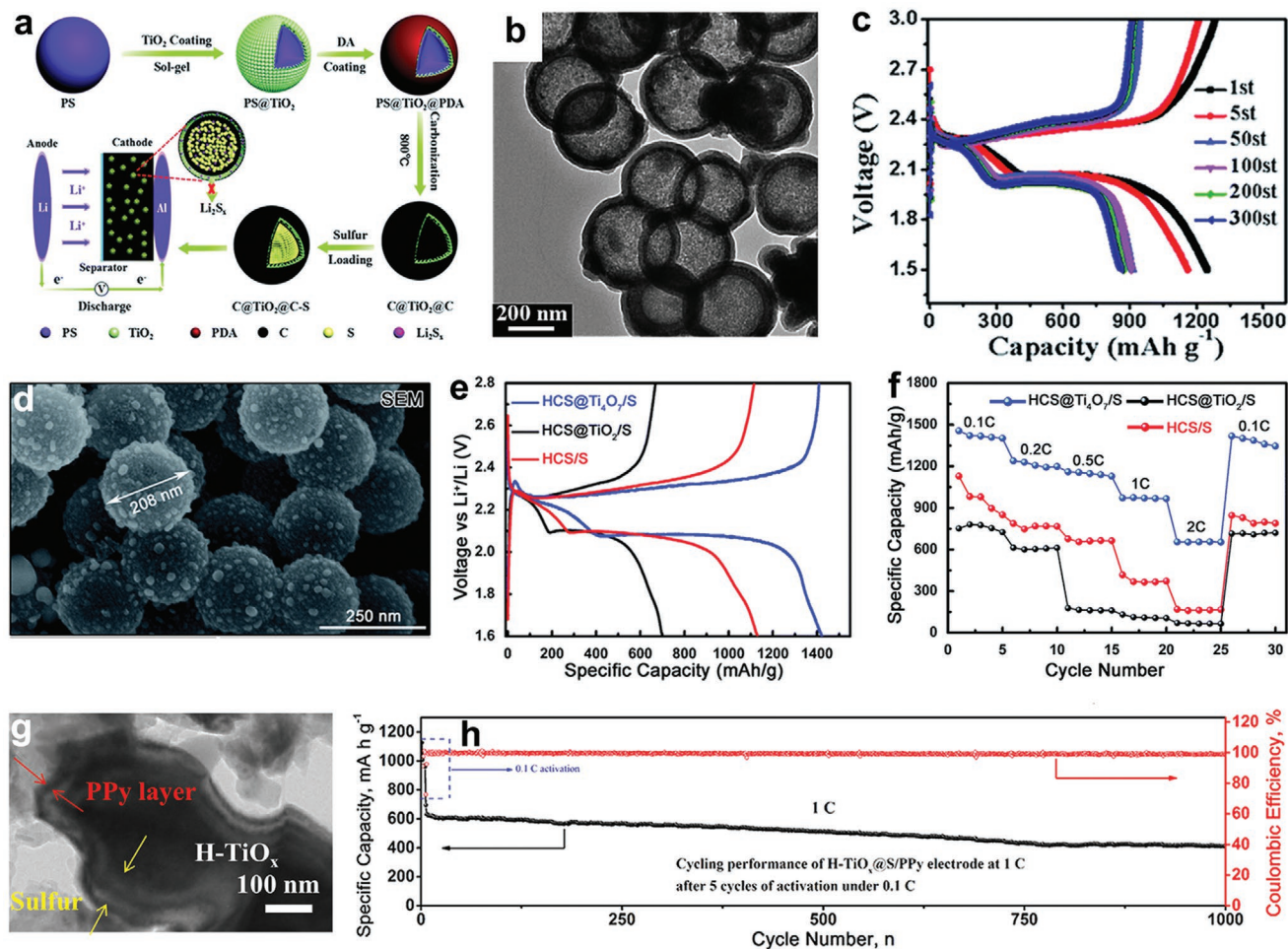
Figure 9. a) Schematic illustration of the preparation of sandwich-type C@TiO$_2$@C-S microspheres. b) TEM image of sandwich-type C@TiO$_2$@C hollow microspheres. c) Voltage profiles of a C@TiO$_2$@C-S cathode at various cycles at 0.2 C. d) SEM image of HCS@Ti$_4$O$_7$. e) Voltage profiles and f) rate performance of HCS@Ti$_4$O$_7$/S. g) TEM image of sandwich-type H-TiO$_x$@S/PPy composites. h) Cycling performance of H-TiO$_x$@S/PPy cathodes. (a–c) Reproduced with permission.[184] Copyright 2018, Royal Society of Chemistry. (d–f) Reproduced with permission.[186] Copyright 2019, Royal Society of Chemistry. (g,h) Reproduced with permission.[187] Copyright 2019, American Chemical Society.

crystal structures combined a hollow morphology with a high surface area of about 100 m^2 g^{-1}. Sulfur was encapsulated in MTDNTs by mixing MTDNTs with a sulfur/CS$_2$ solution to get MTDNT/S composites. TEM and SEM analyses indicated the uniform distribution of sulfur in the mesopores of the as-prepared MTDNT walls. Combined with the fast Li$^+$ transfer facilitated by the hollow structure, the MTDNT/S composite cathodes exhibited desirable cycling stabilities and good rate performance. Even at 8 C, the reversible capacity still reached 610 mAh g^{-1}. Ni et al. introduced mesoporous hollow TiO$_2$ microboxes to improve Li–S batteries.[181] CaTiO$_3$ precursors were employed to synthesize the TiO$_2$ microboxes by a two-step solvothermal reaction. The authors validated that the TiO$_2$/S composite with 70 wt% sulfur showed the optimal electrochemical performance. Ultraviolet–visible spectroscopy (UV–vis) analyses of Li$_2$S$_4$ revealed an efficient polysulfide anchoring by TiO$_2$ microboxes. More recently, Wang et al. investigated oxygen-deficient TiO$_2$ as novel sulfur host.[182] Based on experimental observations and DFT calculations, they found that the oxygen vacancies boosted the polysulfide adsorption by TiO$_2$,

reducing the shuttle effect. In addition, the oxygen vacancies accelerated the charge transfer at the vacancy-enriched electrode surface, hence catalyzing the electrochemical conversion of active sulfur species. The TiO$_2$/S composite cathode delivered high capacities, outstanding rate capabilities, and desirable cycling stabilities.

Combining carbon with TiO$_2$ in sulfur cathodes is beneficial to the electrochemical charge transfer kinetics.[79,183] Yu et al. deposited atomic TiO$_2$ layers on a sulfur cathode constructed from nitrogen-doped graphene (NG).[62] The performance of these composite cathodes was substantially enhanced due to the on-site polysulfide absorption of TiO$_2$ and the accelerated charge transfer. The TiO$_2$ layers in combination with NG offer combined effects: increasing the conductivity of cathodes and alleviating the polysulfide migration. An initial capacity of 1069 mAh g^{-1} at 1 C was reached and showed a capacity retention up to 86% over 500 cycles.

C@TiO$_2$@C hollow microspheres with sandwich structures have been designed as sulfur host to physically and chemically confine polysulfides.[184] As illustrated in **Figure 9**a, TiO$_2$ layers

**ADVANCED
SCIENCE NEWS**
www.advancedsciencenews.com

**ADVANCED
ENERGY
MATERIALS**
www.advenergymat.de

were initially coated on PS microspheres using a sol–gel process. PS@TiO₂ was further covered with a layer of homogenous polydopamine (PDA). Upon carbonization, the final sandwich hollow microspheres were obtained. The TiO₂ layers enabled effective chemical anchoring for polysulfides, while the two carbon shells allowed adequate charge transport pathways and also acted as physical barriers to spatially restrain the movement of polysulfides. Moreover, the hollow cavity structure (Figure 9b) alleviated the volumetric change of sulfur cathodes during (de)lithiation. Such a designed C@TiO₂@C-S host material achieved a high sulfur loading of 76.4 wt%, delivering a high storage capacity of more than 1200 mAh g⁻¹ at 0.2 C (Figure 9c). In addition, TiO₂ nanoparticles were also introduced into a porous carbon matrix. A 3D-ordered macro/mesoporous carbon (3DOMC) was in this way designed by Liang et al. to be a support of TiO₂.[185] The TiO₂/3DOMC exhibited a desirable specific surface area with a large pore volume, indicating a high sulfur loading of more than 73 wt%. The incorporation of TiO₂ nanoparticles successfully inhibited the polysulfide shuttling by their strong electrostatic interaction with polysulfides.

In view of the regular oxygen vacancies in the lattice, the Ti₄O₇ Magnéli phase has been proven high conductivity. The strong adsorption of polysulfides associated with a high conductivity allows Ti₄O₇ to be an effective sulfur host.[78,188,189] Wei et al. prepared mesoporous Magnéli Ti₄O₇ microspheres by an in situ carbonization process to improve the performance of sulfur cathodes.[190] These synthesized Ti₄O₇ microspheres revealed interconnected mesopores with large surface area and pore volume. XPS characterization indicated that the Ti₄O₇ surface formed Ti—S bonding with polysulfides, which enhanced the chemical anchoring with active species. Consequently, the high conductivity of the Magnéli microspheres in combination with the favorable polysulfide anchoring contributed to an improved utilization of these composite cathodes. A high initial capacity of 1317.6 mAh g⁻¹ was attained at 0.1 C.

A similar carbonization reduction process was employed by Wang et al. to introduce Ti₄O₇ nanoparticles on the HCSs.[186] Monodispersed HCS acted as a hard template to coat the TiO₂ shells. Then, the obtained HCS@TiO₂ was covered with another PDA shell. Upon carbonization at high temperatures, TiO₂ was transformed into Ti₄O₇. The grain growth of Ti₄O₇ was restrained by the PDA shells, resulting in Ti₄O₇ nanoparticles with small size and uniform morphology (Figure 9d). The uniformly distributed Ti₄O₇ nanoparticles offered abundant adsorption sites to chemically anchor polysulfides. Compared with the HCS@TiO₂/S and HCS/S electrodes, the HCS@Ti₄O₇/S electrodes showed the smallest electrochemical polarization and highest capacity (Figure 9e). A very high storage capacity of 1421 mAh g⁻¹ at 0.1 C was achieved. Moreover, HCS@Ti₄O₇/S also exhibited significantly enhanced rate capabilities (Figure 9f).

TiO also exhibits excellent conductivity because of the high oxygen and titanium vacancies. The Lou group developed TiO@C hollow spheres to improve sulfur cathodes.[191] These host materials combine a high conductivity with strong polysulfide adsorption. High sulfur content could be loaded into the cavity of the hollow spheres. The polar TiO shell maximized the polysulfide diffusion and enhanced the redox reaction kinetics of sulfur. Further development in their subsequent research demonstrated that the tight packing of the carbon-coated TiO

hollow nanospheres resulted in interconnected microsized clusters, which achieved significantly higher sulfur loadings.[192] The as-obtained hierarchically structured sulfur cathodes revealed high capacities at various current densities.

Chen et al. integrated conductive polypyrrole (PPy) with heterostructured TiOₓ (H-TiOₓ, x = 1, 2) material to assemble multifunctional sulfur hosts.[187] H-TiOₓ was synthesized from the TiO₂ nanoparticle precursors via thermal reduction followed by acid etching. After sulfur loading, the obtained H-TiOₓ@S was further covered with PPy shells. The prepared H-TiOₓ@S/PPy composite revealed a sandwich-type of morphology (Figure 9g). The internal H-TiOₓ with Lewis acid properties was capable of anchoring polysulfides via chemical bonding. The external PPy shell physically blocked polysulfides and also formed polar interactions via N—Li bonds. The multifunctional merits of H-TiOₓ and PPy contributed to an adequate suppression of polysulfide diffusion and improved the electrochemical charge transfer kinetics. Consequently, the H-TiOₓ@S/PPy composite cathode exhibited a very low capacity fading of only 0.04% per cycle over 1000 cycles at 1 C (Figure 9h).

6.1.2. Manganese-Based Oxides

Incorporating sulfur into manganese-based oxide host materials has recently become a promising approach to anchor sulfur species. Among them, MnO₂ has been extensively investigated.[65,89,193,194] For instance, Wang et al. proposed an innovative design of MnO₂ nanosheet-decorated hollow sulfur spheres (hollow S-MnO₂), which efficiently anchored polysulfides.[195] As shown in **Figure 10**a, a bottom-up strategy was initially used to prepare almost monodisperse, PVP-encapsulated, hollow sulfur spheres. KMnO₄ was subsequently introduced to react with PVP, generating dense MnO₂ nanosheets covering the hollow spheres. After removing the extra PVP, hollow S-MnO₂ spheres with crumpled shells were obtained. The resulting hollow S-MnO₂ cathodes showed a 644 mAh g⁻¹ storage capacity after 1500 cycles at 0.5 C with only 0.028% capacity decay per cycle, demonstrating good utilization of active sulfur species (Figure 10b). XPS analyses revealed the interactions between MnO₂ nanosheets and polysulfides. In contrast to the pure MnO₂, the Mn²⁺ contribution from the Mn 2p₃/₂ spectrum of S-MnO₂ indicated a significant increase, implying the partial reduction of MnO₂. The accompanied Li₂S₄ oxidation was also identified from the S2p spectra. Such redox interactions between MnO₂ and polysulfides substantially enhanced the chemical anchoring of sulfur species. DFT calculations further confirmed that the binding energies of S₈, Li₂S₈, Li₂S₆, Li₂S₄, Li₂S₂, and Li₂S with a δ-MnO₂ nanosheet (100) surface increased from 1.60 to 5.15 eV. These strong bonding energies mainly resulted from the formation of Li—O and S=O bonds.

Although the strong chemical binding of δ-MnO₂ nanosheets with polysulfides can substantially decrease the loss of sulfur species, the conductivity of S-MnO₂ composite electrodes is rather poor. Employing a carbon-coated metal oxide nanoboxes strategy, Rehman et al. covered birnessite-type MnO₂ nanosheets with hollow carbon nanoboxes (HCB) to physically and chemically trap polysulfides.[196] The MnCO₃ nanocubes acted as templates to coat thick SiO₂ layers. Then, a thin polymer
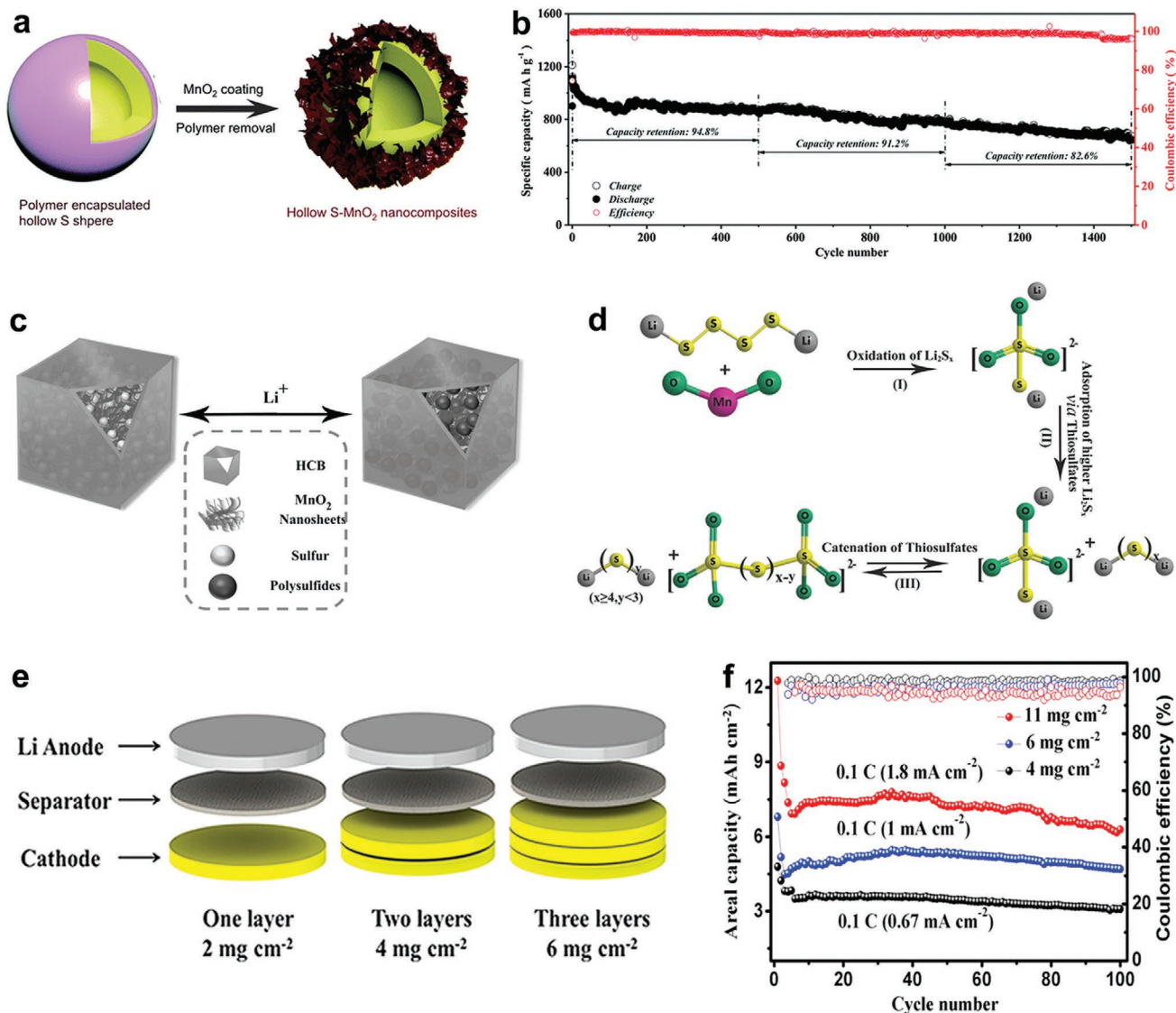
Figure 10. a) Schematic representation of the synthetic process and b) prolonged cycling stability of S-MnO₂ at 0.5 C. c) A reversible electrochemical reaction mechanism of polysulfides retention via MnO₂@HCB/S hybrid nanoboxes. d) Schematic illustration of polysulfide adsorption via MnO₂. e) Enhanced cathode thickness by stacking individual layers. f) Areal capacities of electrodes with different sulfur areal loadings at 0.1 C. (a,b) Reproduced with permission.[195] Copyright 2016, Royal Society of Chemistry. (c,d) Reproduced with permission.[196] Copyright 2017, Wiley-VCH. (e,f) Reproduced with permission.[197] Copyright 2018, American Chemical Society.

coating formed the carbon shells. MnO₂@HCB nanoboxes were prepared via carbonization and SiO₂ elimination. Figure 10c illustrates the structural advantages of these nanoboxes to be applied as sulfur cathodes: 1) the MnO₂ nanosheets with strong chemical bonds restrained polysulfides inside the cavities; 2) HCB enabled a high sulfur content, alleviated the volume swelling of cathodes, and physically restricted polysulfides from migrating out of the nanoboxes; 3) the hierarchically porous carbon layer facilitated the charge transfer kinetics. The authors proposed an anchoring mechanism of polysulfides to the sulfur host as shown in Figure 10d. MnO₂ nanosheets initially in situ oxidized the polysulfides, generating the thiosulfate groups (see reaction step I). Subsequently, the produced polysulfides (step II) were adsorbed by the thiosulfates and converted into

polythionate complexes, which mediated the transformation of polysulfides (step III). Hence, the polythionate complexes had a major effect on the polysulfide mediation and anchoring. The prepared MnO₂@HCB/S composite delivered a significant capacity up to 1042 mAh g⁻¹ at 1 A g⁻¹.

Besides MnO₂, MnO and Mn₃O₄ also have been introduced as sulfur host materials.[198–200] Liu et al. developed MnO nanoparticles to anchor polysulfides.[201] The authors incorporated MnO nanoparticles in micro-mesoporous carbon (MPC), preparing MnO/MPC composites. Because of the intrinsic polarity, MnO nanoparticles significantly anchored polysulfides within the cathodes. Moreover, the deposition of insoluble Li₂S₂ and Li₂S during the discharge process attained substantial improvement, which accelerated the electrochemical charge transfer

**ADVANCED
SCIENCE NEWS**

www.advancedsciencenews.com

**ADVANCED
ENERGY
MATERIALS**

www.advenergymat.de

kinetics. The resulting MnO/MPC@S cathode with 74% sulfur content exhibited increased specific capacities and capacity retention within 150 cycles in comparison to sulfur cathodes without using MnO.

Chen et al. designed a free-standing paper cathode with a layer-by-layer structure.[197] Such a cathode was composed of Mn_3O_4 nanoparticles embedded in nitrogen-doped CNFs with 3D interconnected structures. The authors started the fabrication from electrospun nanofibers. Subsequent carbonization and base etching resulted in the formation of Mn_3O_4@CNF paper composites. By direct stacking the Mn_3O_4@CNF/S layers, the areal sulfur loading can be readily tunable (Figure 10e). On the basis of this approach, the authors investigated the Mn_3O_4@CNF/S cathodes with sulfur loading of 4, 6, and 11 mg cm^{-2}. As shown in Figure 10f, the corresponding cathodes delivered a high initial areal capacity of 5 to 12 mAh cm^{-2} and a favorable capacity retention after 100 cycles. The interconnected CNF network enabled sulfur cathodes to create favorable charge transport pathways. The polysulfide shuttle problem was mostly alleviated by both physical confinement and chemical anchoring to CNF and Mn_3O_4.

6.1.3. Cobalt-Based Oxides

Cobalt-based oxides have been proven excellent electrocatalytic properties, which have been widely investigated for the oxygen reduction and oxygen evolution reaction.[202,203] Using cobalt-based oxides as sulfur hosts has also been reported.[204–206] Derived from ZIF-67 crystals, Xu et al. fabricated a nitrogen-doped Co_3O_4 embedded in nitrogen-doped carbon polyhedrons via simple pyrolysis. With further graphene coating, a nanododecahedral composite was achieved (N-Co_3O_4@N-C/rGO).[207] The synthesized N-Co_3O_4@N-C/rGO possessed well-defined porous structures (**Figure 11**a), desirable conductivities, and special chemical adsorption. As a sulfur host, N-Co_3O_4@N-C/rGO enabled a high sulfur loading, hence achieving a good rate capability of 652 mAh g^{-1} even up to 3 C (Figure 11b). Ex situ Raman spectra verified the strong adsorption of N-Co_3O_4@N-C/rGO toward polysulfides. When the battery was discharged down to 2.1 V for 300 cycles, S_6^{2-} and S_8^{2-} were detected in the N-Co_3O_4@N-C/rGO-S electrode by means of Raman spectroscopy, while the pristine cathode before cycling did not reveal any S_6^{2-} and S_8^{2-} peaks (Figure 11c). Furthermore, first-principle calculations indicated that the favorable chemical bond between polysulfides and Co_3O_4 was causing significantly stronger adsorption energies than rGO. These results demonstrated that Co_3O_4 nanocrystals significantly enhanced the polysulfide anchoring.

Combining carbon with Co_3O_4 leads to better electrochemical charge transfer kinetics. Recently, our group reported carbon-coated Co_3O_4 (Co_3O_4/C) double-shelled nanocages as sulfur host.[58] As illustrated in Figure 11d, the ZIF-67 sacrificial template was transformed into hollow nanocages of layered double hydroxides (LDHs), followed by a PDA layer to form double-shelled LDH/PDA nanocages. Then annealing resulted in the formation of Co_3O_4/C double-shelled nanocages (Figure 11e). The as-prepared S@Co_3O_4/C cathodes exhibited a high capacity at 0.2 C (Figure 11f). Furthermore, it achieved
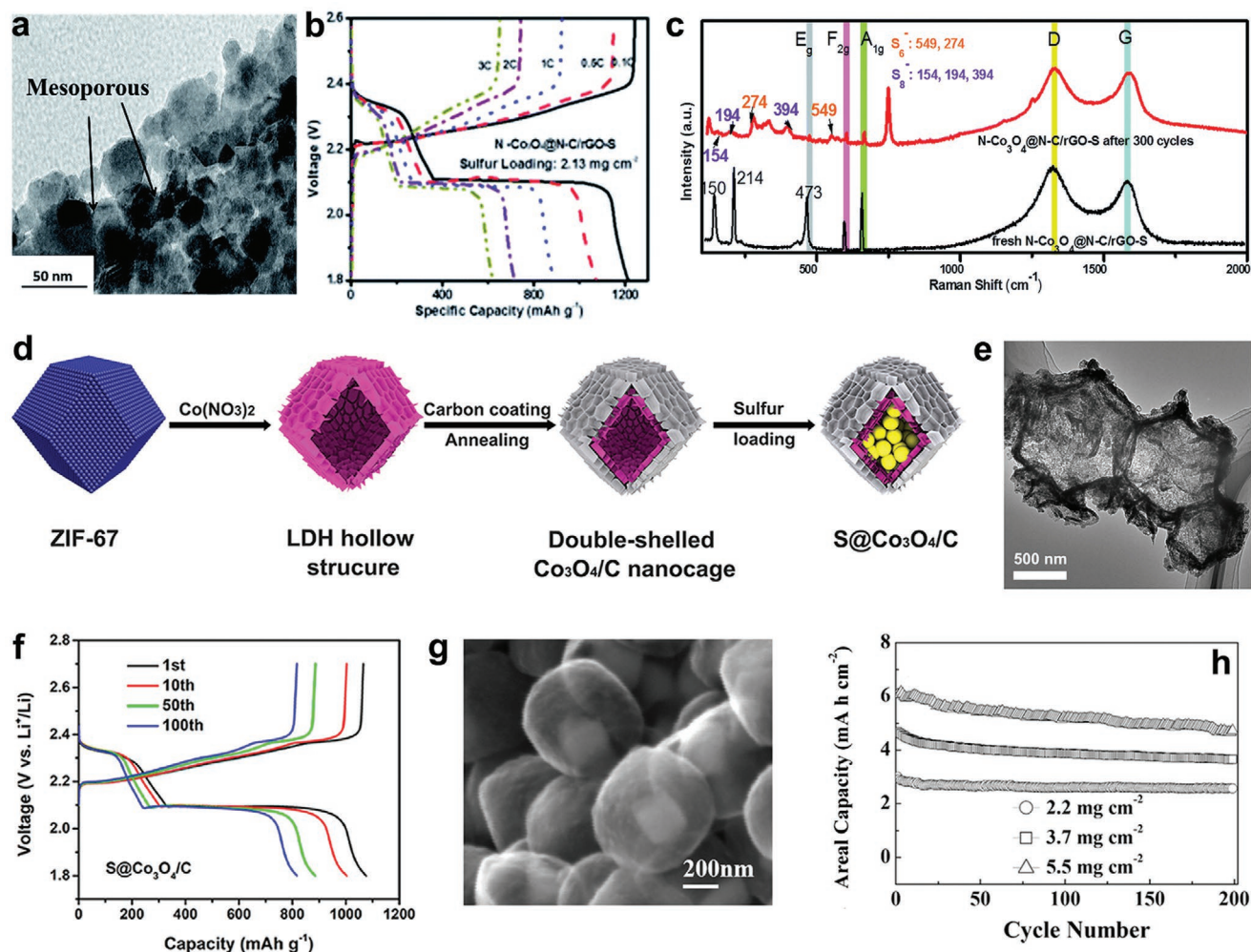
only 0.083% capacity decay per cycle at 1 C for 500 cycles. The chemical interaction between Co_3O_4 nanocages and polysulfides was validated by the upper- and lower-plateau capacities, visual polysulfide adsorption, and XPS measurements. Such double-shelled nanocages had a combined effect on boosting sulfur cathodes. The highly conductive carbon shells resulted in fast electron transference and charge transfer kinetics. Meanwhile, they also physically confined the polysulfide diffusion. The strong chemical anchoring resulting from the inner Co_3O_4 shells was able to chemically adsorb the polysulfides.

There are also studies involving polar CoO to anchor polysulfides. Ren et al. prepared a free-standing 3D PCF cloth with CoO/Co particles as sulfur host.[209] Because of metallic Co and the PCF network, the obtained CoO/Co@PCF host displayed desirable conductivity and therefore the electron transport was greatly accelerated. Moreover, the CoO/Co particles, uniformly dispersed on PCF, allowed abundant adsorption sites to chemically anchor polysulfides. Such strong chemical anchoring was confirmed by immersing CoO/Co@PCF into a Li_2S_4 solution, for which an almost transparent color was observed after 12 h. The corresponding XPS results also demonstrated the presence of electron transfer between Co atoms from CoO/Co and sulfur atoms of Li_2S_4. Advantageously, the prepared CoO/Co@PCF-S cathode loading of 3 mg cm^{-2} sulfur revealed a storage capacity of 1214.2 mAh g^{-1} at 0.1 C. When the sulfur content increased to 5.4 mg cm^{-2}, the composite cathode still attained a favorable capacity up to 508.0 mAh g^{-1} after 100 cycles at 0.5 C.

6.1.4. Iron-Based Oxides

Iron-based oxides like Fe_3O_4 and Fe_2O_3 have been proven to be efficient hosts to improve the cathode performance.[210–212] Considering the superior conductivity and polar property, Manthiram and co-workers introduced Fe_3O_4 with high conductivity (5×10^4 S m^{-1}) to sulfur cathodes. As shown in Figure 11g, the authors employed Fe_3O_4 cubes as core in combination with carbon shells to construct carbon-coated Fe_3O_4 yolk–shelled nanoboxes (YSC@Fe_3O_4).[208] Such a YSC@Fe_3O_4 host revealed unique materials properties for sulfur cathodes: 1) the inner Fe_3O_4 cubes chemically anchored polysulfides within the nanoboxes; 2) the large cavity of the yolk–shell structure enabled adequate sulfur loading and mitigated the cathode swelling during lithiation; 3) the carbon shells physically confined the polysulfide migration; 4) the high conductivity from Fe_3O_4 cubes and carbon shells facilitated the charge transfer kinetics of the sulfur cathodes. The prepared S/YSC@Fe_3O_4 cathodes achieved an areal loading of up to 5.5 mg cm^{-2}, reaching a good areal capacity of 6.1 mAh cm^{-2} (Figure 11h). Moreover, The XPS spectra confirmed the chemical interactions between Fe_3O_4 and polysulfides. After exposure to Fe_3O_4, L_2S_6 revealed a significant binding energy shift for sulfur atoms, implying the presence of electron transfer to Fe_3O_4.

Fe_3O_4 has been combined with various carbon substrate materials to improve sulfur utilization. More recently, employing spray drying, followed by a thermal treatment, Li et al. fabricated 3D porous CNT microspheres with uniformly dispersed Fe_3O_4 nanoparticles (CNT/Fe_3O_4).[213] As sulfur host, the interwoven CNT network accelerated the charge transfer and allowed
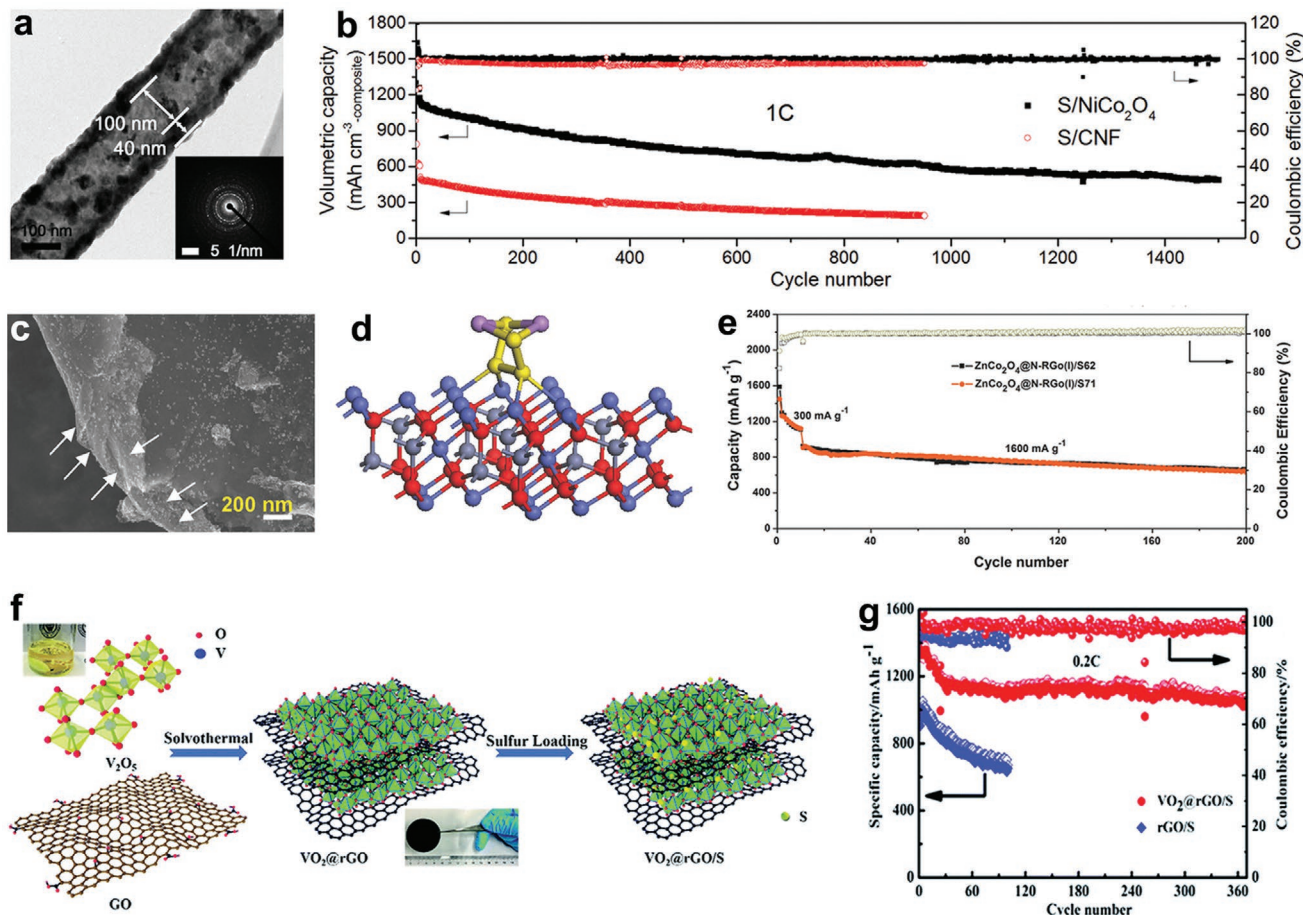
**ADVANCED
SCIENCE NEWS**
www.advancedsciencenews.com

**ADVANCED
ENERGY
MATERIALS**
www.advenergymat.de

Figure 11. a) HRTEM image of N-Co$_3$O$_4$@N-C. b) Voltage profiles of a N-Co$_3$O$_4$@N-C electrode at various rates. c) Ex situ Raman spectra of N-Co$_3$O$_4$@N-C-S before and after 300 cycles (discharged down to 2.1 V). d) Schematic representation of the fabrication and e) TEM image of Co$_3$O$_4$/C nanocages. f) Voltage profiles of a S@Co$_3$O$_4$/C cathode at 0.2 C at various indicated cycle numbers. g) SEM image of yolk-shelled YSC@Fe$_3$O$_4$ nanoboxes. h) Areal capacities of S/YSC@Fe$_3$O$_4$ electrodes with various sulfur loadings. (a–c) Reproduced with permission.[207] Copyright 2018, Royal Society of Chemistry. (d–f) Reproduced with permission.[58] Copyright 2019, American Chemical Society. (g,h) Reproduced with permission.[208] Copyright 2017, Wiley-VCH.

adequate sulfur loading. Moreover, the distributed Fe$_3$O$_4$ nanoparticles were able to improve the chemical anchoring toward polysulfides. Consequently, the S/CNT/Fe$_3$O$_4$ electrode contributed to an increased capacity at 0.2 C of 1270 mAh g^{-1} and favorable rate capability (602 mAh g^{-1} up to 3 C). The catalytic effect of Fe$_3$O$_4$ on the polysulfide conversion has also been reported.[214,215] Ding et al. designed a ternary sulfur host, consisting of Fe$_3$O$_4$ nanoparticles embedded in porous nanocarbon on graphene nanosheets (Fe$_3$O$_4$/NC/G), which revealed the accelerated catalytic conversion of polysulfides.[214] In situ XRD was employed to investigate the polysulfide evolution. The diffraction peaks of polysulfides almost disappeared when the discharging process was finished, meaning that their detrimental migration from cathodes was greatly mitigated. The authors proposed that the polysulfides were effectively anchored and then catalytically converted by Fe$_3$O$_4$ nanoparticles. The prepared Fe$_3$O$_4$/NC/G host loaded with the Li$_2$S$_6$ catholyte achieved a superior rate capability at 3 C of 755 mAh g^{-1}.

6.1.5. Mixed Metal Oxides

Mixed metal oxides or spinels with general formula M^{2+}M$^{3+}_2$O$^{2-}_4$ are good catalysts for various chemical reactions. Benefiting from the interfacial effects between mixed metal ions, their properties are far more superior to those of their single-metal counterparts. Also, they exhibit a better electronic conductivity. Mixed metal oxides like NiCo$_2$O$_4$,[216–219] NiFe$_2$O$_4$,[220,221] and ZnCo$_2$O$_4$ have therefore been introduced as sulfur hosts.

Gao and co-workers fabricated carbon-free NiCo$_2$O$_4$ nanofibers with a high density to anchor sulfur (**Figure 12**a).[222] Such hollow NiCo$_2$O$_4$ nanofibers were prepared by heating the electrospun nanofibers from a mixture of polyacrylonitrile (PAN), Co(OAc)$_2$, and Ni(OAc)$_2$. Different from the traditional lightweight carbon–sulfur hosts, the hollow NiCo$_2$O$_4$ nanofibers achieved S/NiCo$_2$O$_4$ composites with high tap density. The volumetric capacity of S/NiCo$_2$O$_4$ reached 1867 mAh cm^{-3} (composite-based). Moreover, an 1171 mAh cm^{-3} capacity in

**ADVANCED
SCIENCE NEWS**

www.advancedsciencenews.com

**ADVANCED
ENERGY
MATERIALS**

www.advenergymat.de

Figure 12. a) TEM image of NiCo$_2$O$_4$ nanofibers and the corresponding SAED pattern (inset). b) Prolonged cycle life of an S/NiCo$_2$O$_4$ electrode at 1 C. c) SEM image of ZnCo$_2$O$_4$@N-RGO. d) Optimized atomic geometries of Li$_2$S$_4$ adsorbed at ZnCo$_2$O$_4$ (111) crystal plane. e) Cycle life of ZnCo$_2$O$_4$@N-RGO/S with 71 wt% sulfur content. f) Fabrication scheme of the fabrication and g) cycle life performance of VO$_2$@rGO/S composites. (a,b) Reproduced with permission.[222] Copyright 2019, Wiley-VCH. (c–e) Reproduced with permission.[224] Copyright 2018, Wiley-VCH. (f,g) Reproduced with permission.[225] Copyright 2019, Royal Society of Chemistry.

the first cycle was achieved at 1 C. The corresponding electrode stability was excellent. Only 0.039% per cycle was lost during 1500 cycles (Figure 12b). Optically transparent cells indicated a strong polysulfide adsorption at the polar NiCo$_2$O$_4$ nanofibers. Visual observation at various depth-of-discharge evidently revealed that the electrolyte with S/NiCo$_2$O$_4$ cathodes was almost transparent and colorless except for the pale yellow color in the low voltage plateau range. The redox reaction kinetics of the polysulfides was also enhanced by the strong chemical interactions between NiCo$_2$O$_4$ and the polysulfides. Using a similar electrospinning strategy, Gao et al. fabricated nickel ferrite (NiFe$_2$O$_4$) nanofibers as a novel sulfur host material.[223] The resulting NiFe$_2$O$_4$ nanofibers with strong polarity showed favorable adsorption of polysulfides, significantly inhibiting the shuttle effect of the sulfur cathodes. Because of the high tap density, the obtained S/NiFe$_2$O$_4$ electrode revealed an initial volumetric capacity up to 1281.7 mAh cm^{-3} at 0.1 C on the basis of the composite content.

Combining mixed metal oxides with highly conductive carbon structures is also beneficial to the redox kinetics of sulfur species. Sun et al. employed highly conductive N-doped RGO with stable network structures to support ZnCo$_2$O$_4$ nanocubes

(ZnCo$_2$O$_4$@N-RGO).[224] As shown in Figure 12c, numerous ZnCo$_2$O$_4$ nanocubes were uniformly dispersed on both sides of the graphene sheets (indicated by white arrows), forming a sandwich-like microstructure. Such architecture can significantly enhance the adsorption of polysulfides due to the chemical anchoring of ZnCo$_2$O$_4$ and N-RGO. The interaction between ZnCo$_2$O$_4$ and polysulfides has been investigated by calculating the binding energies of Li$_2$S$_4$ with ZnCo$_2$O$_4$ based on DFT. The optimized model (Figure 12d) revealed the presence of a strong binding energy of 3.1 eV between the (111) planes of ZnCo$_2$O$_4$ and Li$_2$S$_4$. The doped nitrogen atoms from N-RGO and the metal ions from ZnCo$_2$O$_4$ gave rise to dual chemical anchoring toward polysulfides. As a result, the ZnCo$_2$O$_4$@N-RGO host loading 71% sulfur revealed a capacity of 905 mAh g^{-1} in the first cycle at a current of 1600 mA g^{-1} and maintained 71% of its capacity after 200 cycles (Figure 12e).

6.1.6. Other Oxides

There also have been other metal oxides applied as sulfur host material to improve the electrode performance, some of

**ADVANCED
SCIENCE NEWS**

www.advancedsciencenews.com

**ADVANCED
ENERGY
MATERIALS**

www.advenergymat.de

which exhibit considerably increased effects on the storage capacity and cycle life performance of sulfur cathodes, such as SiO_2,[226–228] VO_2,[229] V_2O_3,[230,231] V_2O_5,[90,232] Al_2O_3,[233,234] ZnO,[235–237] and MgO.[238,239] For instance, Rehman et al. fabricated a cross-linked Si/SiO_2 hierarchically porous carbonsphere hybrid material ($Si/SiO_2/C$).[240] As sulfur host, such $Si/SiO_2/C$ spheres disclosed several structural advantages: 1) the cross-linked architecture restrained polysulfide leakage by physical confinement inside the porous carbon structures and by electrostatic interactions with Si/SiO_2; 2) the favorable porosities with high surface area enabled high sulfur loading and facilitated the charge transfer reaction, leading to desirable rate capabilities; 3) the cross-linked Si/SiO_2 species also boosted the electrochemical charge transfer kinetics of sulfur cathodes. Benefiting from these characteristics, an optimal $Si/SiO_2@C$-S cathode was loaded with 69.6 wt% sulfur, exhibiting a capacity up to 825 mAh g^{-1} during the first cycle at 2 C and a high storage capacity was maintained even after 500 cycles.

Li et al. designed a binary sulfur host, comprising in situ grown VO_2 nanoflakes at rGO ($VO_2@rGO$).[225] As shown in Figure 12f, The $VO_2@rGO$ composite was obtained via a facile solvothermal reaction. The prepared VO_2 nanoflakes exhibited intense chemical anchoring toward polysulfides and also accelerated the conversion between polysulfides and Li_2S_2/Li_2S, thus reducing the shuttle problem. Additionally, rGO nanosheets spatially confined polysulfides and enhanced the conductivity of sulfur cathodes, significantly promoting the electrode redox kinetics. The CV curves at various scan rates indicated that the $VO_2@rGO$ hosts accelerated the redox kinetics and Li$^+$ diffusion of the cathodes. With the combined effects from VO_2 and rGO, the $VO_2@rGO$/S cathode demonstrated a superior prolonged cycle life at 0.2 C (Figure 12g). An initial capacity of 1358 mAh g^{-1} was reached and 77% of its capacity was retained after 370 cycles, which resulted in a capacity fading of 0.06% per cycle. Ma et al. synthesized Al_2O_3-doped ZnO coated with CNT (AZO/CNT) as sulfur hosts through a hydrothermal process, followed by a solid state reaction.[241] The AZO component provided a strong chemical bonding to polysulfides, which significantly inhibited the polysulfide shuttling. Moreover, the Al atoms doping into the ZnO lattice increased the electron density of ZnO, thus increasing the electronic conductivity and facilitating the redox kinetics. The AZO@S/CNT cathode, containing 60 wt% sulfur content, delivered a capacity of 1100 mAh g^{-1} in the first cycle at 0.2 C and remained 700 mAh g^{-1} over 200 cycles.

By tailoring the structure and configuration, metal oxides can improve the chemical bonding and accelerate the polysulfide conversion. The present results allow us to have a better understanding of the interactions between metal oxides and polysulfides. Future research on metal oxides has to focus on more efficient adsorption and conversion of polysulfides, high conductivity, and higher cost-effectiveness for practical applications.
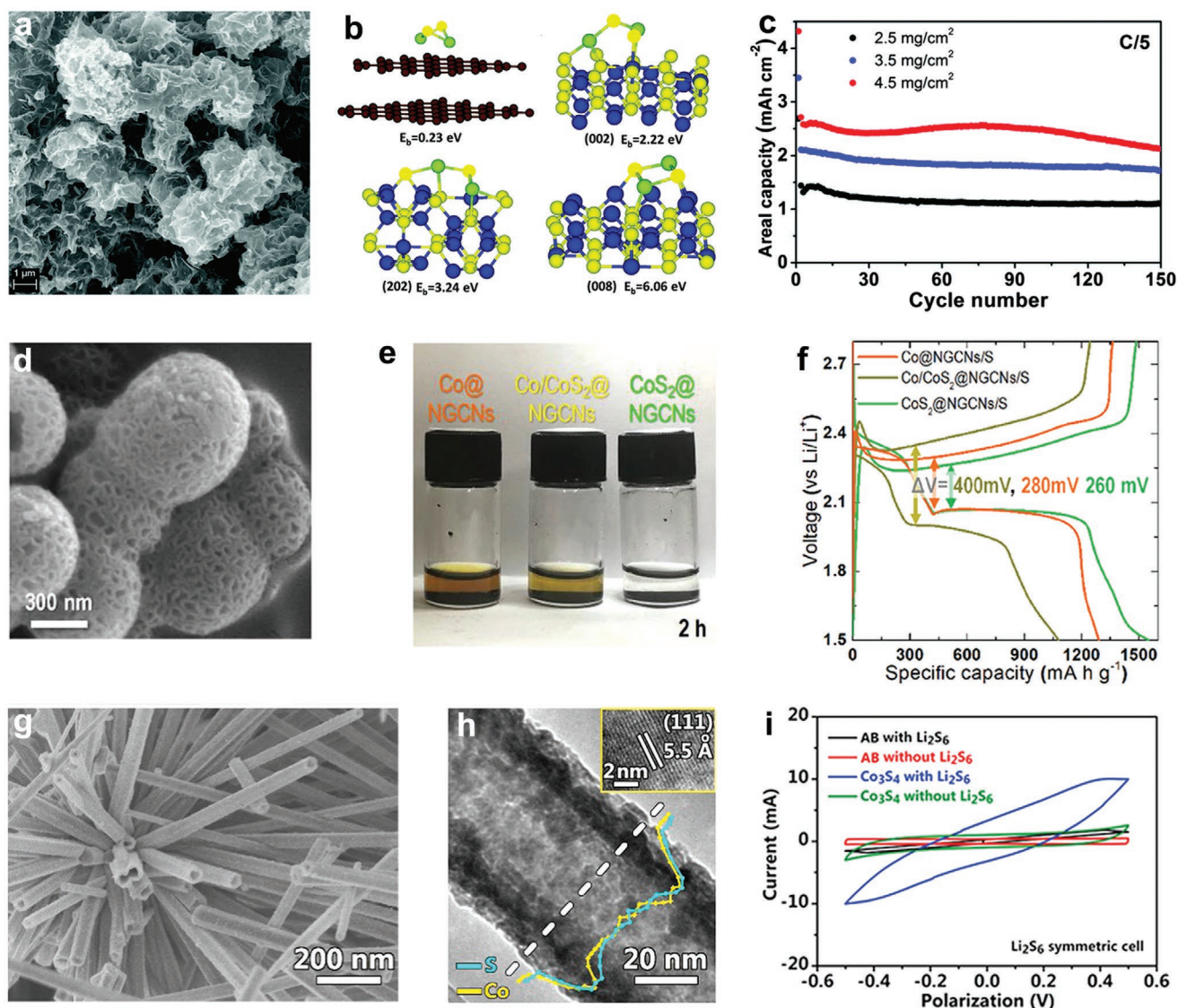
6.2. Metal Sulfides

Metal sulfides have been explored as sulfur host materials, since their strong polar character induces significant chemical interaction with active sulfur.[242] Most metal sulfides typically lithiate at voltages below 1.5 V versus Li$^+$/Li, avoiding parasitic reactions of host materials within the operating voltage window of sulfur cathodes. Another important property that has been described in recent literature is that some metal sulfides reveal high catalytic effects, promoting the conversion of polysulfides and, consequently, improving the charge transfer kinetics.[243] Moreover, in contrast to metal oxides, metal sulfides typically show better conductivities, which is beneficial for the electrochemistry of sulfur cathodes.

6.2.1. Cobalt-Based Sulfides

Cobalt-based sulfides, such as Co_9S_8,[81,244,245] CoS_2,[30,246] and Co_3S_4,[247,248] have been studied in detail to be applied as sulfur hosts to boost the electrode performance. All of them own superior room temperature conductivity (1.36 S m^{-1} for Co_9S_8, 6.7×10^5 S m^{-1} for CoS_2, and 3.3×10^5 S m^{-1} for Co_3S_4).[247] Pang et al. proposed a graphene-like Co_9S_8 nanosheet material as sulfur host because of the high conductivity of Co_9S_8 and the strong chemical interaction with polysulfides.[244] This graphene-like Co_9S_8, synthesized by a facile microwave solvothermal method, exhibited a 3D network comprising interconnected nanosheets (**Figure 13**a). The authors studied three different lattice planes of Co_9S_8 to determine the binding effects of Co and S atoms on polysulfides (Figure 13b). The (002) surface with a Co/S ratio of 1:4 showed a binding energy of 2.22 eV to Li_2S_2, while the (202) surface with a higher Co/S ratio increased the energy to 3.24 eV to finally reach 6.06 eV for the (008) surface, comprising pure cobalt atoms. The higher Co/S ratio indicated the stronger binding energy, implying that Co-S interactions were mainly responsible for the chemical bonding to polysulfides. XPS results also demonstrated the presence of electron transfer between Li_2S_4 and Co_9S_8. As a result, Co_9S_8 hosts loaded with 75 wt% sulfur exhibited an ultralow 0.045% capacity loss per cycle during 1500 cycles at 0.5 C. In particular, a cathode loaded with 4.5 mg cm^{-2} sulfur exhibited a stable cycling performance of over 150 cycles (Figure 13c). Such a result demonstrated the merit of Co_9S_8 nanosheets for sulfur cathodes with high energy density.

Using a self-template method followed by sulfidation, Chen et al. synthesized Co_9S_8 nanocrystals embedded in hollow carbon nanopolyhedra (Co_9S_8/C).[81] Such a Co_9S_8/C composite structure has many advantages: 1) the large internal void was capable of incorporating high sulfur contents and buffered the electrode swelling during cycling; 2) the embedded Co_9S_8 nanocrystals effectively anchored polysulfides and restrained their migration out of the cathodes; 3) the 3D conductively porous networks offered adequate charge transfer pathways. Quantum density functional theory (QDFT) simulations revealed that the adsorption energies of Co_9S_8 nanoparticles toward various sulfur species were in the range of 2.97 to 6.08 eV, suggesting strong chemisorption. A visual adsorption test revealed that Li_2S_4 exposed to Co_9S_8/C hollow nanopolyhedra became nearly transparent after a short period of time. The chemical interaction between active sulfur and Co_9S_8 mainly resulted from the formation of Co−S and Li−S bonds. The resulting Co_9S_8/C-S composite cathode stabilized at 560 mAh g^{-1} over 1000 cycles at 2.0 C.

**ADVANCED
SCIENCE NEWS**

www.advancedsciencenews.com

**ADVANCED
ENERGY
MATERIALS**

www.advenergymat.de

Figure 13. a) SEM image of graphene-like Co_9S_8. b) Schematic representation of the most stable Li_2S_2 binding geometric configuration for double-layered graphitic carbon and four-layered Co_9S_8 surface slabs. c) Cycling performance of the $Co_9S_8/S75$ electrodes at 0.2 C. d) SEM image of mesoporous hollow $CoS_2@NGCNs$. e) Li_2S_6 adsorption with the addition of $CoS_2@NGCNs$. f) Voltage profile of a hollow $CoS_2@NGCN$ electrode. SEM (g) and TEM (h) images of Co_3S_4 nanotubes. The inset in (h) is the HRTEM image of Co_3S_4 nanotube walls. The plots are EDX of Co and S. i) CV curves of Li_2S_6 symmetrical cells. (a–c) Reproduced with permission.[244] Copyright 2016, Royal Society of Chemistry. (d–f) Reproduced with permission.[249] Copyright 2019, Wiley-VCH. (g–i) Reproduced with permission.[247] Copyright 2017, Elsevier.

CoS_2 was initially introduced as an additive to sulfur cathodes by Yuan et al.[30] They found that the introduced CoS_2 exhibited strong interaction with polysulfides and thus accelerated redox reactions of polysulfides. This discovery has promoted the application of CoS_2 in sulfur cathodes. More recently, Seo et al. designed mesoporous HCSs with brain-coral-like structures, which were assembled by N-doped graphitic carbon nanoshells (NGCNs) embedded with CoS_2 nanoparticles.[249] As shown in Figure 13d, the mesoporous hollow $CoS_2@NGCN$ nanostructure was composed of numerous surface pores. Because of the large internal voids, $CoS_2@NGCN$ host materials offer sufficient space for sulfur infusion and volume changes during (de)lithiation. Polar CoS_2 nanoparticles in combination with

NGCNs not only chemically adsorb polysulfides but also facilitate the charge transfer reaction. Figure 13e illustrated the strong adsorption of $CoS_2@NGCN$ toward polysulfides. After exposing $CoS_2@NGCN$, the Li_2S_6 solution became transparent in 2 h. The voltage curves in Figure 13f show that the $CoS_2@NGCN/S$ cathode delivered a higher specific capacity with mitigated polarization than the other two counterparts. It was concluded that $CoS_2@NGCN$ was beneficial for the utilization of sulfur cathodes and increased polysulfide reaction kinetics. The $CoS_2@NGCN/S$ composite cathode maintained a steady capacity of more than 900 mAh g^{-1} at 0.1 C after 100 cycles.

Inspired by the high electrocatalytic activity of Co_3S_4 for oxygen reduction, Pu et al. proposed that Co_3S_4 could also

catalyze the conversion of sulfur species, since both sulfur and oxygen belong to the chalcogen group.[247] The authors proposed a facile strategy to fabricate $Co_3S_4@S$ nanotubes for high-performance Li–S batteries. The SEM image in Figure 13g clearly indicates the hollow structure of the Co_3S_4 nanotubes. A 15 nm thick wall was revealed from the TEM image (Figure 13h). Nanoscale Co_3S_4 nanotubes with abundant sites ensured the chemical absorption of sulfur species. Symmetric cells were constructed to investigate the catalytic properties of Co_3S_4 for the polysulfide conversion reactions. The CV curve of the symmetrical Co_3S_4 cell revealed that Co_3S_4 accelerated the conversion of polysulfides (Figure 13i). As for the cells without the Li_2S_6 electrolyte, both the Co_3S_4 and acetylene black (AB) cells barely displayed a current response. However, Co_3S_4 indicated significantly enhanced currents than AB after adding Li_2S_6. Furthermore, $Co_3S_4@S$ nanotube-based cathodes showed a prolonged cycle life of more than 1000 cycles at 5 C.

6.2.2. Molybdenum Disulfide

Molybdenum disulfide (MoS_2), consisting of 2D layered structures, has been proven to have a high electrochemical activity for water splitting. The application of MoS_2 has also been explored to be applied in sulfur cathodes.[250–252] By controlling the sulfur deficiency of few-layer MoS_2 nanoflakes, Lin et al. designed rGO decorated with sulfur-deficient MoS_2 nanoflakes (MoS_{2-x}/rGO) that showed electrocatalytic activities for the polysulfide conversion.[67] Because of the sulfur deficiencies, the conversion of sulfur species at MoS_{2-x}/rGO experienced an energetically favorable pathway, resulting in accelerated redox kinetics and consequently in high sulfur utilization. Similarly, the integration of layered MoS_2 nanosheets with a rGO foam was reported by You et al. to construct sulfur cathodes.[82] As illustrated in **Figure 14**a, a facile hydrothermal process was conducted to synthesize MoS_2/rGO foams, producing 3D
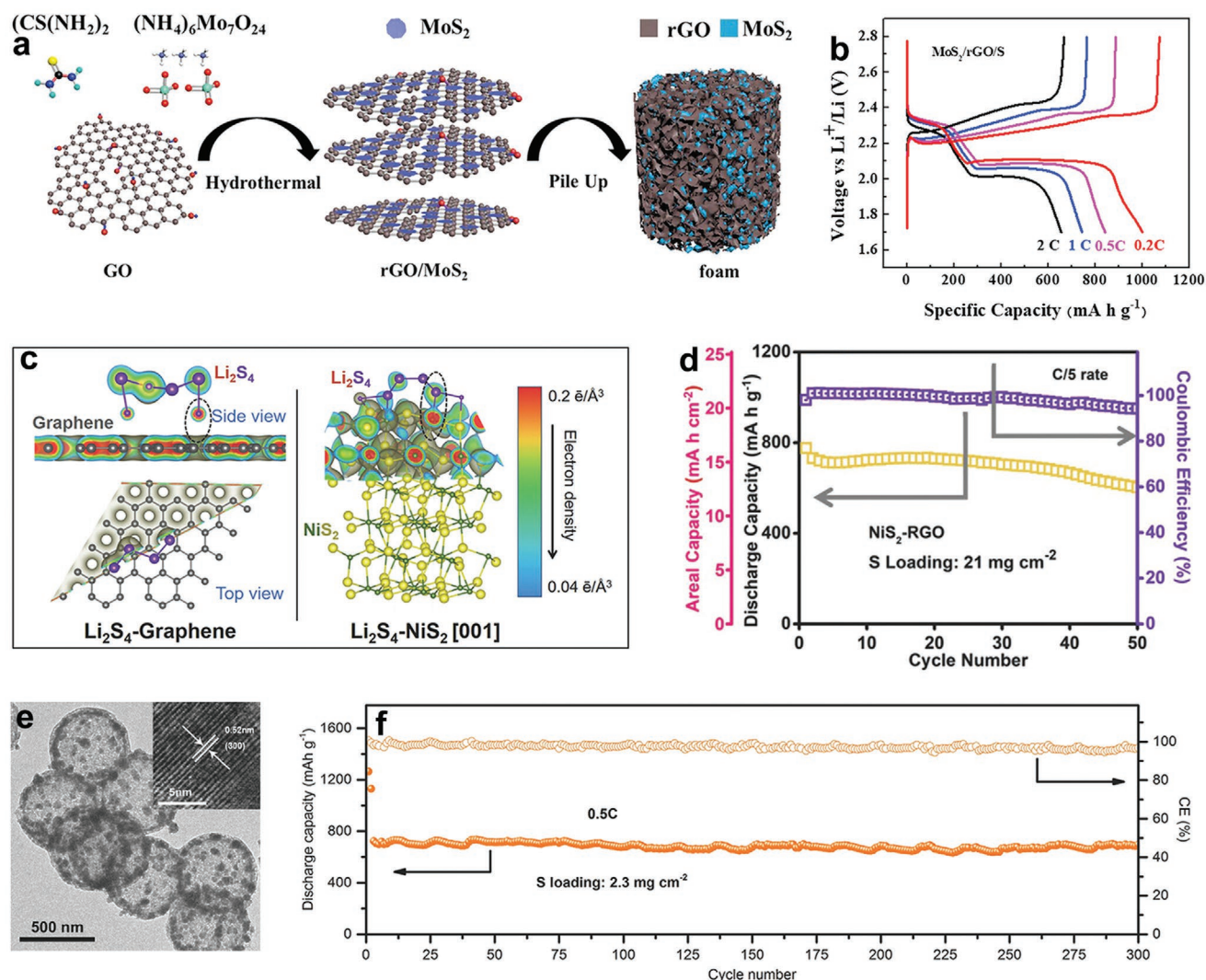
Figure 14. a) Synthesis scheme of MoS_2/rGO foam. b) Voltage profiles of MoS_2/rGO/S at various current rates. c) Binding geometries and electron densities of Li_2S_4 at graphene and NiS_2. d) Cycle life performance of NiS_2-RGO cathodes with higher sulfur loading. e) TEM image of NiS@C-HS and HRTEM of NiS in the inset. f) Cycle life of an S/NiS@C-HS electrode. (a,b) Reproduced with permission.[82] Copyright 2019, Elsevier. (c,d) Reproduced with permission.[253] Copyright 2018, Wiley-VCH. (e,f) Reproduced with permission.[254] Copyright 2017, Wiley-VCH.

interconnected porous networks. The highly conductive rGO nanosheets with large surface areas exhibited desirable elasticity, which was suitable to load sulfur into the networks. The MoS_2 nanosheets possessed strong bonding and therefore a high electrocatalytic activity toward polysulfides. These features have been validated by the visualized adsorption of Li_2S_6 and CV curves of symmetrical electrochemical cells. As a result, the obtained $MoS_2/rGO/S$ cathodes exhibited enhanced rate capability at various current densities than rGO/S cathodes (Figure 14b). Porous MoS_2/rGO foams are therefore promising to be applied for sulfur cathodes.

Due to the ultrathin property, MoS_2 nanosheets were also coated on other matrixes to confine polysulfides. Hu et al. designed MoS_2 nanosheet-coated hierarchical carbon spheres (MoS_2@HCS) to improve sulfur cathodes.[255] A Ni-MOF precursor was used to fabricate HCS consisting of hollow carbon nanobubbles. The HCS was subsequently covered with a layer of MoS_2 nanosheets by making use of a solvothermal process. The as-prepared MoS_2@HCS host materials revealed some interesting characteristics: 1) the hollow carbon bubbles provided many voids for sulfur loading and alleviated the electrode swelling upon lithiation; 2) highly conductive HCS ensured the charge transport, hence improving the sulfur utilization; 3) the polar MoS_2 dispersed at HCS inhibited the polysulfide shuttling process and prolonged the electrodes cycle life by effective polysulfide adsorption; 4) the introduced MoS_2 accelerated the electrochemical redox kinetics. Taking advantage of these structural properties, the capacity of S/MoS_2@HCS cathodes reached 1048 mAh g^{-1} at 0.2 C. CV revealed the accelerated polysulfide redox kinetics by MoS_2. Compared with the pure sulfur cathode, MoS_2/S cathodes showed significantly reduced overpotentials for the reduction and oxidation reactions.

6.2.3. Nickel-Based Sulfides

Nickel-based sulfides like NiS_2,[256,257] NiS,[254] and Ni_3S_2[258,259] have been employed as sulfur host material because of the desirable sulfiphilicity and accelerated redox kinetics of polysulfides. For example, Luo et al. synthesized a novel 3D polysulfide reservoir by integrating NiS_2 nanoparticles with RGO frameworks.[253] Such a NiS_2-RGO sponge hybrid was constructed by biomolecule-assisted self-assembly. Uniform NiS_2 nanoparticles with porous morphology were in situ grown on a RGO substrate by a hydrothermal reaction. The hybrid NiS_2-RGO sponge delivered multiple benefits: 1) the porous RGO matrix provided sulfur species with sufficient space, facilitated 3D electron pathways, and physical blocking; 2) uniformly dispersed NiS_2 nanoparticles offered abundant sites for the chemical anchoring of polysulfides; 3) the strong chemically coupled NiS_2-RGO enabled continuous electron channels from RGO to the adsorption interface of NiS_2-polysulfides, considerably boosting the conversion of polysulfides and rate capabilities. DFT calculations visualized in Figure 14c revealed a high binding energy of 3.60 eV between Li_2S_4 and NiS_2, which was much stronger than that of graphene. In addition, the electron density distribution provided a more straightforward comparison. Compared to the C–Li
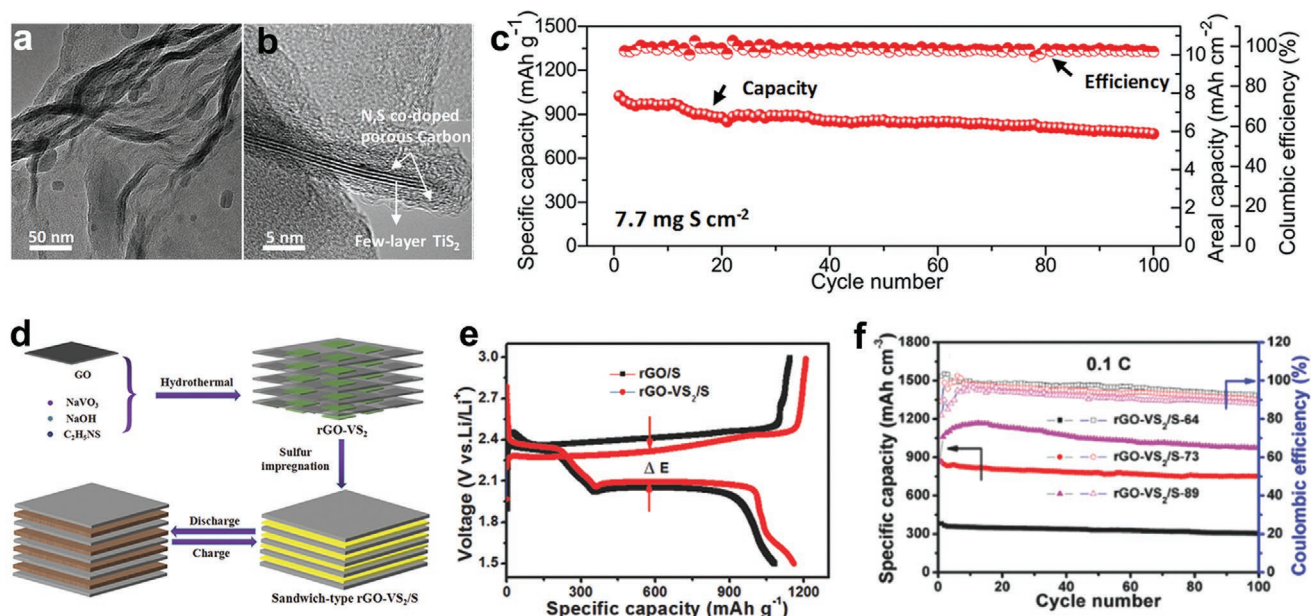
bonding, the electron density between Ni atoms of NiS_2 and Li atoms of Li_2S_4 was evidently enhanced (highlighted with a black circle). These features enabled the NiS_2-RGO sponge host loaded with a 75 wt% sulfur content. The obtained sulfur cathodes with a 21 mg cm^{-2} areal loading achieved a 16 mAh cm^{-2} areal capacity (Figure 14d).

Combining nanosized NiS with 3D carbon hollow spheres is another effective approach to confine polysulfides. Combining an in situ thermal reduction with the sulfidation process, Ye et al. fabricated a hybrid sulfur host consisting of NiS nanoparticles homogeneously dispersed on 3D carbon hollow spheres (NiS@C-HS).[254] Such a 3D network enlarged the chemical anchoring of NiS nanoparticles toward polysulfides by exposing many more active sites (Figure 14e). Moreover, C-HS provided the 3D electron transport pathways and sufficient physical blocking for polysulfides. The strong coupling interaction between the NiS nanoparticles and C-HS networks accelerated the electrode redox kinetics. The hybrid NiS@C-HS loaded with 2.3 mg cm^{-2} sulfur attained a very stable cycle life of over 300 cycles at 0.5 C (Figure 14f). The authors compared the adsorption capability of the hosts by visual adsorption tests, finding that NiS@C-HS exhibited stronger adsorption than other compared host materials. After treatment with polysulfides, the Raman spectra revealed that the four main peaks of NiS showed a slight redshift, indicating chemical bonding of NiS toward polysulfides.

6.2.4. Titanium Disulfide

Titanium disulfide (TiS_2) is a cathode material which was first investigated in rechargeable lithium batteries. Because of its high conductivity and effective adsorption for polysulfides, TiS_2 has been demonstrated a promising sulfur host material.[260,261] Chung et al. employed conductive TiS_2 to adsorb polysulfides.[83] The authors encapsulated the fabricated TiS_2-polysulfide in carbon electrode shells, assembling a so-called core–shell composite cathode. A catholyte composed of a high concentration of Li_2S_6 was employed to be the active species. Sulfur loading reached as high as 12 mg cm^{-2}. Even with a low electrolyte content of 5 µL electrolyte per mg sulfur, this hybrid cathode achieved a 10 mAh cm^{-2} areal capacity after 200 cycles at 0.2 C,

Recently, Huang et al. initially reported sandwich-like ultrathin TiS_2 nanosheets encapsulated in the N and S co-doped porous carbon (TiS_2@NSC).[262] TiS_2@NSC was prepared from the $Ti_3C_2T_x$ MXene precursor via PDA coating and sulfuration process. From TEM observations (**Figure 15**a,b) it has been concluded that TiS_2@NSC consisted of few-layer TiS_2 nanosheets sandwiched by a thin layer of porous carbon. Such an architecture was beneficial for trapping polysulfides and therefore greatly promoted the use of sulfur. Integrated with cotton-derived carbon fibers (CFs), TiS_2@NSC gave a freestanding cathode (TiS_2@NSC@CFs) with high areal sulfur loading up to 7.7 mg cm^{-2}. The freestanding sulfur cathode achieved a high initial areal capacity of 7.9 mAh cm^{-2} and maintained 5.9 mAh cm^{-2} after 100 cycles (Figure 15c). These results position TiS_2@NSC as one of the best sulfur hosts reported at that time.

**ADVANCED
SCIENCE NEWS**

www.advancedsciencenews.com

**ADVANCED
ENERGY
MATERIALS**

www.advenergymat.de

Figure 15. a) TEM and b) HRTEM of TiS$_2$@NSC. c) Cycle life performance of freestanding S/TiS$_2$@NSC@CFs cathodes. d) Schematic illustration for the synthesis of a sandwich-structured rGO-VS$_2$/S composite. e) Voltage profile of rGO-VS$_2$/S at 0.2 C. f) Volumetric capacities of VS$_2$-rGO/S with various sulfur contents. (a–c) Reproduced with permission.[262] Copyright 2019, Wiley-VCH. (d–f) Reproduced with permission.[263] Copyright 2018, Wiley-VCH.

6.2.5. Other Metal Sulfides

Some other metal sulfides involving VS$_2$,[264,265] ZnS,[266] FeS$_2$,[20,267] WS$_2$,[268,269] and NiCo$_2$S$_4$[270,271] have also been explored as sulfur host electrode material. For instance, integrating VS$_2$ grown on rGO sheets with sulfur layers into an alternating structure, Wang and co-workers developed a variety of flexible sandwich-like cathodes (rGO-VS$_2$/S).[263] As illustrated in Figure 15d, a facile hydrothermal process produced rGO-VS$_2$ nanosheets. rGO-VS$_2$/S composites with various sulfur loadings were obtained by tuning the content of sulfur infusion, revealing the following materials properties: 1) the sandwich-like structure mitigated the cathode swelling during lithiation; 2) a low content of VS$_2$ enhanced the conductivity and tap density of the sulfur cathodes; 3) the spatial confinement and chemical anchoring from rGO-VS$_2$ gave rise to reduced polysulfide shuttling; 4) the catalytic activity of VS$_2$ promoted the cathode reaction kinetics. Benefiting from these features, the rGO-VS$_2$/S cathode displayed longer discharge plateaus and higher capacity than rGO/S (Figure 15e). The cell polarization was also mitigated, that is, ΔE shows a smaller potential gap. The authors further evaluated rGO-VS$_2$/S electrodes with various sulfur loading, reporting that cathodes with 89 wt% sulfur exhibited an optimal volumetric capacity of up to 1182 mAh cm^{-3} (Figure 15f). This performance is highly competitive with state-of-the-art capacities in Li–S batteries.

Polar WS$_2$ nanosheets deposited on CNFs were first developed by Lei et al. via a facile hydrothermal process.[272] Such a C@WS$_2$ composite revealed a freestanding architecture, in which dense WS$_2$ nanosheets were vertically arranged along CNFs. DFT calculations revealed that WS$_2$ exhibited binding strengths to polysulfides throughout lithiation process. Active sulfur species were adequately anchored by the physical forces of CNFs and the chemical adsorption of WS$_2$. The initial

capacity of the freestanding C@WS$_2$/S cathode reached about 1500 mAh g^{-1} at 0.1 C. Even at 2 C, a prolonged cycling stability of 1500 cycles was obtained with an extremely low capacity loss of only 0.00072% per cycle. More recently, Lu et al. synthesized NiCo$_2$S$_4$ nanosheets, in situ grown on carboxylated CNTs by a simple hydrothermal reaction.[273] The NiCo$_2$S$_4$ flake morphology revealed abundant micropores, firmly anchored at the surface of CNTs. As a sulfur host, such a composite structure showed a better electrode conductivity and anchoring of polysulfides. The corresponding NiCo$_2$S$_4$@CNT/S electrode sustained a 1000 cycle life at 0.6 C with a capacity loss as low as 0.049% per cycle. The authors proposed a mechanism to unveil the role of the NiCo$_2$S$_4$@CNT host. CNTs provided highly electron conductive pathways, effectively improving the charge transport inside the cathodes. Furthermore, the bimetallic NiCo$_2$S$_4$ nanosheets facilitated strong adsorption toward polysulfides, effectively suppressing the diffusion of polysulfides.

The excellent conductivity, strong chemical adsorption of polysulfides, and good electrocatalytic activity of metal sulfides significantly increased the utilization of sulfur cathodes. The current exploration of metal sulfides for Li–S batteries gradually focuses on the catalytic effect on active sulfur species. However, the catalytic mechanism has not been well unveiled, which should be further investigated in future studies.

6.3. Metal Hydroxides

Compared with metal oxides and sulfides, hydroxides employed as a sulfur host material is rather limited, which may result from their relatively low conductivity and weak adsorption with polysulfides. The research mainly focuses on the performance of nickel hydroxides and layered double hydroxides.
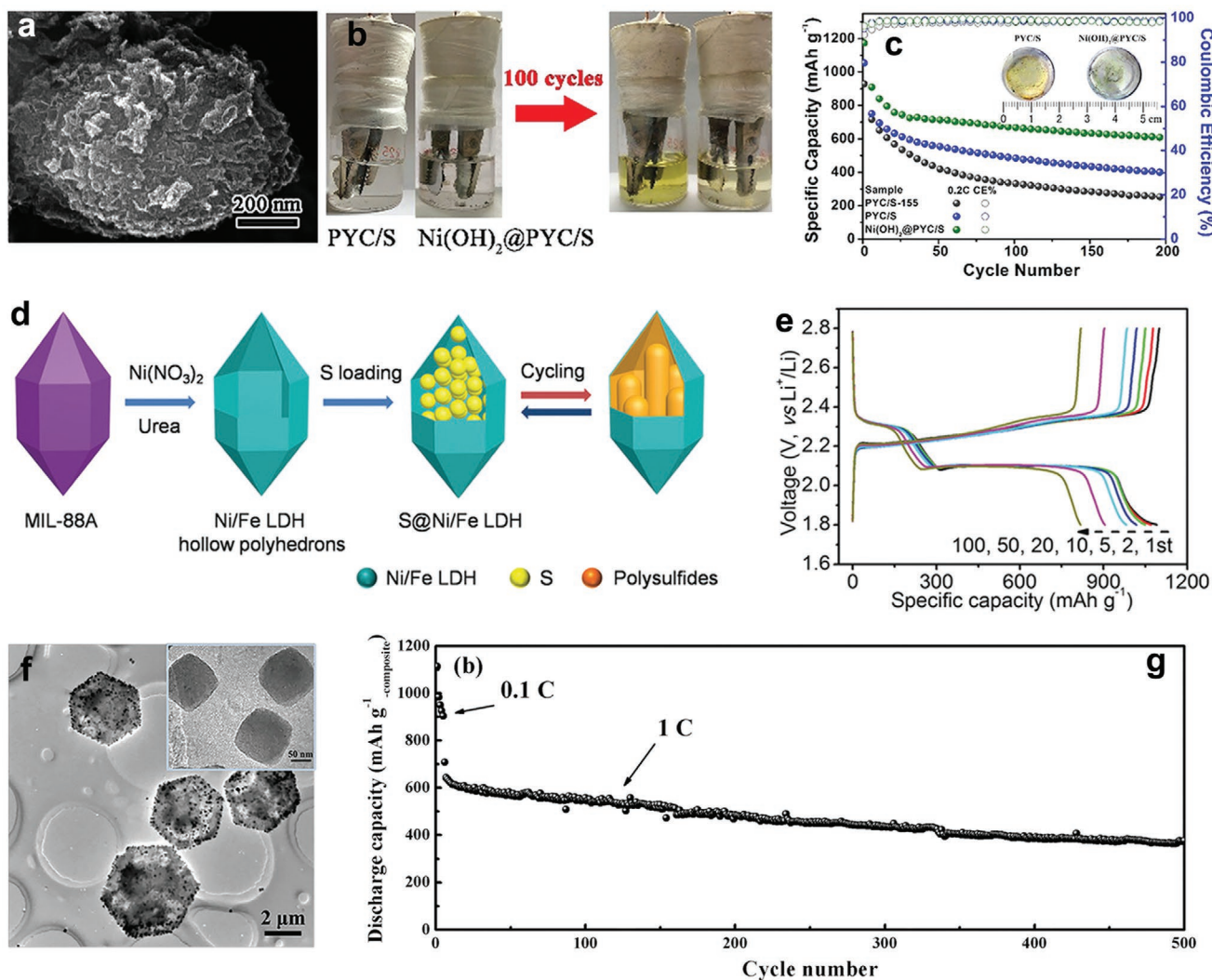
Figure 16. a) SEM image of Ni(OH)$_2$@PYC/S composites. b) Photos of PYC and Ni(OH)$_2$@PYC/S before and after 100 cycles. c) Cycling stability of Ni(OH)$_2$@PYC/S at 0.2 C. d) Synthesis scheme of S@Ni/Fe LDH. e) Voltage profiles of a S@Ni/Fe LDH cathode at 0.2 C. f) TEM image of CoOOH sheets. g) Long-term cycle life test of an S/CoOOH electrode. (a–c) Reproduced with permission.[277] Copyright 2018, Elsevier. (d,e) Reproduced with permission.[57] Copyright 2018, Wiley-VCH. (f,g) Reproduced with permission.[278] Copyright 2019, Wiley-VCH.

6.3.1. Nickel Hydroxides

Nickel hydroxides (Ni(OH)$_2$) with layered structures are typically employed as coating layers to inhibit the active sulfur dissolution into electrolytes by both their physical confinement and chemical adsorption.[274–276] For example, Xia et al. modified a thin Ni(OH)$_2$ layer on porous yeast carbon/sulfur (PYC/S) microspheres.[277] As illustrated in **Figure 16**a, the obtained Ni(OH)$_2$@PYC/S was coated with fluffy Ni(OH)$_2$ layers, resulting in a unique core–shell structure. The conductive porous PYC matrices are favorable for electrolyte penetration and effective electron transport, as well as to provide sufficient internal voids for sulfur loading. In addition, the polar Ni(OH)$_2$ shells ensured the strong chemical adsorption of polysulfides, effectively suppressing the polysulfide shuttling. Visual cycling tests confirmed the electrochemical stability

of Ni(OH)$_2$@PYC/S cathodes (Figure 16b). The electrolyte in Ni(OH)$_2$@PYC/S nearly kept transparent for more than 100 cycles, implying good adsorption of polysulfides. By contrast, the electrolyte in PYC/S clearly changed into yellow, indicating that polysulfides diffused out of the cathode. Due to these structural characteristics, the Ni(OH)$_2$@PYC/S composite cathodes exhibited a good cycling stability for more than 200 cycles at 0.2 C and the separator color remained unchanged during the cycling process (Figure 16c).

Another research, involving nickel-based hydroxides (NNHs) in sulfur cathodes, was developed by Meng et al.[279] They designed a thin-layered NNH to wrap the activated carbon cloth/sulfur composite (ACC/S). First, sulfur was infused into ACC by a facile "ethanol-transfer-adsorption" process. Then, a hydrothermal reaction resulted in the formation of NNH coated on ACC/S (NNH/ACC/S). The microporous ACC was an

effective sulfur scaffold which provided many electronic pathways. The outer NNH layers acted as a shield to spatially inhibit the polysulfide migration. Furthermore, the oxygen-containing groups at NNH chemically adsorbed polysulfides. Interestingly, an irreversible reaction of NNH with lithium generated a mixed hydroxide protection layer with good ionic conductivity for lithium. The XPS spectra proved the chemical interaction between NNH and polysulfides as electronic charge was transferred from oxygen of NNH to the lithium in the polysulfides, forming Li–O bonds. Consequently, a freestanding NNH/ACC/S cathode loaded with 4.3 mg cm^{-2} sulfur has a high and stable areal storage capacity of 4.3 mAh cm^{-2} at 0.15 C.

6.3.2. Layered Double Hydroxides

LDHs are a class of inorganic lamellar compounds composed of metal ions with different valences octahedrally coordinating the hydroxyl groups. The general formula is $[M^{2+}_{1-x}M^{3+}_x(OH)_2]^{x+}[A^{n-}_{x/n}]^{x-}\cdot mH_2O$, where M^{2+} and M^{3+} represent divalent and trivalent metal cations, respectively, while A^{n-} are interlayer anions. Due to the high chemical activity of LDHs, they are widely used as nanocomposites, catalysts, and anion exchangers. LDHs have also been introduced to sulfur cathodes because of ample sulfiphilic and hydroxyl groups, as well as its electrocatalytic properties, accelerating the redox kinetics of polysulfides.[280–282]

Lou and co-workers developed different LDHs to improve sulfur cathodes.[280] Recently, they fabricated MOF-derived hollow Ni/Fe LDH polyhedrons to host sulfur.[57] As illustrated in Figure 16d, polyhedral MIL-88A particles were employed as sacrificial template. With a facile solvothermal reaction, MIL-88A converted into hollow Ni/Fe LDH polyhedrons. The final S@Ni/Fe LDH composite was obtained by sulfur melting infusion. As sulfur host, The Ni/Fe LDH polyhedrons displayed several characteristics: 1) the polar shells lead to abundant sulfiphilic sites, chemically anchoring polysulfides; 2) the hollow cavities enabled numerous sulfur storage and also buffered the cathode swelling; 3) the redox reaction kinetics of polysulfides was accelerated, achieving a uniform deposition of solid discharge products. Consequently, S@Ni/Fe LDH cathodes exhibited a 1091 mAh g^{-1} storage capacity in the first cycle at 0.2 C (Figure 16e). The initial capacity at 1 C reached 844 mAh g^{-1} and could be cycled for more than 1000 cycles with only 40% capacity loss.

Another strategy, proposed by Chen et al., was to cover P-doped activated biomass-derived carbons (PAB) with NiAl-LDH fences by a simple hydrothermal process.[283] The prepared NiAl@PAB hybrid host combined the merits of PAB and NiAl-LDH, the cooperative interface of which effectively encapsulated polysulfides through physical confinement and chemical adsorption. Moreover, the decorated NiAl-LDH fences with sufficient adsorption sites had a catalytic effect on the polysulfide conversion, hence substantially boosting the electrode reaction kinetics. The NiAl–LDH modification increased the Li$_2$S$_4$ adsorption as was demonstrated by DFT calculations with an enhanced binding energy of 3.03 eV. Therefore, the prepared NiAl@PAB/S composite loaded with 66 wt% sulfur delivered a 1216.3 mAh g^{-1} initial storage capacity at 0.2 C.

6.3.3. Other Hydroxides

Cobalt-based hydroxides have also been investigated as sulfur host. Niu et al. coated Co(OH)$_2$ nanosheets on a sulfur/conductive carbon black (CCB) electrode by thermal and hydrothermal reactions, in which CCB provided the conductive network and Co(OH)$_2$ nanosheets stabilized the electrode surface to prevent the polysulfide diffusion from CCB.[284] The obtained composite cathode (Co(OH)$_2$@S/CCB) delivered an optimal capacity of 1026 mAh g^{-1} at 0.1 C and 71.2% capacity retention over 200 cycles at 1 C, better than those of S/CCB electrodes. It was shown that Co(OH)$_2$ nanosheets considerably inhibited the diffusion of polysulfides.

More recently, Wang et al. proposed CoOOH sheets with high conductivity to anchor sulfur.[278] The synthesized CoOOH sheets displayed uniformly hexagonal morphology with tiny cubes at the surface (Figure 16f). As a carbon-free sulfur host, the highly conductive CoOOH sheets revealed specific electrode properties. The large surface area exposed adequate active sites to anchor and then catalyze polysulfides. On the basis of these structural features, the authors proposed a two-step reaction process between polysulfides and CoOOH. Co–O bonds were partially split and polysulfides were oxidized to thiosulfate/polythionate species. The exposed Co atoms received electrons from the polysulfides, forming Co–S bonds by Lewis acid–base interactions. This process effectively promoted the polysulfide conversion and mitigated the shuttling process. Taking advantage of these favorable anchoring effects, the prepared sulfur/CoOOH composite cathode was successfully loaded with 91.8 wt% sulfur, attaining 1.26 g cm^{-3} in tap density. At 1 C, a good cycle life was obtained for more than 500 cycles with only 0.09% capacity loss per cycle (Figure 16g).

6.4. Metal Carbides

Metal carbides have been investigated as electrocatalyst due to their excellent conductivity, unique structure, and low material cost. These intrinsic natures make them interesting to improve sulfur cathodes. Some transition metal carbides such as TiC, Fe$_3$C, and Mo$_2$C have been introduced as sulfur host, which exhibit a considerably enhanced electrochemical performance for Li–S batteries.

6.4.1. Titanium Carbides

Polar titanium carbides (TiC) with high conductivity were initially applied for sulfur cathodes by Peng et al.[285] Analyzing the charge transfer kinetics of sulfur species at various substrates, the authors concluded that conductive polar TiC had strong interactions with polysulfides and played a crucial role in the redox kinetics. First-principle calculations as shown in **Figure 17**a revealed that the binding energies of the TiC (100) surface with Li$_2$S$_4$ and Li$_2$S were 1.89 and 2.75 eV, respectively. Such affinity was substantially stronger than those with graphene. Polysulfide conversion studies were conducted with carbon-fiber paper (CP), CP-supported TiO$_2$ (CP-TiO$_2$), and CP-supported TiC (CP-TiC) electrodes. The electrochemical
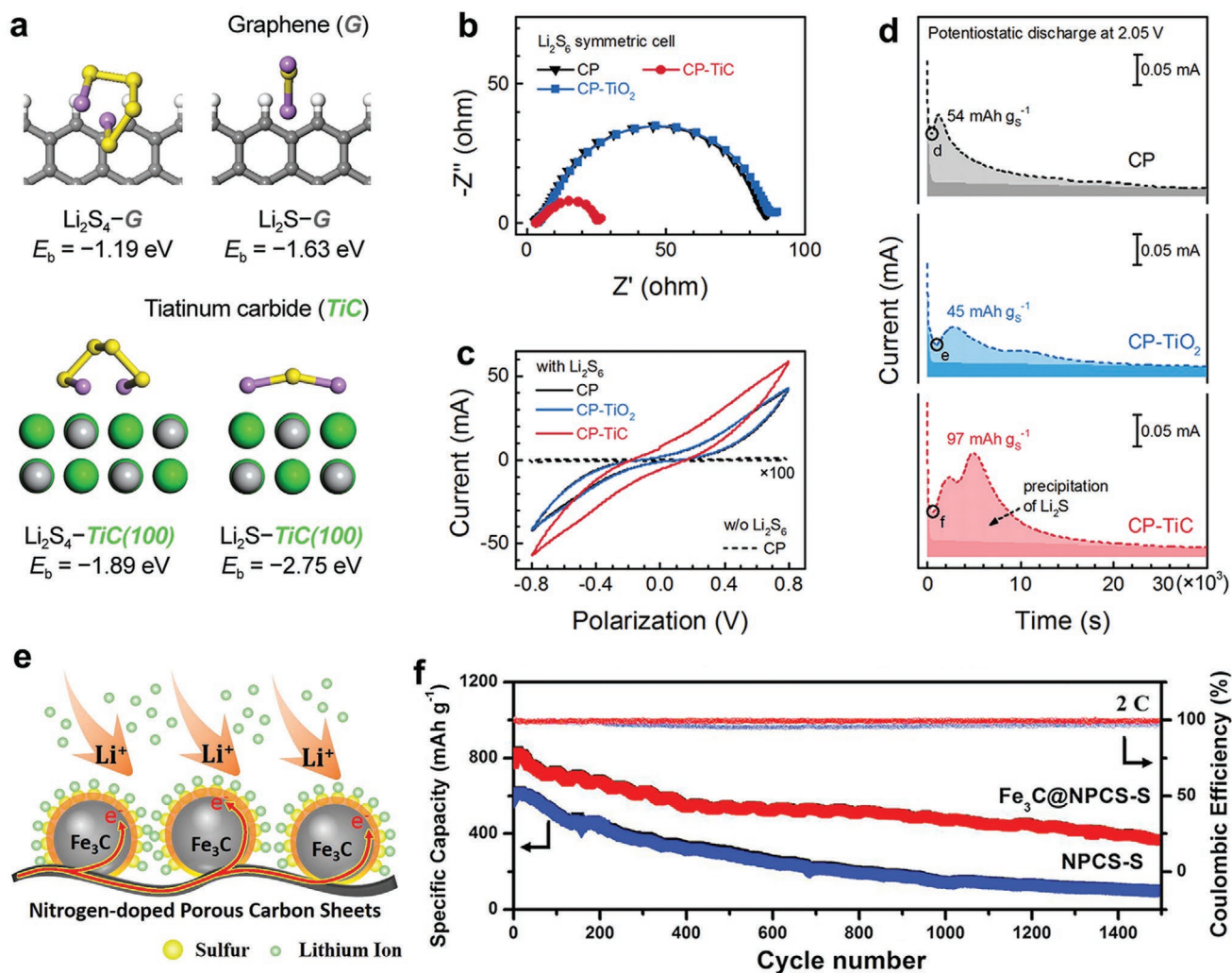
Figure 17. a) Binding energies of TiC at Li_2S_4 and Li_2S compared to pristine graphene. b) EIS and c) CV of symmetric cells. d) Potentiostatic current discharge curves of a Li_2S_8 tetraglyme solution at different substrates. e) Schematic illustration of the role of $Fe_3C@NPCS$ upon cycling. f) Cycling performance of the $Fe_3C@NPCS$-S electrodes at 2 C. (a–d) Reproduced with permission.[285] Copyright 2016, Wiley-VCH. (e,f) Reproduced with permission.[286] Copyright 2019, Elsevier.

impedance spectroscopy (EIS) of symmetric cells in Figure 17b revealed that CP-TiC delivered a significantly decreased impedance, indicating the improved interfacial bonding of TiC with polysulfides. Moreover, a higher redox current of CP-TiC in CV curves (Figure 17c) indicated that conductivity was another favorable impact on the polysulfide conversion. TiC also effectively induced and accelerated the Li_2S precipitation. This can be validated by the potentiostatic discharge tests in a Li_2S_8/tetraglyme solution. As shown in Figure 17d, CP-TiC exhibited a higher capacity of the Li_2S precipitation than CP and CP-TiO$_2$. The authors designed a hybrid sulfur host, incorporating TiC nanoparticles in a mesoporous graphene framework (TiC@G), to validate the superiority of TiC. As a result, a TiC@G/S composite cathode loaded with 3.5 mg cm^{-2} sulfur displayed an enhanced capacity and a more durable lower voltage plateau.

Further research on TiC hosts was based on combining various matrix configurations to improve sulfur cathodes. For instance, Zhou et al. designed a hybrid host covering TiC

nanoparticles at CNFs to develop sulfur cathodes.[287] Taking advantage of the desired conductivity and intense adhesion, the prepared hybrid host material provided fast electron transport pathways and abundant active sites, hence significantly enhancing the cathode utilization.

Cao et al. employed a facile reduction process to incorporate TiC nanoparticles on hollow carbon nanospheres (TiC@C).[288] The uniformly dispersed TiC nanoparticles showed effective adsorption of polysulfides. The novel TiC@C structure helped the composite cathodes to achieve outstanding long-term cycling stability at high rates. By using a supercritical CO$_2$ liquid process, Huang et al. embedded TiC particles in CMK-3 mesoporous carbon (TiC/C).[289] The prepared TiC/C composite with high mesoporous structures displayed a large surface area. Moreover, the uniform distribution of the embedded TiC particles offered adequate sites to anchor polysulfides. The resulting TiC/C-S cathode delivered good capacities at various current densities. Integrating TiC with other metal compounds as
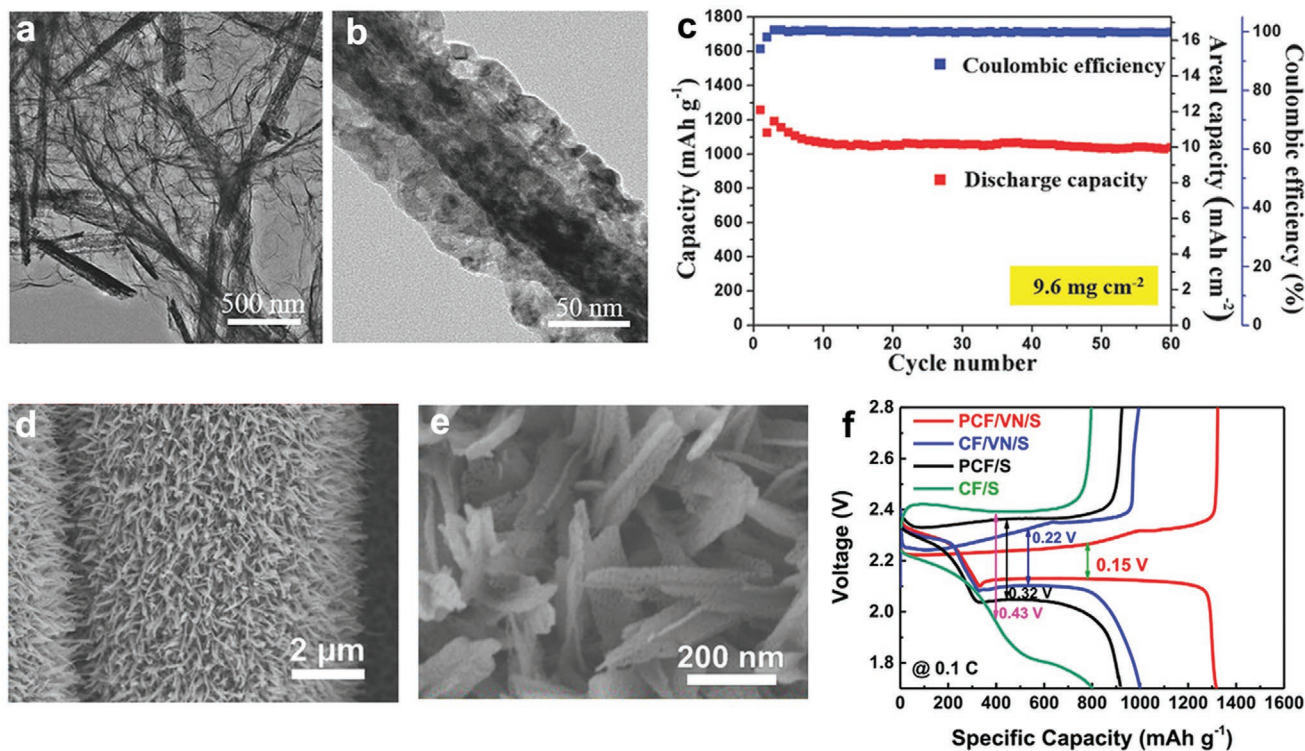
Figure 18. a,b) TEM images of 3DNG/TiN. c) Cycling performance of 3DNG/TiN cathodes with 9.6 mg cm^{-2} sulfur loading. d,e) SEM images of PCF/VN composites. f) Cycling performance of PCF/VN/S cathodes. (a–c) Reproduced with permission.[307] Copyright 2018, Wiley-VCH. (d–f) Reproduced with permission.[48] Copyright 2018, Wiley-VCH.

sulfur host materials may enhance the performance of sulfur cathodes further.

Lang et al. combined the conductivity of TiC and strong adsorption of the TiO$_2$ with respect to polysulfides to synthesize a stable TiO$_2$/TiC composite material as sulfur immobilizers.[290] Such dual effects were reported to be beneficial for the utilization of sulfur cathodes. The TiO$_2$/TiC composites material loaded with various contents of sulfur were investigated. An optimal cathode performance was achieved with 55 wt.% sulfur loading. Another similar TiO$_2$/TiC composite host has also been reported, showing enhanced performance.[291]

6.4.2. Iron Carbides

Due to the high conductivity and effective polysulfide adsorption, iron carbides (Fe$_3$C) have also been employed as sulfur hosts. Wang et al. incorporated uniformly dispersed Fe$_3$C nanoparticles in NPC sheets (NPCS) via a simple carbonization reaction, producing a porous Fe$_3$C@NPCS nanocomposite with high conductivity.[286] As shown in Figure 17e, the carbon sheets allowed the uniform distribution of the Fe$_3$C nanoparticles and accommodated sulfur to mitigate its volume expansion during cycling. The redox kinetics was also accelerated due to the highly conductive NPCS and Fe$_3$C nanoparticles. Moreover, the Fe$_3$C nanoparticles offered strong chemical adsorption to polysulfides, which was confirmed by DFT calculations. The calculated binding energies of the Fe$_3$C (100) surface to Li$_2$S

and Li$_2$S$_2$ were 4.87 and 6.37 eV, respectively. The Fe$_3$C@NPCS composite significantly boosted the utilization of active sulfur species and accelerated the electrochemical performance. Based on these features, the prepared Fe$_3$C@NPCS-S composite delivered electrochemical stability for 1500 cycles at 2 C with only 0.036% capacity loss per cycle (Figure 17f).

Li and co-workers proposed a novel mechanism of polysulfide anchoring by built-in magnetic field enhancement. The authors employed a facile thermal treatment to produce activated cotton textile (ACT), in which ferromagnetic iron/iron carbide (Fe/Fe$_3$C) nanoparticles were in situ grown.[292] The resulting ACT@Fe/Fe$_3$C/S composite revealed a uniform distribution of sulfur. Owing to the ferromagnetic Fe/Fe$_3$C nanoparticles, an intrinsic magnetic field was introduced, which formed a Lorenz force for the cathode. Such effects changed the diffusion pathway of the polysulfide anions and effectively restrained the ions into the cathode. The composite cathode exhibited a distinct electrochemistry. Only a single discharge plateau was observed in the voltage profiles.

Similarly, Liu et al. encapsulated nitrogen-doped CNTs with Fe/Fe$_3$C nanoparticles (Fe/Fe$_3$C@N-CNT) in a carbonized melamine sponge, forming freestanding conductive frameworks to anchor sulfur.[293] As a sulfur host, the hierarchical porosities have large internal voids, allowing a 14.44 mg cm^{-2} sulfur loading. The wrapped Fe/Fe$_3$C nanoparticles in N-CNT effectively suppressed the polysulfide shuttling. The prepared freestanding Fe/Fe$_3$C@N-CNT/S cathodes exhibited remarkably good electrochemical performance. On the basis

of DFT calculations, Li et al. synthesized Fe_3C nanosheets with an ultra-thin thickness of about 1 nm, grown on mesoporous carbon (Fe_3C-MC).[294] The Fe_3C nanosheets provided sufficient active sites to chemically anchor and convert polysulfides. The Fe_3C-MC sulfur composite cathode delivered a 1530 mAh g^{-1} capacity during the initial cycles at 0.1 C.

Using an evaporation-induced self-assembly approach, Wei et al. prepared ordered mesoporous graphitic carbon/Fe_3C nanocomposites (GC/Fe_3C) as sulfur host.[295] The obtained mesoporous GC/Fe_3C composite revealed an ultra-high surface area of more than 3000 m^2 g^{-1}. Together with the high porosities, 85 wt% sulfur was loaded. Due to the desirable charge transport pathways, the prepared sulfur cathode revealed high capacities of up to 1350 mAh g^{-1} at 0.1 C.

6.4.3. Other Carbides

Other carbides, such as B_4C,[296,297] Mo_2C,[298–300] MoC,[301,302] NbC,[84,303] and WC,[304] have also been investigated as sulfur host. For example, Luo et al. designed a simple catalyst-assisted approach to grow B_4C nanowires at CNFs.[296] The obtained B_4C@CNF composite owned several merits for sulfur cathodes: Experimental analyses in combination with DFT calculations confirmed that the chemical anchoring of the B_4C nanowires resulted in the strong polysulfide adsorption. Moreover, B_4C also exhibited a high catalytic activity for sulfur conversion, accelerating the cathode redox kinetics. Such favorable electrode properties contributed to outstanding storage capacities and rate capabilities. As a result, sulfur cathodes, employing B_4C@CNF as host materials, maintained 80% of its original storage capacity after 500 cycles at 1 C.

Wang et al. reported porous molybdenum carbide nanorods (Mo_2C NRs) as a bifunctional sulfur host.[299] XPS spectra proved that Mo_2C NRs strongly anchored polysulfides due to the strong chemical interactions between Mo_2C and polysulfides, resulting in the formation of Mo—S bonds. Due to the introduction of Mo_2C, the activation overpotential of Li_2S was significantly mitigated, implying that Mo_2C facilitated the decomposition of Li_2S during charging. Benefiting from these positive effects, the Mo_2CNRs-S cathodes sustained a long-lasting cycle life of over 500 cycles at 2 C.

Shen et al. incorporated conductive NbC nanoparticles in bowl-like trichoderma spore carbon (TSC) with nitrogen and phosphorus codoping, forming a highly porous TSC/NbC network.[84] As sulfur host, the codoped TSC and conductive NbC enhanced the electron transport and the chemical anchoring of polysulfides. Moreover, the porosities of TSC/NbC networks allowed the uniform distribution of sulfur. The TSC/NbC-S cathode exhibited a discharge capacity of 810 mAh g^{-1} at even 5 C-rate.

6.5. Metal Nitrides

Similar to metal carbides, metal nitrides with polarity also show desirable conductivity and good structural stability, some of which, such as TiN and VN, have been developed to confine active sulfur species.[305]

6.5.1. Titanium Nitrides

Goodenough and co-workers initially introduced mesoporous titanium nitride (TiN) to sulfur cathodes. The prepared TiN-S composite electrodes revealed a good reversibility of more than 500 cycles.[306] Further studies showed that TiN is beneficial to improve the electrochemistry of sulfur cathodes. Li et al. introduced TiN nanowires to in situ grow these on 3D nitrogen-doped graphene (3DNG), forming a freestanding architecture.[307] As shown in **Figure 18**a, uniform TiN nanowires were tightly attached to the wrinkled graphene nanosheets. The TiN surface was coarse and porous (Figure 18b). This structure was able to provide abundant sites to adsorb polysulfides. DFT calculations showed that the TiN nanowires revealed strong chemical bonding with polysulfides. The binding energies of various sulfur species on TiN (200) surfaces were in a range from 3.28 to 4.60 eV. This result was consistent with the XPS analyses, in which the S—N—Ti bonding was observed. When employed as sulfur host, the interconnected 3DNG/TiN networks enabled efficient pathways for charge transfer and enough space for sulfur loading. The composite cathode loaded with 4.8 mg cm^{-2} sulfur delivered a capacity of 1510 mAh g^{-1} at 0.5 C. Moreover, with a higher sulfur loading up to 9.6 mg cm^{-2}, 3DNG/TiN achieved an ultrahigh areal capacity of 12.0 mAh cm^{-2} (Figure 18c). This work provided a high potential for high energy density Li–S batteries.

Considering the inherent surface properties, Lim et al. designed a hierarchically porous TiN (h-TiN) to boost high-rate sulfur cathodes.[308] The hierarchical porosities were generated via a tunable evaporation-induced self-assembly approach. Owing to the multiscale porous structure, the prepared h-TiN effectively anchored sulfur species. This has been confirmed by XPS studies. In contrast to bare h-TiN, Li_2S_8-treated h-TiN showed new peaks of Ti—S and Ti—N—S bonds, implying the chemical bonding between Li_2S_8 and h-TiN. h-TiN also showed good electrocatalytic properties. Compared with the mesoporous carbon, h-TiN exhibited enhanced current intensities and beneficial peak shifts in CV, implying mitigated polarization and facilitated redox reactions of sulfur species. Because of these advantages, the h-TiN hosts, loaded with 72 wt% sulfur, sustained over 1000 cycles at 5 C with a storage capacity of up to 557 mAh g^{-1}. Besides, various structures of TiN, such as hollow spheres[32,309,310] and tubes,[311] have been studied to make sulfur cathodes more efficient.

6.5.2. Vanadium Nitrides

Vanadium nitrides (VN) have desirable conductivities and strong bonding capabilities with respect to polysulfides. Combining porous VN nanoribbons with graphene, Sun et al. confirmed that VN was able to anchor polysulfides and accelerated their electrochemical conversion. By facile chemical etching, associated with a solvothermal-supercritical fluid process, Zhong et al. fabricated VN arrays onto PCFs.[48] An acid-etched PCF was used as substrate to grow V_2O_5 via a solvothermal reaction. Subsequent annealing under NH_3 produced PCF/VN scaffolds. From the SEM observation (Figure 18d,e), vertically aligned VN nanobelts with an average of 150–200 nm in diameter were uniformly covering PCF. The interconnected porous PCF exhibited a large surface area, allowing high sulfur

loadings and physically retarding the polysulfide shuttling. In addition, the conductive VN arrays showed strong chemical adsorption, tightly locking polysulfides inside the pores. Consequently, the designed PCF/VN/S electrode achieved a highly steady capacity of more than 1300 mAh g^{-1} (Figure 18f). The structural merits made PCF/VN/S lower cell polarization with the smallest voltage gap than other counterparts.

Ren et al. also noticed the positive effects of VN on the polysulfide immobilization. They synthesized homogenous yolk–shell VN nanospheres with cobalt doping (Co-VN) by a template-free solvothermal reaction followed by a calcination process.[312] A thin nitrogen-doped carbon was further coated on Co-VN to prepare a Co-VN@C composite as sulfur host. This yolk–shell structure confined polysulfides in the enclosed cavities and alleviated the volumetric swelling upon cycling. The conductive polar VN gave rise to good electronic conductivity and strong affinity with respect to polysulfides. Co-doped VN also showed good electrocatalytic properties. The electrode capacity of Co-VN@C/S reached nearly 1400 mAh g^{-1} at 0.1 C. The results of other investigations, including VN nanowires[313] and nanobubbles,[314] have also been reported, showing the efficient suppression of polysulfide shuttling.

6.5.3. Other Nitrides

The exploration of various other nitrides to confine sulfur species has also been carried out. Such sulfur hosts include Co$_4$N,[85,315,316] WN,[317,318] NbN,[319] BN,[320] and MoN.[321] For instance, Xiao et al. fabricated Co$_4$N nanoparticles homogeneously embedded in 2D nitrogen-doped carbon grown onto carbon cloth.[85] As a freestanding electrode, it significantly boosted the rate capabilities and cycling performance. Theoretical simulations and experimental results showed that Co$_4$N nanoparticles were able to generate strong chemical anchoring toward polysulfides. Moreover, the catalytic activities of Co$_4$N benefited the conversion of polysulfides and the precipitation of Li$_2$S, resulting in accelerated redox kinetics and mitigated cell polarization. These freestanding sulfur cathodes achieved a high capacity up to 1425 mAh g^{-1} at 0.1 C. A storage capacity still reached 745 mAh g^{-1} after 400 cycles.

Huang and co-workers explored the interaction between WN and polysulfides.[317] They designed 3D porous WN foam blocks as reservoirs to spatially confine sulfur species inside the pores. Theoretical calculations demonstrated that the chemisorption strength of WN toward active sulfur species varied during the lithiation process. For soluble polysulfides, the binding energies gradually decreased from Li$_2$S$_8$ to Li$_2$S$_4$, while a significant binding energy recovery occurred for the insoluble Li$_2$S$_2$ and Li$_2$S. The prepared composite cathode delivered high rate capabilities. The capacities at 0.5 and 5 C reached 1090 and 510 mAh g^{-1}, respectively. Ye et al. fabricated a 2D MoN-VN heterostructure as a model sulfur host material.[321] The integration of V allowed tailoring the electronic structure of MoN. The strong coupling between MoN and VN considerably promoted the polysulfide adsorption. MoN-VN-based cathodes loaded with 3.0 mg cm^{-2} sulfur combined a storage capacity of up to 708 mAh g^{-1} at 2 C with a relatively low capacity loss of 0.068% per cycle during the first 500 cycles.

6.6. MXenes

MXenes are a class of 2D transition metal carbides, nitrides, or carbonitrides with only a few atom-thick layers.[322] Their typical formula is M$_{n+1}$X$_n$T$_x$ ($n = 1–3$), in which M represents transition metals, X refers to carbon and/or nitrogen, and T$_x$ stands for surface functional groups, such as hydroxyl, oxygen, or fluorine. In an MXene structure, $n+1$ M layers and n X layers alternately stack, forming an [MX]$_n$M arrangement. Various MXene compositions have successively been synthesized since they were first reported in 2011.[323] Due to the structural characteristics, MXenes have high conductivity and are rich in the number of active surface sites, which make them promising candidates for sulfur host materials.[324–326] The number of MXene chemistries are meanwhile expanding, for example, to Ti$_3$C$_2$T$_x$,[327,328] Ti$_2$CT$_x$,[88] and Mo$_2$CT$_x$.[329]

Nazar and co-workers initially investigated the application of MXenes for sulfur cathodes. They proposed Ti$_2$C to be an excellent sulfur host.[88] Benefiting from the high metallic conductivity and desirable anchoring effect, Ti$_2$C with 70 wt% sulfur content displayed a long-term cycling stability. XPS analyses determined that the exposed terminal Ti atoms acted as Lewis acid sites to form strong Ti—S bonds with active sulfur species.

In their follow-up study, the authors further investigate the surface interaction between polysulfide species and two new MXene materials (Ti$_3$C$_2$ and Ti$_3$CN).[91] XPS studies (**Figure 19**a,b) revealed that both of the Li$_2$S$_4$-treated Ti$_3$C$_2$ and Ti$_3$CN composites indicated significant Ti-S interaction by a peak from a Ti—S bond (455.6 eV). This can be ascribed to the strong Lewis acid–base interaction between Ti atoms and polysulfide ions. The corresponding S 2p spectra of the Li$_2$S$_4$-treated MXene confirmed the formation of thiosulfate and polythionate complexes, implying the reduction of the hydroxyl terminal groups on MXene. On the basis of the XPS analyses, a two-step process was proposed to describe the interaction between MXene and polysulfides, as illustrated in Figure 19c. The hydroxyl groups of Ti$_3$C$_2$ and Ti$_3$CN initially underwent a redox process with polysulfides to produce thiosulfate/polythionate species, resulting in the cleavage of Ti—OH bonds and exposure of acid-active sites. Subsequently, the exposed Ti atoms with empty orbitals accepted electrons from the electronegative polysulfides, forming S—Ti bonds through Lewis acid–base interactions. Such dual adsorption of polysulfides enabled uniform Li$_2$S deposition and substantially suppressed the diffusion of polysulfides. The authors incorporated CNTs into these TMXene layers, building sulfur hosts with a porous conductive network. The storage capacities of about 450 mAh g^{-1} after 1200 cycles were achieved with a fading rate of 0.043% per cycle.

6.6.1. Functionalized MXenes

Considering the abundant surface functional groups of MXenes, investigating their interactions with polysulfide species is beneficial to the design of better sulfur-anchoring host materials. Relevant theoretical studies have been conducted on O/F-functionalized Ti-based MXenes.[332–334] These simulation results demonstrated that O/F-functionalized groups can
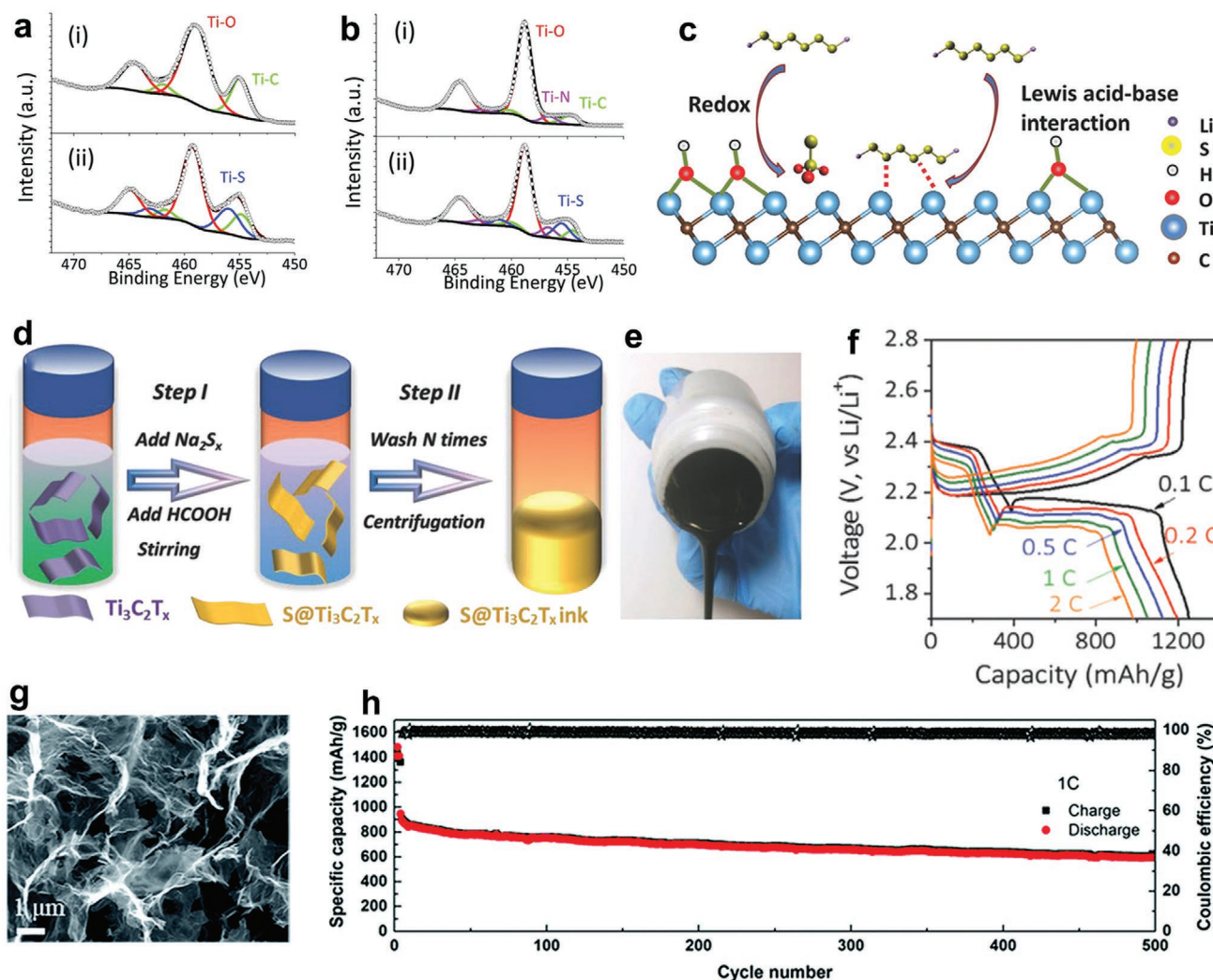
Figure 19. a) Ti 2p spectra of Ti$_3$C$_2$ (i) and Ti$_3$C$_2$-Li$_2$S$_4$ (ii). b) Ti 2p spectra of Ti$_3$CN (i) and Ti$_3$CN-Li$_2$S$_4$ (ii). c) Schematic representation of the interaction between a representative hydroxyl-decorated MXene phase and polysulfides. d) Preparation scheme and e) optical image of S@Ti$_3$C$_2$T$_x$ ink. f) Voltage profiles of 70% S@Ti$_3$C$_2$T$_x$ at various current rates. g) SEM image of a MX/G-30 aerogel. h) Long-term cycle life performance of a Li–S cell with a MX/G-30 cathode for 500 cycles at 1 C. (a–c) Reproduced with permission.[91] Copyright 2017, Wiley-VCH. (d–f) Reproduced with permission.[330] Copyright 2018, Wiley-VCH. (g,h) Reproduced with permission.[331] Copyright 2019, Royal Society of Chemistry.

effectively anchor active sulfur species. Experimental results further revealed their immobilization mechanism.

For instance, Tang et al. encapsulated nanoscale sulfur particles into 2D Ti$_3$C$_2$T$_x$ nanosheets to form a viscous aqueous ink. By vacuum-filtration, such ink could directly form a freestanding and flexible S@Ti$_3$C$_2$T$_x$ electrode.[330] A facile two-step process resulted in the formation of an S@Ti$_3$C$_2$T$_x$ ink (Figure 19d). With sodium polysulfides and formic acid in a Ti$_3$C$_2$T$_x$ suspension, sulfur was in situ formed. The uniform and viscous S@Ti$_3$C$_2$T$_x$ ink was obtained after washing and centrifugation (Figure 19e). According to the experimental analyses, the authors discovered that a thick sulfate complex layer was in situ formed as protective barrier, mitigating the migration of polysulfides from the sulfur cathodes. Consequently, the S@Ti$_3$C$_2$T$_x$ electrodes with 70 wt% sulfur loading revealed favorable rate capabilities. A good capacity of 1244 mAh mg^{-1} at 0.1 C was achieved (Figure 19f).

On the basis of a similar strategy, Tang et al. further developed another robust and freestanding Ti$_3$C$_2$T$_x$/S paper by a filtration–evaporation approach. As a sulfur cathode, this Ti$_3$C$_2$T$_x$/S paper exhibited a durable cycling performance and ultralow capacity fading.[335] Besides, S-functionalized groups have also been introduced to MXenes for anchoring polysulfides.[336] The moderate adsorption of polysulfides from S-functionalized V$_2$C not only effectively restricted the shuttling but also prevented polysulfide decomposition.

6.6.2. MXene Composites

Due to the hydrogen bond formation, surface functional groups in MXenes may cause the restacking of MXene nanosheets. Such aggregation considerably decreases the active area and the number of anchoring sites. Therefore,

various conductive carbons and inorganic compounds have been integrated with Mxenes in order to achieve enhanced capacity and increased cycle life.[337–341] The Wang group developed a series of 3D MXene/carbon hybrid structures to further improve Li–S batteries.[331,342,343] For example, they reported a hybrid 3D $Ti_3C_2T_x$@mesoporous carbon architecture ($Ti_3C_2T_x$@Meso-C) as sulfur host material.[342] The introduced Meso-C has a homogeneously porous structure, which offered sufficient voids for sulfur incorporation and effectively reduced the swelling of sulfur cathodes. Moreover, due to the strong hydrophilic surface, the $Ti_3C_2T_x$ nanosheets were successfully stabilized by Meso-C. XPS analyses demonstrated the chemisorptive nature of $Ti_3C_2T_x$ nanosheets. With sulfur loading, S—Ti—C bonds were formed during the heat treatment. The resulting $Ti_3C_2T_x$@Meso-C/S cathodes attained an initial storage capacity of 1225.8 mAh g^{-1} at 0.5 C and 704.6 mAh g^{-1} after 300 cycles.

Wang and co-workers further designed a freestanding 3D porous $Ti_3C_2T_x$/rGO hybrid aerogel (MX/G) as polysulfide reservoir.[331] An MX/G composite cathode was directly obtained with the Li_2S_6 catholyte. The 3D interconnected network (Figure 19g) offered high conductivity and enabled fast Li^+ diffusion. The planar polar interface of $Ti_3C_2T_x$ chemically anchored polysulfides via Ti—S bonds. This 3D porous MX/G substantially boosted the cathode utilization and improved the sulfur reaction kinetics. The optimal MX/G aerogel cathode with 30% $Ti_3C_2T_x$ (MX/G-30) revealed a high capacity of 1270 mAh g^{-1} at 0.1 C and a prolonged cycle life with very low capacity fading of only 0.07% per cycle (Figure 19h). In addition, cathodes loaded with high sulfur content up to 6 mg cm^{-2} attained a 5.27 mAh cm^{-2} areal capacity. The Wang group also explored the heteroatom doping strategy to MXenes.[31] Nitrogen doping applied to MXene nanosheets revealed a strong physical and chemical adsorption toward polysulfides.

6.7. Metal–Organic Frameworks

MOFs are compounds composed of metal ions coordinated with organic linkers. Due to the diversity of the coordination between metal ions and organic linkers, MOFs possess tunable chemical composition, structures, and porosity making these materials highly interesting for applications in energy, catalysis, and gas storage. With regard to Li–S batteries, the intrinsic porosity of MOFs enables high sulfur loading and deep electrolyte penetration. In addition, MOFs have abundant metal sites, which can serve as Lewis acid to anchor sulfur species. Based on these advantages, MOFs are promising candidates to be applied as sulfur host materials. Another merit is that the tunable properties allow MOFs as good precursor materials to construct various nanoscale materials with favorable porosity. By either direct annealing or template-engaged reactions, MOF precursors can readily convert into porous/hollow nanocarbon or metal-based architectures, including oxides, hydroxides, and sulfides. Such MOF-derived materials are also promising sulfur hosts, which have been discussed in detail above. In this section, we mainly focus on pristine MOFs and MOF composites as sulfur host materials.

6.7.1. Pristine MOFs

Pristine MOFs were initially introduced to Li–S batteries by Tarascon and co-workers. They employed MIL-100 (Cr) as the sulfur host.[344] Combining TEM and XPS analyses, the pores of MIL-100 (Cr) were confirmed to reversibly capture and release polysulfides upon cycling, and the S-MOF interaction was demonstrated. Such effects contributed to the increased capacity retention of sulfur cathodes. The adsorption of MOFs toward polysulfides has been investigated by theoretical calculations. Park et al. revealed that the coordinately unsaturated metal sites (CUS) of MOFs were responsible for the dominant adsorption of all sulfur species.[345] The anchoring of polysulfides was tunable by substituting CUS. Sixteen metal-substituted variants of MOF-74 were computationally screened as optimal compositions, exhibiting outstanding anchoring to polysulfides. Li et al. investigated the adsorption of a Cu-benzenehexathiol (Cu-BHT) monolayer toward sulfur species via first-principles calculations.[346] The results showed that the Cu-BHT monolayer had a moderate interaction with polysulfides to suppress their dissolution. In addition, Cu-BHT enabled the uniform deposition of Li_2S, improving the sulfur utilization and enhancing the conversion between polysulfides and Li_2S.

Due to the nature of MOFs as Lewis acid, tailoring the coordination of metal ions is a major strategy to anchor polysulfides.[347] Baumann et al. systematically analyzed favorable sulfur adsorption sites of CuBTC via theoretical calculations and experiments.[348] They found that the decrease in particle size of CuBTC caused increased density of Cu sites, which substantially improved the polysulfide retention and discharge capacity. Hong et al. developed a bi-functional nano-sized MOF (Cu-TDPAT) as a sulfur host material.[349] Cu-TDPAT combined the Cu(II) Lewis acidic sites with the nitrogen Lewis basic sites from the ligands to anchor sulfur species and lithium ions. By further optimizing the particle size, Cu-TDPAT with an average size of 100 nm effectively anchored polysulfides. The prepared S@Cu-TDPAT cathode exhibited a prolonged 500 cycle cell lifespan at 1 C with a stable capacity of about 745 mAh g^{-1}.

Liu et al. synthesized a unique manganese cluster-based porous MOF (Mn-CC-xH$_2$O).[350] As illustrated in **Figure 20**a, the coordinated water molecules in Mn-CC-xH$_2$O were readily removed by thermal activation, resulting in the conversion from the central Mn ions to unsaturated metal sites. With the elimination of coordinated water molecules, the activated Mn-CC provided abundant open metal Lewis acid sites to anchor polysulfides. Integrating the porosity of Mn-CC as sulfur host effectively inhibited the polysulfide shuttling through spatial confinement and chemical anchoring. The resulting composite cathode delivered a 1420 mAh g^{-1} capacity during the initial cycles at 0.2 C and stabilized at 990 mAh g^{-1} after 200 cycles (Figure 20b). Other research involving highly conductive Ni-based MOF of $Ni_3(HITP)_2$ has been synthesized by Cai et al., which revealed favorable adsorption of polysulfides and enhanced electrochemical performance.[351]

6.7.2. MOF Composites

Despite the superiority of MOFs, their poor conductivity incurs severe cell polarization and sluggish redox kinetics of sulfur
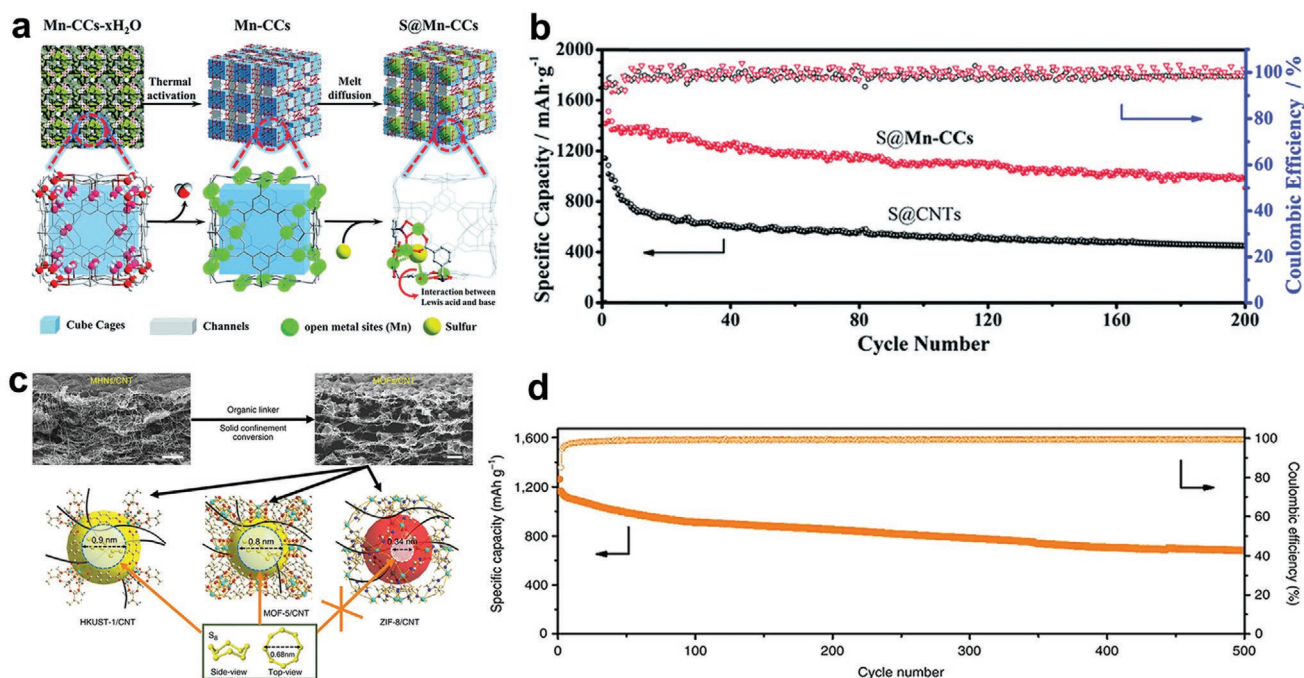
Figure 20. a) Schematic diagram of the various synthesis steps to produce S@Mn-CC. b) Voltage profiles of an S@Mn-CC and S@CNT electrodes at 0.2 C. c) Synthesis of S_8 loaded MOF/CNT composite thin films. d) Cycle life of an S@HKUST-1/CNT electrode. (a,b) Reproduced with permission.[350] Copyright 2019, Royal Society of Chemistry. (c,d) Reproduced with permission.[352] Copyright 2017, Springer Nature.

cathodes. Moreover, the structural fragility of MOFs also causes performance instability of batteries upon prolonged cycling. Constructing flexible and highly conductive MOF composites is capable of overcoming these hurdles. There have been many studies that introduce CNTs,[352–354] rGO,[355] polymers,[356] and other carbon materials[357] to MOFs to produce composite materials. For instance, Mao et al. designed a foldable interpenetrated MOF/CNT thin film as binder-free and flexible host.[352] Such films possess a hierarchically porous structure of 3D conductive networks, in which sulfur species were anchored by the hierarchical pores and open metal sites of MOFs. The interwoven CNTs contributed to the enhanced conductivity and structural integrity of electrodes. The authors compared three MOFs (HKUST-1, MOF-5, and ZIF-8) with different pore sizes to determine the porosity effects on the electrochemistry of sulfur cathodes (Figure 20c). The results revealed that the loaded S_8 ring with a diameter of 0.68 nm was barely encapsulated in the cavity of ZIF-8 with an entrance of 0.34 nm, which was mainly dispersed at the surface of ZIF-8. The narrow pore effect gave rise to poor utilization of sulfur and fast capacity decay. With regard to MOF-5, the 0.8 nm entrance size was sufficient for S_8 to access the cavity, but such size was still smaller than HKUST-1. These relatively small pores resulted in fast capacity fading in the initial cycles. Furthermore, the open copper sites of HKUST-1 were able to anchor polysulfides via Lewis acid–base interactions, while the lack of open metal sites in MOF-5 and ZIF-8 was not. Benefiting from these advantages, the selfstanding S@HKUST-1/CNT cathode exhibited an initial capacity of 1263 mAh g^{-1} at 0.2 C and sustained 500 cycles, in which the capacity decayed only 0.08% per cycle (Figure 20d).

The enhancement in conductivity of MOFs will contribute to high rate sulfur cathodes. Jiang et al. combined PPy with

MOFs, resulting in increased conductivity by 5 to 7 orders of magnitude.[358] The constructed PPy-MOF composites with proper ion channels promoted ion diffusion and achieved high rate performance. PCN-224 with cross-linked pores and tunnels enabled shortest ion diffusion pathways and provided the largest pore apertures, leading to the fastest ion transfer. As a result, even at 10 C, the PPy-S-in-PCN-224 composite cathode exhibited a 680 mAh g^{-1} capacity from the first cycle and sustained 440 mAh g^{-1} after 1000 cycles.

Liu et al. presented a 3D free-standing monolithic electrode comprising ZIF-67 and HKUST-1 well dispersed in highly conductive N, P codoped carbon.[359] The 3D monolithic carbon network enabled the encapsulation and electrical correlation of MOF nanodomains, which were responsible for prolonged capacity retention of sulfur species and increased sulfur loading. An optimized 3D carbon-HKUST-1 cathode achieved high areal and volume capacities of 16 mAh cm^{-2} and 1231 mAh cm^{-3} at 0.2 C, respectively. Besides, the combination of PPy and ZIF-67 has also been proven to have improved electrochemical performance for Li–S batteries.[360] These results demonstrated that MOFs with proper entrance pore sizes and open metal sites are favorable for high volumetric energy density cathodes.

Overall, various metal compound host materials employed in Li–S batteries significantly improve the sulfur utilization and battery cycling stability. Their strong polysulfide anchoring, resulting from chemical bonding, effectively inhibits the shuttle problem of polysulfides. Furthermore, in combination with other nanostructured carbon, metal compound hosts are able to improve the electrochemical performance enabling long-life Li–S batteries. **Table 3** summarizes the latest research advances on metal compound host materials applied in Li–S batteries.

Table 3. Summary of performance parameters for metal compound host materials used in Li–S batteries.

Host material	Sulfur content [wt%][a]	Sulfur loading [mg cm^{-2}]	Voltage range [V]	Rate [C][b]	Cycle number	Initial capacity [mAh g^{-1}]	Retained capacity [mAh g^{-1}]	Ref.
TiO$_2$ microboxes	49	1.0	1.8–2.6	1.0	500	605	626	[181]
C@TiO$_2$@C	61	2.5	1.5–3.0	2.0	500	774	511	[184]
HCS@Ti$_4$O$_7$	56	N/A	1.6–2.8	0.5	800	1168	609	[186]
Heterostructured TiO$_x$	46.4	0.8–1.0	1.7–2.8	1.0	1000	694	412	[187]
MnO$_2$	56.6	1.7–2.1	1.5–3.0	0.5	1500	898	644	[195]
MnO$_2$@HCB	51	0.7–1.0	1.7–2.8	4.0 (A g^{-1})	200	496	N/A	[196]
MnO/MPC	52	2.8	1.0–2.8	1.6 (A g^{-1})	150	475	290	[201]
Mn$_3$O$_4$@CNF	50	11.0	1.7–2.8	0.1	70	1055	744	[197]
N-doped Co$_3$O$_4$	60	2.13	1.7–2.7	2.0	1000	≈900[c]	611	[207]
Co$_3$O$_4$/C	56	1.4	1.8–2.7	1.0	500	889	520	[58]
CoO/Co	61.2	3.0	1.7–2.8	1.0	300	N/A	514	[209]
YSC@Fe$_3$O$_4$	64	5.5	1.8–2.8	0.1	200	1104	854	[208]
Fe$_3$O$_4$ nanoparticles	N/A	3.85	1.7–2.8	0.1	100	N/A	1007	[214]
NiCo$_2$O$_4$	52.5	1.3–1.5	1.7–2.8	1.0	1500	1171 (mAh cm^{-3})[d]	487 (mAh cm^{-3})[d]	[222]
ZnCo$_2$O$_4$	50	1.1-1.3	1.7–2.8	0.8 (A g^{-1})	200	1322	761	[224]
VO$_2$@rGO	53	1.5	1.7–2.8	0.2	370	1358	1049	[225]
Co$_9$S$_8$	60	1.5	1.8–3.0	0.5	1500	≈890[c]	≈290[e]	[244]
Co$_3$S$_4$	59	2.0	1.6–2.6	5.0	1000	517	305	[247]
MoS$_{2-x}$/rGO	60	1.5	1.8–2.6	0.5	600	≈1200[c]	628	[67]
MoS$_2$/rGO	56	0.85	1.7–2.8	1.0	300	≈830[c]	480	[82]
NiS@C-HS	50	2.3	1.7–2.8	0.5	300	723	695	[254]
NiS$_2$-RGO	75	21	1.7–2.8	0.2	50	776	N/A	[253]
TiS$_2$	65	12	1.7–3.0	0.2	200	959	605	[83]
TiS$_2$ nanosheets	56	7.7	1.8–2.8	0.1	100	1025	767	[262]
rGO-VS$_2$	51.2	1.15	1.5–3.0	1.0	1200	1130	879	[263]
C@WS$_2$	11	1.0–1.2	1.7–2.7	2.0	1500	563	502	[272]
Nickel-based hydroxide	32	4.3	1.8–2.8	0.5	350	838	650	[279]
Ni/Fe LDH	49	2.0–3.0	1.7–2.8	1.0	1000	844	501	[57]
CoOOH	64	1.0–1.3	1.6–2.8	1.0	500	N/A	376[d]	[278]
TiC	55	3.5	1.7–2.8	0.2	100	1032	670	[285]
Fe$_3$C@NPCS	59.6	1.5	1.8–2.8	2.0	1500	≈800[c]	≈370[e]	[286]
B$_4$C@CNF	70	2.0	1.6–3.0	1.0	500	1020	815	[296]
Mo$_2$C	53	0.8–1.2	1.6–2.8	1.0	500	968	669	[299]
TiN	N/A	9.6	1.6–2.8	0.5	60	≈1250[c]	≈1000[e]	[307]
Porous TiN	57.6	1.5–2.0	1.7–2.8	5.0	1000	662	557	[308]
PCF/VN	60.1	8.1	1.7–2.8	0.1	250	1310	1052	[48]
VN nanospheres	49	1.3–1.5	1.6–3.0	1.0	300	800	602	[312]
WN	47	0.92	1.7–2.8	2.0	500	1050	358	[317]
MoN-VN	58.5	3.0	1.7–2.8	2.0	500	N/A	708	[321]
Ti-based MXenes	≈64	1.5	1.7–3.0	0.5	1200	N/A	450	[91]
Ti$_3$C$_2$T$_x$	70	2.49	1.7–2.8	0.2	800	1184	724	[330]
MX/G	45	6.0	1.7–2.8	1.0	500	946	596	[331]
Cu-TDPAT	40	1.2	1.8–2.8	1.0	500	900[c]	745	[349]
Mn-CC	49	2.0	1.7–2.8	0.2	200	1420	990	[350]
HKUST-1/CNT	40	1.0	1.7–2.8	0.2	500	1263	758	[352]

[a]Sulfur content in cathodes; [b]1 C ≈ 1675 mA g^{-1}; [c]Initial; [d]Capacity with respect to composites; [e]Retained capacity estimated from the figure as the specific value was not given in the reference.

ADVANCED
SCIENCE NEWS
www.advancedsciencenews.com

ADVANCED
ENERGY
MATERIALS
www.advenergymat.de

7. Conclusions and Outlook

In this review, recent advances in various sulfur host materials anchoring polysulfides have been comprehensively discussed. Two anchoring strategies were shown to be important: physical confinement and chemical bonding. With regard to physical confinement, sulfur hosts with porous and layered or shelled electrode structures can serve as physical barriers to successfully confine polysulfides upon cycling. As for chemical bonding, four chemical interactions between sulfur hosts and active sulfur species have been identified: 1) polar–polar interactions; 2) Lewis acid–base interactions; 3) redox interactions; 4) covalent binding interactions. These four interactions can effectively confine polysulfides by chemical anchoring.

Combining the characteristics of the physical confinement and chemical bonding, various sulfur hosts have been proposed and synthesized. Subsequently, three classes of sulfur host materials have been discussed: 1) nanostructured carbon; 2) polymers; 3) metal compounds. A number of studies have demonstrated that all three materials are able to inhibit active sulfur species from diffusing into the electrolyte. Nanostructured carbon hosts generally suppress the polysulfide diffusion from cathodes by physical confinement due to their diverse structures and large surface area. Soluble polysulfides can be tightly stowed away in the pores, cavities, or layers of the carbon architecture, leading to significant increases in sulfur utilization and electrochemical performance. Furthermore, nonpolar carbon-based materials can also be converted into polar host materials by adopting certain approaches, such as doping. Consequently, these polar carbon hosts simultaneously own the physical confinement and chemical bonding toward sulfur species.

The multifunctional advantages of polymers also play an essential role in enhancing the utilization of sulfur cathodes. Their readily tunable structure and abundant surface groups integrate the physical confinement and chemical bonding ability to anchor sulfur species. Another important characteristic is that polymers can immobilize sulfur by covalent bonding. In sulfurized polymers, sulfur is covalently bonded to the backbones of polymers via the C—S bonds. As a result, no soluble polysulfides exist during the whole charging and discharging process. The shuttle problem can, therefore, be completely eliminated.

Metal compounds are another major type of sulfur host. The anchoring of polysulfides by metal compound hosts has been developed making use of the various mechanisms. Several metal compound hosts have been analyzed with respect to their fundamental polysulfide-anchoring properties. The intrinsic polarity allows metal compounds to strongly bind with polar polysulfides. The active sites of metal compounds can chemically anchor polysulfides via polar–polar and Lewis acid–base interactions. Some of the metal compounds have been shown to catalyze the conversion of active sulfur species by redox interactions. The chemical interactions concluded in this review are able to explain most anchoring mechanisms of metal compound hosts toward polysulfides. On the other hand, the poor conductivity of many metal compounds also incurs a sluggish charge transfer and high electrochemical polarization. These drawbacks impede the charge transfer reaction kinetics. The prevalent solution is, therefore, to integrate highly conductive carbon with metal compounds to fabricate composite host materials.

The discussion above has identified that the three classes of host materials are promising for high-performance Li–S batteries. However, the different types of host materials exhibit distinct improvement in terms of battery capacity, cycle life, and rate capability. Due to the high conductivity and large surface area, nanostructured carbon hosts favor a high rate capability. They can facilitate electron/ion pathways and accelerate charge transfer. Therefore, battery polarization is significantly mitigated. Some of the conductive polymer hosts also reveal such characteristics. In addition, sulfurized polymers can achieve more durable cycle life owing to the elimination of polysulfide shuttling. As regards metal compounds, their favorable chemical bonding to polysulfides suppresses the polysulfide loss and improves the utilization of active species. Thus, better battery capacity and cycle life are expected. If we take all characteristics into account, conductive polar metal compounds would be the most promising host materials at this moment, which can achieve high sulfur utilization and fast redox kinetics. This class of host materials intrinsically possesses two major advantages: 1) high conductivity for charge transfer; 2) strong anchoring effects on polysulfides. Integrating rational structural design and tailoring, they are expected to solve the current problems of sulfur cathodes. Significant outcomes have confirmed that some conductive polar metal compounds, such as manganese oxides,[89,195] titanium oxides,[78,191] cobalt sulfides,[81,244,247] and VN,[52] can successfully achieve balanced performance in terms of capacities and rate capabilities.

By reviewing various sulfur host materials, it can be concluded that there are still several problems that should be further investigated. The first one is the amount of host material in the electrodes. Since the major merit of Li–S batteries compared with traditional Li-ion counterparts is the high energy density, the electroactive species in sulfur cathodes should be kept as high as possible to achieve this highly relevant energy density. The reported sulfur/host composites normally contain 20–30 wt% host materials. Together with the conductive agent and binder, the actual active sulfur mass in the electrodes is mostly below 75 wt%. This value is notably inferior to that of commercial Li-ion batteries, in which the electroactive species can account for as high as 95 wt% of the whole electrode. Moreover, because of the low density of sulfur and the large porosity of cathodes, Li–S batteries typically exhibit only limited volumetric energy densities. The excessive use of host materials will further decease this volumetric energy density.

In order to achieve commercial applications, decreasing the content of host materials should therefore be explored in more detail. The present approach mainly focuses on ex situ integrating host materials with sulfur to fabricate host/sulfur composites. The exploration of the in situ formation of robust protection layers at the surface of sulfur cathodes might be effective to protect sulfur species from dissolving into the electrolyte. Electrolyte tuning or physical/chemical pre-treatment may play a vital role in constructing such layers. Relevant studies are barely reported.

Another problem that has been extensively addressed is the interaction between sulfur hosts and polysulfides. Both theoretical calculations and experimental results have

**ADVANCED
SCIENCE NEWS**

www.advancedsciencenews.com

**ADVANCED
ENERGY
MATERIALS**

www.advenergymat.de

demonstrated that these interactions contribute to the polysulfide confinement. However, there have not been sufficient studies to clarify the underlying interaction mechanisms. The chemical bonding between the surface sites of the host materials and sulfur species typically combined different interactions, for example, polar–polar and Lewis acid–base interactions, which are difficult to be distinguished using a single characterization approach. In addition, the interaction strength is another major factor that affects the utilization of sulfur cathodes. The stronger the interaction, the stronger the bonding. However, a too strong bonding will negatively influence the conversion of sulfur species and cause their decomposition and consequently capacity loss. A more detailed understanding of the mechanisms will help to design even more efficient host materials and reduce the host material content in sulfur electrodes.

The third problem is related to the catalytic properties of host materials. Many metal compounds exhibit high electrocatalytic activities that facilitate the electrochemical conversion of active sulfur species during cycling. This promotes sulfur utilization and the redox kinetics, significantly improving the battery performance. However, the catalytic mechanism of host materials is still inadequate, which is expected to be further elucidated from theoretical and experimental analyses. In addition, host materials with favorable catalytic properties only are unable to prevent the polysulfide diffusion from the cathodes. For instance, when a sulfur cathode partly discharges above 2 V and then stops, in which sulfur species mainly exist in the form of soluble polysulfides, the catalytic effects will also stop. In this case, polysulfides will dissolve and diffuse into the electrolyte if the host material does not have any confinement. Therefore, the principal concern is still to confine polysulfides into the cathode. Combined confinement and electrocatalytic conversion is therefore of critical importance for the design of efficient sulfur host materials. As long as a host can effectively confine polysulfides during the whole discharge stage, the catalytic effect will contribute to the performance increase.

Li–S batteries have fulfilled a major breakthrough over the last few years. However, recent research on sulfur host materials seems to level off. Designing an ideal host material still faces some challenges. As a conversion reaction electrode, sulfur converts into various soluble polysulfide intermediates during (de)lithiation. A sulfur host is essential for polysulfide anchoring in the cathode. At present, there has not been a single host material that can address all the problems. Integrating the advantages of different types of host materials will further boost the performance of Li–S batteries.

Despite many problems and difficulties faced by sulfur cathodes, it is believed that Li–S batteries, which exhibit high energy density and long-term cycling stability, will eventually be commercialized through further theoretical studies and experimental analyses.

Acknowledgements

Conflict of Interest

The authors declare no conflict of interest.

Keywords

[1] B. Dunn, H. Kamath, J.-M. Tarascon, *Science* **2011**, *334*, 928.
[2] P. G. Bruce, S. A. Freunberger, L. J. Hardwick, J. M. Tarascon, *Nat. Mater.* **2012**, *11*, 19.
[3] D. Lin, Y. Liu, Y. Cui, *Nat. Nanotechnol.* **2017**, *12*, 194.
[4] A. Manthiram, X. Yu, S. Wang, *Nat. Rev. Mater.* **2017**, *2*, 16103.
[5] K. Chayambuka, G. Mulder, D. L. Danilov, P. H. L. Notten, *Adv. Energy Mater.* **2018**, *8*, 1800079.
[6] X. Hong, J. Mei, L. Wen, Y. Tong, A. J. Vasileff, L. Wang, J. Liang, Z. Sun, S. X. Dou, *Adv. Mater.* **2019**, *31*, 1802822.
[7] J. B. Goodenough, K. S. Park, *J. Am. Chem. Soc.* **2013**, *135*, 1167.
[8] M. Li, J. Lu, Z. Chen, K. Amine, *Adv. Mater.* **2018**, *30*, 1800561.
[9] T. Kim, W. Song, D.-Y. Son, L. K. Ono, Y. Qi, *J. Mater. Chem. A* **2019**, *7*, 2942.
[10] Q. Pang, X. Liang, C. Y. Kwok, L. F. Nazar, *Nat. Energy* **2016**, *1*, 16132.
[11] X. Liu, J. Q. Huang, Q. Zhang, L. Mai, *Adv. Mater.* **2017**, *29*, 1601759.
[12] S.-H. Chung, C.-H. Chang, A. Manthiram, *Adv. Funct. Mater.* **2018**, *28*, 1801188.
[13] T. Li, X. Bai, U. Gulzar, Y.-J. Bai, C. Capiglia, W. Deng, X. Zhou, Z. Liu, Z. Feng, R. Proietti Zaccaria, *Adv. Funct. Mater.* **2019**, *29*, 1901730.
[14] R. Fang, S. Zhao, Z. Sun, D. W. Wang, H. M. Cheng, F. Li, *Adv. Mater.* **2017**, *29*, 1606823.
[15] G. Li, Z. Chen, J. Lu, *Chem* **2018**, *4*, 3.
[16] H. Yuan, H.-J. Peng, J.-Q. Huang, Q. Zhang, *Adv. Mater. Interfaces* **2019**, *6*, 1802046.
[17] X. Ji, K. T. Lee, L. F. Nazar, *Nat. Mater.* **2009**, *8*, 500.
[18] J. Xu, T. Lawson, H. Fan, D. Su, G. Wang, *Adv. Energy Mater.* **2018**, *8*, 1702607.
[19] J. Ren, Y. Zhou, L. Xia, Q. Zheng, J. Liao, E. Long, F. Xie, C. Xu, D. Lin, *J. Mater. Chem. A* **2018**, *6*, 13835.
[20] K. Xi, D. He, C. Harris, Y. Wang, C. Lai, H. Li, P. R. Coxon, S. Ding, C. Wang, R. V. Kumar, *Adv. Sci.* **2019**, *6*, 1800815.
[21] F. Li, Q. Liu, J. Hu, Y. Feng, P. He, J. Ma, *Nanoscale* **2019**, *11*, 15418.
[22] A. Eftekhari, D.-W. Kim, *J. Mater. Chem. A* **2017**, *5*, 17734.
[23] S. Bai, X. Liu, K. Zhu, S. Wu, H. Zhou, *Nat. Energy* **2016**, *1*, 16094.
[24] Z. A. Ghazi, X. He, A. M. Khattak, N. A. Khan, B. Liang, A. Iqbal, J. Wang, H. Sin, L. Li, Z. Tang, *Adv. Mater.* **2017**, *29*, 1606817.
[25] T. Zhou, W. Lv, J. Li, G. Zhou, Y. Zhao, S. Fan, B. Liu, B. Li, F. Kang, Q.-H. Yang, *Energy Environ. Sci.* **2017**, *10*, 1694.
[26] Y. C. Jeong, J. H. Kim, S. Nam, C. R. Park, S. J. Yang, *Adv. Funct. Mater.* **2018**, *28*, 1707411.
[27] W. Chen, T. Lei, C. Wu, M. Deng, C. Gong, K. Hu, Y. Ma, L. Dai, W. Lv, W. He, X. Liu, J. Xiong, C. Yan, *Adv. Energy Mater.* **2018**, *8*, 1702348.
[28] Q. Pang, A. Shyamsunder, B. Narayanan, C. Y. Kwok, L. A. Curtiss, L. F. Nazar, *Nat. Energy* **2018**, *3*, 783.
[29] J. Zheng, G. Ji, X. Fan, J. Chen, Q. Li, H. Wang, Y. Yang, K. C. DeMella, S. R. Raghavan, C. Wang, *Adv. Energy Mater.* **2019**, *9*, 1803774.

[30] Z. Yuan, H. J. Peng, T. Z. Hou, J. Q. Huang, C. M. Chen, D. W. Wang, X. B. Cheng, F. Wei, Q. Zhang, *Nano Lett.* **2016**, *16*, 519.

[31] W. Bao, L. Liu, C. Wang, S. Choi, D. Wang, G. Wang, *Adv. Energy Mater.* **2018**, *8*, 1702485.

[32] Y. Wang, R. Zhang, Y.-c. Pang, X. Chen, J. Lang, J. Xu, C. Xiao, H. Li, K. Xi, S. Ding, *Energy Storage Mater.* **2019**, *16*, 228.

[33] Y. He, Z. Chang, S. Wu, H. Zhou, *J. Mater. Chem. A* **2018**, *6*, 6155.

[34] Z. W. Seh, Y. Sun, Q. Zhang, Y. Cui, *Chem. Soc. Rev.* **2016**, *45*, 5605.

[35] A. Manthiram, Y. Fu, S.-H. Chung, C. Zu, Y.-S. Su, *Chem. Rev.* **2014**, *114*, 11751.

[36] C. Deng, Z. Wang, S. Wang, J. Yu, *J. Mater. Chem. A* **2019**, *7*, 12381.

[37] S. S. Zhang, *J. Power Sources* **2013**, *231*, 153.

[38] S. Rehman, K. Khan, Y. Zhao, Y. Hou, *J. Mater. Chem. A* **2017**, *5*, 3014.

[39] O. Ogoke, G. Wu, X. Wang, A. Casimir, L. Ma, T. Wu, J. Lu, *J. Mater. Chem. A* **2017**, *5*, 448.

[40] Y. Yang, G. Zheng, S. Misra, J. Nelson, M. F. Toney, Y. Cui, *J. Am. Chem. Soc.* **2012**, *134*, 15387.

[41] J. Liang, Z.-H. Sun, F. Li, H.-M. Cheng, *Energy Storage Mater.* **2016**, *2*, 76.

[42] Z. Li, Y. Huang, L. Yuan, Z. Hao, Y. Huang, *Carbon* **2015**, *92*, 41.

[43] C. Chen, D. Li, L. Gao, P. P. R. M. L. Harks, R.-A. Eichel, P. H. L. Notten, *J. Mater. Chem. A* **2017**, *5*, 1428.

[44] J. L. Wang, J. Yang, J. Y. Xie, N. X. Xu, Y. Li, *Electrochem. Commun.* **2002**, *4*, 499.

[45] J. Wang, L. Liu, Z. Ling, J. Yang, C. Wan, C. Jiang, *Electrochim. Acta* **2003**, *48*, 1861.

[46] Y. Zhong, X. Xia, S. Deng, J. Zhan, R. Fang, Y. Xia, X. Wang, Q. Zhang, J. Tu, *Adv. Energy Mater.* **2018**, *8*, 1701110.

[47] J. Ren, Y. Zhou, H. Wu, F. Xie, C. Xu, D. Lin, *J. Energy Chem.* **2019**, *30*, 121.

[48] Y. Zhong, D. Chao, S. Deng, J. Zhan, R. Fang, Y. Xia, Y. Wang, X. Wang, X. Xia, J. Tu, *Adv. Funct. Mater.* **2018**, *28*, 1706391.

[49] X. Zhang, Y. Zhong, X. Xia, Y. Xia, D. Wang, C. a. Zhou, W. Tang, X. Wang, J. B. Wu, J. Tu, *ACS Appl. Mater. Interfaces* **2018**, *10*, 13598.

[50] Z. Cheng, H. Pan, H. Zhong, Z. Xiao, X. Li, R. Wang, *Adv. Funct. Mater.* **2018**, *28*, 1707597.

[51] G. Li, J. Sun, W. Hou, S. Jiang, Y. Huang, J. Geng, *Nat. Commun.* **2016**, *7*, 10601.

[52] Z. Sun, J. Zhang, L. Yin, G. Hu, R. Fang, H. M. Cheng, F. Li, *Nat. Commun.* **2017**, *8*, 14627.

[53] F. Wu, J. Li, Y. Su, J. Wang, W. Yang, N. Li, L. Chen, S. Chen, R. Chen, L. Bao, *Nano Lett.* **2016**, *16*, 5488.

[54] H. Chen, C. Wang, Y. Dai, S. Qiu, J. Yang, W. Lu, L. Chen, *Nano Lett.* **2015**, *15*, 5443.

[55] K. Xi, S. Cao, X. Peng, C. Ducati, R. V. Kumar, A. K. Cheetham, *Chem. Commun.* **2013**, *49*, 2192.

[56] L. Ni, Z. Wu, G. Zhao, C. Sun, C. Zhou, X. Gong, G. Diao, *Small* **2017**, *13*, 1603466.

[57] J. Zhang, Z. Li, Y. Chen, S. Gao, X. W. D. Lou, *Angew. Chem., Int. Ed.* **2018**, *57*, 10944.

[58] L. Zhou, H. Li, X. Wu, Y. Zhang, D. L. Danilov, R.-A. Eichel, P. H. L. Notten, *ACS Appl. Energy Mater.* **2019**, *2*, 8153.

[59] L. Lin, F. Pei, J. Peng, A. Fu, J. Cui, X. Fang, N. Zheng, *Nano Energy* **2018**, *54*, 50.

[60] H. Liu, Z. Chen, L. Zhou, K. Pei, P. Xu, L. Xin, Q. Zeng, J. Zhang, R. Wu, F. Fang, R. Che, D. Sun, *Adv. Energy Mater.* **2019**, *9*, 1901667.

[61] W. Zhou, Y. Yu, H. Chen, F. J. DiSalvo, H. D. Abruña, *J. Am. Chem. Soc.* **2013**, *135*, 16736.

[62] M. Yu, J. Ma, H. Song, A. Wang, F. Tian, Y. Wang, H. Qiu, R. Wang, *Energy Environ. Sci.* **2016**, *9*, 1495.

[63] H. Kim, J. T. Lee, D.-C. Lee, A. Magasinski, W.-i. Cho, G. Yushin, *Adv. Energy Mater.* **2013**, *3*, 1308.

[64] M. Yu, W. Yuan, C. Li, J.-D. Hong, G. Shi, *J. Mater. Chem. A* **2014**, *2*, 7360.

[65] Z. Li, J. Zhang, X. W. Lou, *Angew. Chem., Int. Ed.* **2015**, *54*, 12886.

[66] S. B. Patil, H. J. Kim, H.-K. Lim, S. M. Oh, J. Kim, J. Shin, H. Kim, J. W. Choi, S.-J. Hwang, *ACS Energy Lett.* **2018**, *3*, 412.

[67] H. Lin, L. Yang, X. Jiang, G. Li, T. Zhang, Q. Yao, G. W. Zheng, J. Y. Lee, *Energy Environ. Sci.* **2017**, *10*, 1476.

[68] W. Tian, B. Xi, Z. Feng, H. Li, J. Feng, S. Xiong, *Adv. Energy Mater.* **2019**, *9*, 1901896.

[69] C. Li, Z. Xi, D. Guo, X. Chen, L. Yin, *Small* **2018**, *14*, 1701986.

[70] J. Balach, J. Linnemann, T. Jaumann, L. Giebeler, *J. Mater. Chem. A* **2018**, *6*, 23127.

[71] L. Ji, M. Rao, H. Zheng, L. Zhang, Y. Li, W. Duan, J. Guo, E. J. Cairns, Y. Zhang, *J. Am. Chem. Soc.* **2011**, *133*, 18522.

[72] K. Chen, Z. Sun, R. Fang, Y. Shi, H.-M. Cheng, F. Li, *Adv. Funct. Mater.* **2018**, *28*, 1707592.

[73] S.-K. Park, J.-K. Lee, Y. C. Kang, *Adv. Funct. Mater.* **2018**, *28*, 1705264.

[74] M. Kim, J. Lee, Y. Jeon, Y. Piao, *Nanoscale* **2019**, *11*, 13758.

[75] J. Wang, H. Yang, Z. Chen, L. Zhang, J. Liu, P. Liang, H. Yang, X. Shen, Z. X. Shen, *Adv. Sci.* **2018**, *5*, 1800621.

[76] J. Ren, L. Xia, Y. Zhou, Q. Zheng, J. Liao, D. Lin, *Carbon* **2018**, *140*, 30.

[77] H.-J. Peng, T.-Z. Hou, Q. Zhang, J.-Q. Huang, X.-B. Cheng, M.-Q. Guo, Z. Yuan, L.-Y. He, F. Wei, *Adv. Mater. Interfaces* **2014**, *1*, 1400227.

[78] Q. Pang, D. Kundu, M. Cuisinier, L. F. Nazar, *Nat. Commun.* **2014**, *5*, 4759.

[79] X. Shang, P. Guo, T. Qin, M. Liu, M. Lv, D. Liu, D. He, *Adv. Mater. Interfaces* **2018**, *5*, 1701602.

[80] K. Lu, H. Zhang, S. Gao, H. Ma, J. Chen, Y. Cheng, *Adv. Funct. Mater.* **2019**, *29*, 1807309.

[81] T. Chen, L. Ma, B. Cheng, R. Chen, Y. Hu, G. Zhu, Y. Wang, J. Liang, Z. Tie, J. Liu, Z. Jin, *Nano Energy* **2017**, *38*, 239.

[82] Y. You, Y. Ye, M. Wei, W. Sun, Q. Tang, J. Zhang, X. Chen, H. Li, J. Xu, *Chem. Eng. J.* **2019**, *355*, 671.

[83] S.-H. Chung, L. Luo, A. Manthiram, *ACS Energy Lett.* **2018**, *3*, 568.

[84] S. Shen, X. Xia, Y. Zhong, S. Deng, D. Xie, B. Liu, Y. Zhang, G. Pan, X. Wang, J. Tu, *Adv. Mater.* **2019**, *31*, 1900009.

[85] K. Xiao, J. Wang, Z. Chen, Y. Qian, Z. Li, L. Zhang, X. Chen, J. Liu, X. Fan, Z. X. Shen, *Small* **2019**, *15*, 1901454.

[86] H. Al Salem, G. Babu, C. V. Rao, L. M. Arava, *J. Am. Chem. Soc.* **2015**, *137*, 11542.

[87] J. Zheng, J. Tian, D. Wu, M. Gu, W. Xu, C. Wang, F. Gao, M. H. Engelhard, J. G. Zhang, J. Liu, J. Xiao, *Nano Lett.* **2014**, *14*, 2345.

[88] X. Liang, A. Garsuch, L. F. Nazar, *Angew. Chem., Int. Ed.* **2015**, *54*, 3907.

[89] X. Liang, C. Hart, Q. Pang, A. Garsuch, T. Weiss, L. F. Nazar, *Nat. Commun.* **2015**, *6*, 5682.

[90] X. Liang, C. Y. Kwok, F. Lodi-Marzano, Q. Pang, M. Cuisinier, H. Huang, C. J. Hart, D. Houtarde, K. Kaup, H. Sommer, T. Brezesinski, J. Janek, L. F. Nazar, *Adv. Energy Mater.* **2016**, *6*, 1501636.

[91] X. Liang, Y. Rangom, C. Y. Kwok, Q. Pang, L. F. Nazar, *Adv. Mater.* **2017**, *29*, 1603040.

[92] G. Zhou, H. Tian, Y. Jin, X. Tao, B. Liu, R. Zhang, Z. W. Seh, D. Zhuo, Y. Liu, J. Sun, J. Zhao, C. Zu, D. S. Wu, Q. Zhang, Y. Cui, *Proc. Natl. Acad. Sci. U. S. A.* **2017**, *114*, 840.

[93] S. S. Zhang, *Front. Energy Res.* **2013**, *1*, 10.

[94] B. Duan, W. Wang, A. Wang, K. Yuan, Z. Yu, H. Zhao, J. Qiu, Y. Yang, *J. Mater. Chem. A* **2013**, *1*, 13261.

[95] X. Wang, Y. Qian, L. Wang, H. Yang, H. Li, Y. Zhao, T. Liu, *Adv. Funct. Mater.* **2019**, *29*, 1902929.

[96] M. Frey, R. K. Zenn, S. Warneke, K. Müller, A. Hintennach, R. E. Dinnebier, M. R. Buchmeiser, *ACS Energy Lett.* **2017**, *2*, 595.

[97] Z. Li, H. B. Wu, X. W. Lou, *Energy Environ. Sci.* **2016**, *9*, 3061.

[98] X.-X. Peng, Y.-Q. Lu, L.-L. Zhou, T. Sheng, S.-Y. Shen, H.-G. Liao, L. Huang, J.-T. Li, S.-G. Sun, *Nano Energy* **2017**, *32*, 503.

[99] S. Liu, X. Hong, D. Wang, Y. Li, J. Xu, C. Zheng, K. Xie, *Electrochim. Acta* **2018**, *279*, 10.

[100] F. Pei, T. An, J. Zang, X. Zhao, X. Fang, M. Zheng, Q. Dong, N. Zheng, *Adv. Energy Mater.* **2016**, *6*, 1502539.

[101] C. Hernández-Rentero, R. Córdoba, N. Moreno, A. Caballero, J. Morales, M. Olivares-Marín, V. Gómez-Serrano, *Nano Res.* **2018**, *11*, 89.

[102] X. Qin, J. Wu, Z.-L. Xu, W. G. Chong, J.-Q. Huang, G. Liang, B. Li, F. Kang, J.-K. Kim, *Carbon* **2019**, *141*, 16.

[103] S. Xin, L. Gu, N.-H. Zhao, Y.-X. Yin, L.-J. Zhou, Y.-G. Guo, L.-J. Wan, *J. Am. Chem. Soc.* **2012**, *134*, 18510.

[104] Y. Xu, Y. Wen, Y. Zhu, K. Gaskell, K. A. Cychosz, B. Eichhorn, K. Xu, C. Wang, *Adv. Funct. Mater.* **2015**, *25*, 4312.

[105] Q. Zhu, Q. Zhao, Y. An, B. Anasori, H. Wang, B. Xu, *Nano Energy* **2017**, *33*, 402.

[106] B. Q. Li, S. Y. Zhang, L. Kong, H. J. Peng, Q. Zhang, *Adv. Mater.* **2018**, *30*, 1707483.

[107] F. Pei, L. Lin, D. Ou, Z. Zheng, S. Mo, X. Fang, N. Zheng, *Nat. Commun.* **2017**, *8*, 482.

[108] J. Schuster, G. He, B. Mandlmeier, T. Yim, K. T. Lee, T. Bein, L. F. Nazar, *Angew. Chem., Int. Ed.* **2012**, *51*, 3591.

[109] S. K. Park, J. Lee, T. Hwang, B. Jang, Y. Piao, *ACS Appl. Mater. Interfaces* **2017**, *9*, 2430.

[110] Z. Li, Y. Jiang, L. Yuan, L. Yi, C. Wu, Y. Liu, P. Strasser, Y. Huang, *ACS Nano* **2014**, *8*, 9295.

[111] M. Chen, S. Jiang, S. Cai, X. Wang, K. Xiang, Z. Ma, P. Song, A. C. Fisher, *Chem. Eng. J.* **2017**, *313*, 404.

[112] W. Hooch Antink, Y. Choi, K.-d. Seong, J. M. Kim, Y. Piao, *Adv. Mater. Interfaces* **2018**, *5*, 1701212.

[113] G. Zhou, S. Pei, L. Li, D. W. Wang, S. Wang, K. Huang, L. C. Yin, F. Li, H. M. Cheng, *Adv. Mater.* **2014**, *26*, 625.

[114] H. Li, Y. Tao, C. Zhang, D. Liu, J. Luo, W. Fan, Y. Xu, Y. Li, C. You, Z.-Z. Pan, M. Ye, Z. Chen, Z. Dong, D.-W. Wang, F. Kang, J. Lu, Q.-H. Yang, *Adv. Energy Mater.* **2018**, *8*, 1703438.

[115] J. Song, Z. Yu, M. L. Gordin, D. Wang, *Nano Lett.* **2016**, *16*, 864.

[116] L. Duan, L. Zhao, H. Cong, X. Zhang, W. Lu, C. Xue, *Small* **2019**, *15*, 1804347.

[117] Z. Zhang, L.-L. Kong, S. Liu, G.-R. Li, X.-P. Gao, *Adv. Energy Mater.* **2017**, *7*, 1602543.

[118] Z. Wang, Y. Dong, H. Li, Z. Zhao, H. B. Wu, C. Hao, S. Liu, J. Qiu, X. W. Lou, *Nat. Commun.* **2014**, *5*, 5002.

[119] G. Hu, C. Xu, Z. Sun, S. Wang, H. M. Cheng, F. Li, W. Ren, *Adv. Mater.* **2016**, *28*, 1603.

[120] J. L. Gómez-Urbano, J. L. Gómez-Cámer, C. Botas, N. Díez, J. M. López del Amo, L. M. Rodríguez-Martinez, D. Carriazo, T. Rojo, *Carbon* **2018**, *139*, 226.

[121] C. Tang, Q. Zhang, M. Q. Zhao, J. Q. Huang, X. B. Cheng, G. L. Tian, H. J. Peng, F. Wei, *Adv. Mater.* **2014**, *26*, 6100.

[122] P. Xiao, F. Bu, G. Yang, Y. Zhang, Y. Xu, *Adv. Mater.* **2017**, *29*, 1703324.

[123] R. Chu, J. Lin, C. Wu, J. Zheng, Y. Chen, J. Zhang, R. Han, Y. Zhang, H. Guo, *Nanoscale* **2017**, *9*, 9129.

[124] J. L. Gómez-Urbano, J. L. Gómez-Cámer, C. Botas, T. Rojo, D. Carriazo, *J. Power Sources* **2019**, *412*, 408.

[125] H. Yang, X. Zhang, W. Zhu, F. Wang, Y. Li, Q. Fan, X. Hiao, F. Zhang, *ChemElectroChem* **2019**, *6*, 1115.

[126] D. Gueon, J. T. Hwang, S. B. Yang, E. Cho, K. Sohn, D. K. Yang, J. H. Moon, *ACS Nano* **2018**, *12*, 226.

[127] A. Abdul Razzaq, Y. Yao, R. Shah, P. Qi, L. Miao, M. Chen, X. Zhao, Y. Peng, Z. Deng, *Energy Storage Mater.* **2019**, *16*, 194.

[128] M. Zheng, Y. Chi, Q. Hu, H. Tang, X. Jiang, L. Zhang, S. Zhang, H. Pang, Q. Xu, *J. Mater. Chem. A* **2019**, *7*, 17204.

[129] J. Guo, Y. Xu, C. Wang, *Nano Lett.* **2011**, *11*, 4288.

[130] L. Sun, M. Li, Y. Jiang, W. Kong, K. Jiang, J. Wang, S. Fan, *Nano Lett.* **2014**, *14*, 4044.

[131] R. Fang, G. Li, S. Zhao, L. Yin, K. Du, P. Hou, S. Wang, H.-M. Cheng, C. Liu, F. Li, *Nano Energy* **2017**, *42*, 205.

[132] M. Yan, H. Chen, Y. Yu, H. Zhao, C.-F. Li, Z.-Y. Hu, P. Wu, L. Chen, H. Wang, D. Peng, H. Gao, T. Hasan, Y. Li, B.-L. Su, *Adv. Energy Mater.* **2018**, *8*, 1801066.

[133] X.-B. Cheng, J.-Q. Huang, Q. Zhang, H.-J. Peng, M.-Q. Zhao, F. Wei, *Nano Energy* **2014**, *4*, 65.

[134] Z. Yuan, H.-J. Peng, J.-Q. Huang, X.-Y. Liu, D.-W. Wang, X.-B. Cheng, Q. Zhang, *Adv. Funct. Mater.* **2014**, *24*, 6105.

[135] L. Ma, H. L. Zhuang, S. Wei, K. E. Hendrickson, M. S. Kim, G. Cohn, R. G. Hennig, L. A. Archer, *ACS Nano* **2016**, *10*, 1050.

[136] P. Zhu, J. Zhu, C. Yan, M. Dirican, J. Zang, H. Jia, Y. Li, Y. Kiyak, H. Tan, X. Zhang, *Adv. Mater. Interfaces* **2018**, *5*, 1701598.

[137] Q. Li, J. Guo, J. Zhao, C. Wang, F. Yan, *Nanoscale* **2019**, *11*, 647.

[138] G. Zheng, Y. Yang, J. J. Cha, S. S. Hong, Y. Cui, *Nano Lett.* **2011**, *11*, 4462.

[139] G. Zheng, Q. Zhang, J. J. Cha, Y. Yang, W. Li, Z. W. Seh, Y. Cui, *Nano Lett.* **2013**, *13*, 1265.

[140] X.-Q. Zhang, B. He, W.-C. Li, A.-H. Lu, *Nano Res.* **2018**, *11*, 1238.

[141] J. S. Lee, W. Kim, J. Jang, A. Manthiram, *Adv. Energy Mater.* **2017**, *7*, 1601943.

[142] J. H. Yun, J. H. Kim, D. K. Kim, H. W. Lee, *Nano Lett.* **2018**, *18*, 475.

[143] Q. Pang, X. Liang, C. Y. Kwok, J. Kulisch, L. F. Nazar, *Adv. Energy Mater.* **2017**, *7*, 1601630.

[144] X. Zhao, M. Kim, Y. Liu, H.-J. Ahn, K.-W. Kim, K.-K. Cho, J.-H. Ahn, *Carbon* **2018**, *128*, 138.

[145] L. Fan, H. L. Zhuang, K. Zhang, V. R. Cooper, Q. Li, Y. Lu, *Adv. Sci.* **2016**, *3*, 1600175.

[146] X. Song, S. Wang, Y. Bao, G. Liu, W. Sun, L.-X. Ding, H. Liu, H. Wang, *J. Mater. Chem. A* **2017**, *5*, 6832.

[147] X. Zhou, X. Ma, C. Ding, W. Meng, S. Xu, L. Chen, D. Duan, S. Liu, *Mater. Lett.* **2019**, *251*, 180.

[148] N. Deng, W. Kang, J. Ju, L. Fan, X. Zhuang, X. Ma, H. He, Y. Zhao, B. Cheng, *J. Power Sources* **2017**, *346*, 1.

[149] Y. Z. Zhang, Z. Zhang, S. Liu, G. R. Li, X. P. Gao, *ACS Appl. Mater. Interfaces* **2018**, *10*, 8749.

[150] G. Zhou, E. Paek, G. S. Hwang, A. Manthiram, *Nat. Commun.* **2015**, *6*, 7760.

[151] C. Jin, W. Zhang, Z. Zhuang, J. Wang, H. Huang, Y. Gan, Y. Xia, C. Liang, J. Zhang, X. Tao, *J. Mater. Chem. A* **2017**, *5*, 632.

[152] S. Liu, J. Li, X. Yan, Q. Su, Y. Lu, J. Qiu, Z. Wang, X. Lin, J. Huang, R. Liu, B. Zheng, L. Chen, R. Fu, D. Wu, *Adv. Mater.* **2018**, *30*, 1706895.

[153] K. Mi, S. Chen, B. Xi, S. Kai, Y. Jiang, J. Feng, Y. Qian, S. Xiong, *Adv. Funct. Mater.* **2017**, *27*, 1604265.

[154] Q. Lu, Y. Zhong, W. Zhou, K. Liao, Z. Shao, *Adv. Mater. Interfaces* **2018**, *5*, 1701659.

[155] W. Ai, W. Zhou, Z. Du, Y. Chen, Z. Sun, C. Wu, C. Zou, C. Li, W. Huang, T. Yu, *Energy Storage Mater.* **2017**, *6*, 112.

[156] L. Chen, J. Feng, H. Zhou, C. Fu, G. Wang, L. Yang, C. Xu, Z. Chen, W. Yang, Y. Kuang, *J. Mater. Chem. A* **2017**, *5*, 7403.

[157] Q. Pang, J. Tang, H. Huang, X. Liang, C. Hart, K. C. Tam, L. F. Nazar, *Adv. Mater.* **2015**, *27*, 6021.

[158] M. Chen, S. Jiang, C. Huang, X. Wang, S. Cai, K. Xiang, Y. Zhang, J. Xue, *ChemSusChem* **2017**, *10*, 1803.

[159] W. Ai, J. Li, Z. Du, C. Zou, H. Du, X. Xu, Y. Chen, H. Zhang, J. Zhao, C. Li, W. Huang, T. Yu, *Nano Res.* **2018**, *11*, 4562.

[160] T. S. Miller, A. B. Jorge, T. M. Suter, A. Sella, F. Cora, P. F. McMillan, *Phys. Chem. Chem. Phys.* **2017**, *19*, 15613.

[161] Q. Pang, L. F. Nazar, *ACS Nano* **2016**, *10*, 4111.

[162] J. Liang, L. Yin, X. Tang, H. Yang, W. Yan, L. Song, H. M. Cheng, F. Li, *ACS Appl. Mater. Interfaces* **2016**, *8*, 25193.

[163] Y. Gong, C. Fu, G. Zhang, H. Zhou, Y. Kuang, *Electrochim. Acta* **2017**, *256*, 1.

[164] M. Wang, Q. Liang, J. Han, Y. Tao, D. Liu, C. Zhang, W. Lv, Q.-H. Yang, *Nano Res.* **2018**, *11*, 3480.

[165] J. Song, S. Feng, C. Zhu, J.-I. Lee, S. Fu, P. Dong, M.-K. Song, Y. Lin, *Electrochim. Acta* **2017**, *248*, 541.

[166] J. Wang, Z. Meng, W. Yang, X. Yan, R. Guo, W. Q. Han, *ACS Appl. Mater. Interfaces* **2019**, *11*, 819.

[167] Y. Yang, G. Yu, J. J. Cha, H. Wu, M. Vosgueritchian, Y. Yao, Z. Bao, Y. Cui, *ACS Nano* **2011**, *5*, 9187.

[168] W. Li, G. Zheng, Y. Yang, Z. W. Seh, N. Liu, Y. Cui, *Proc. Natl. Acad. Sci. USA* **2013**, *110*, 7148.

[169] W. Li, Q. Zhang, G. Zheng, Z. W. Seh, H. Yao, Y. Cui, *Nano Lett.* **2013**, *13*, 5534.

[170] S. Lim, R. L. Thankamony, T. Yim, H. Chu, Y. J. Kim, J. Mun, T. H. Kim, *ACS Appl. Mater. Interfaces* **2015**, *7*, 1401.

[171] P. Jia, T. Hu, Q. He, X. Cao, J. Ma, J. Fan, Q. Chen, Y. Ding, J. Pyun, J. Geng, *ACS Appl. Mater. Interfaces* **2019**, *11*, 3087.

[172] H. Kang, H. Kim, M. J. Park, *Adv. Energy Mater.* **2018**, *8*, 1802423.

[173] Y. Liu, A. K. Haridas, K.-K. Cho, Y. Lee, J.-H. Ahn, *J. Phys. Chem. C* **2017**, *121*, 26172.

[174] Z. Cheng, H. Pan, Z. Xiao, D. Chen, X. Li, R. Wang, *J. Mater. Chem. A* **2018**, *6*, 7375.

[175] H. Kim, J. Lee, H. Ahn, O. Kim, M. J. Park, *Nat. Commun.* **2015**, *6*, 7278.

[176] S. Zhang, *Energies* **2014**, *7*, 4588.

[177] H. M. Kim, J. Y. Hwang, D. Aurbach, Y. K. Sun, *J. Phys. Chem. Lett.* **2017**, *8*, 5331.

[178] C.-H. Tsao, C.-H. Hsu, J.-D. Zhou, C.-W. Chin, P.-L. Kuo, C.-H. Chang, *Electrochim. Acta* **2018**, *276*, 111.

[179] Z. Wei Seh, W. Li, J. J. Cha, G. Zheng, Y. Yang, M. T. McDowell, P. C. Hsu, Y. Cui, *Nat. Commun.* **2013**, *4*, 1331.

[180] X. Qian, X. Yang, L. Jin, D. Rao, S. Yao, X. Shen, K. Xiao, S. Qin, J. Xiang, *Mater. Res. Bull.* **2017**, *95*, 402.

[181] J. Ni, L. Jin, M. Xue, J. Zheng, J. P. Zheng, C. Zhang, *Electrochim. Acta* **2019**, *296*, 39.

[182] H.-E. Wang, K. Yin, N. Qin, X. Zhao, F.-J. Xia, Z.-Y. Hu, G. Guo, G. Cao, W. Zhang, *J. Mater. Chem. A* **2019**, *7*, 10346.

[183] C. Zha, F. Yang, J. Zhang, T. Zhang, S. Dong, H. Chen, *J. Mater. Chem. A* **2018**, *6*, 16574.

[184] M. Fang, Z. Chen, Y. Liu, J. Quan, C. Yang, L. Zhu, Q. Xu, Q. Xu, *J. Mater. Chem. A* **2018**, *6*, 1630.

[185] C. Liang, X. Zhang, Y. Zhao, T. Tan, Y. Zhang, *J. Solid State Electrochem.* **2019**, *23*, 565.

[186] F. Wang, X. Ding, R. Shi, M. Li, Y. Lei, Z. Lei, G. Jiang, F. Xu, H. Wang, L. Jia, R. Jiang, Z. Liu, J. Sun, *J. Mater. Chem. A* **2019**, *7*, 10494.

[187] G. Chen, W. Zhong, Y. Li, Q. Deng, X. Ou, Q. Pan, X. Wang, X. Xiong, C. Yang, M. Liu, *ACS Appl. Mater. Interfaces* **2019**, *11*, 5055.

[188] S. Mei, C. J. Jafta, I. Lauermann, Q. Ran, M. Kärgell, M. Ballauff, Y. Lu, *Adv. Funct. Mater.* **2017**, *27*, 1701176.

[189] M. Chen, S. Jiang, C. Huang, J. Xia, X. Wang, K. Xiang, P. Zeng, Y. Zhang, S. Jamil, *ACS Appl. Mater. Interfaces* **2018**, *10*, 13562.

[190] H. Wei, E. F. Rodriguez, A. S. Best, A. F. Hollenkamp, D. Chen, R. A. Caruso, *Adv. Energy Mater.* **2017**, *7*, 1601616.

[191] Z. Li, J. Zhang, B. Guan, D. Wang, L. M. Liu, X. W. Lou, *Nat. Commun.* **2016**, *7*, 13065.

[192] Z. Li, B. Y. Guan, J. Zhang, X. W. Lou, *Joule* **2017**, *1*, 576.

[193] J. Zhang, Y. Shi, Y. Ding, W. Zhang, G. Yu, *Nano Lett.* **2016**, *16*, 7276.

[194] S. Huang, L. Liu, Y. Wang, Y. Shang, L. Zhang, J. Wang, Y. Zheng, O. G. Schmidt, H. Y. Yang, *J. Mater. Chem. A* **2019**, *7*, 6651.

[195] X. Wang, G. Li, J. Li, Y. Zhang, A. Wook, A. Yu, Z. Chen, *Energy Environ. Sci.* **2016**, *9*, 2533.

[196] S. Rehman, T. Tang, Z. Ali, X. Huang, Y. Hou, *Small* **2017**, *13*, 1700087.

[197] X. Chen, L. Yuan, Z. Hao, X. Liu, J. Xiang, Z. Zhang, Y. Huang, J. Xie, *ACS Appl. Mater. Interfaces* **2018**, *10*, 13406.

[198] T. An, D. Deng, M. Lei, Q.-H. Wu, Z. Tian, M. Zheng, Q. Dong, *J. Mater. Chem. A* **2016**, *4*, 12858.

[199] J. Zhu, R. Pitcheri, T. Kang, Y. Guo, J. Li, Y. Qiu, *Ceram. Int.* **2018**, *44*, 16837.

[200] X. Wen, K. Xiang, Y. Zhu, L. Xiao, X. Chen, H. Chen, *Mater. Lett.* **2018**, *229*, 272.

[201] Y. Liu, G. Feng, X. Guo, Z. Wu, Y. Chen, W. Xiang, J. Li, B. Zhong, *J. Alloys Compd.* **2018**, *748*, 100.

[202] Y. Liang, Y. Li, H. Wang, J. Zhou, J. Wang, T. Regier, H. Dai, *Nat. Mater.* **2011**, *10*, 780.

[203] L. Xu, Q. Jiang, Z. Xiao, X. Li, J. Huo, S. Wang, L. Dai, *Angew. Chem., Int. Ed.* **2016**, *55*, 5277.

[204] J. Zhou, X. Liu, L. Zhu, J. Zhou, Y. Guan, L. Chen, S. Niu, J. Cai, D. Sun, Y. Zhu, J. Du, G. Wang, Y. Qian, *Joule* **2018**, *2*, 2681.

[205] Z. Chang, H. Dou, B. Ding, J. Wang, Y. Wang, X. Hao, D. R. MacFarlane, *J. Mater. Chem. A* **2017**, *5*, 250.

[206] Y. Chen, X. Ji, *J. Alloys Compd.* **2019**, *777*, 688.

[207] J. Xu, W. Zhang, Y. Chen, H. Fan, D. Su, G. Wang, *J. Mater. Chem. A* **2018**, *6*, 2797.

[208] J. He, L. Luo, Y. Chen, A. Manthiram, *Adv. Mater.* **2017**, *29*, 1702707.

[209] W. Ren, W. Ma, M. M. Umair, S. Zhang, B. Tang, *ChemSusChem* **2018**, *11*, 2695.

[210] C. Zhao, C. Shen, F. Xin, Z. Sun, W. Han, *Mater. Lett.* **2014**, *137*, 52.

[211] N. Zhang, B. D. A. Levin, Y. Yang, D. A. Muller, H. D. Abruña, *J. Electrochem. Soc.* **2018**, *165*, A1656.

[212] L. Fan, H. Wu, X. Wu, M. Wang, J. Cheng, N. Zhang, Y. Feng, K. Sun, *Electrochim. Acta* **2019**, *295*, 444.

[213] B. Li, Z. Sun, Y. Zhao, Z. Zhang, *Mater. Lett.* **2019**, *255*, 126529.

[214] M. Ding, S. Huang, Y. Wang, J. Hu, M. E. Pam, S. Fan, Y. Shi, Q. Ge, H. Y. Yang, *J. Mater. Chem. A* **2019**, *7*, 25078.

[215] Y. Zhang, R. Gu, S. Zheng, K. Liao, P. Shi, J. Fan, Q. Xu, Y. Min, *J. Mater. Chem. A* **2019**, *7*, 21747.

[216] L. Hu, C. Dai, H. Liu, Y. Li, B. Shen, Y. Chen, S.-J. Bao, M. Xu, *Adv. Energy Mater.* **2018**, *8*, 1800709.

[217] D. Xiao, H. Zhang, C. Chen, Y. Liu, S. Yuan, C. Lu, *ChemElectroChem* **2017**, *4*, 2959.

[218] A. Iqbal, Z. Ali Ghazi, A. Muqsit Khattak, A. Ahmad, *J. Solid State Chem.* **2017**, *256*, 189.

[219] D. Luo, G. Li, Y. P. Deng, Z. Zhang, J. Li, R. Liang, M. Li, Y. Jiang, W. Zhang, Y. Liu, W. Lei, A. Yu, Z. Chen, *Adv. Energy Mater.* **2019**, *9*, 1900228.

[220] Q. Fan, W. Liu, Z. Weng, Y. Sun, H. Wang, *J. Am. Chem. Soc.* **2015**, *137*, 12946.

[221] Z. Zhang, S. Basu, P. Zhu, H. Zhang, A. Shao, N. Koratkar, Z. Yang, *Carbon* **2019**, *142*, 32.

[222] Y.-T. Liu, D.-D. Han, L. Wang, G.-R. Li, S. Liu, X.-P. Gao, *Adv. Energy Mater.* **2019**, *9*, 1803477.

[223] Z. Zhang, D.-H. Wu, Z. Zhou, G.-R. Li, S. Liu, X.-P. Gao, *Sci. China Mater.* **2019**, *62*, 74.

[224] Q. Sun, B. Xi, J.-Y. Li, H. Mao, X. Ma, J. Liang, J. Feng, S. Xiong, *Adv. Energy Mater.* **2018**, *8*, 1800595.

[225] S. Li, Y. Cen, Q. Xiang, M. K. Aslam, B. Hu, W. Li, Y. Tang, Q. Yu, Y. Liu, C. Chen, *J. Mater. Chem. A* **2019**, *7*, 1658.

[226] X. Ji, S. Evers, R. Black, L. F. Nazar, *Nat. Commun.* **2011**, *2*, 325.

[227] R. Wang, K. Wang, S. Gao, M. Jiang, M. Zhou, S. Cheng, K. Jiang, *Nanoscale* **2017**, *9*, 14881.

[228] H. Wu, Q. Tang, H. Fan, Z. Liu, A. Hu, S. Zhang, W. Deng, X. Chen, *Electrochim. Acta* **2017**, *255*, 179.

[229] Y. Song, W. Zhao, X. Zhu, L. Zhang, Q. Li, F. Ding, Z. Liu, J. Sun, *ACS Appl. Mater. Interfaces* **2018**, *10*, 15733.

[230] Y. Song, W. Zhao, N. Wei, L. Zhang, F. Ding, Z. Liu, J. Sun, *Nano Energy* **2018**, *53*, 432.

[231] M. Zhu, S. Li, J. Liu, B. Li, *Appl. Surf. Sci.* **2019**, *473*, 1002.

[232] R. Carter, L. Oakes, N. Muralidharan, A. P. Cohn, A. Douglas, C. L. Pint, *ACS Appl. Mater. Interfaces* **2017**, *9*, 7185.

[233] M. Yu, W. Yuan, C. Li, J.-D. Hong, G. Shi, *J. Mater. Chem. A* **2014**, *2*.

[234] Y. Wu, Q. Xiao, S. Huang, K. Wang, *Mater. Chem. Phys.* **2019**, *221*, 258.

[235] Y. Kong, J. Luo, C. Jin, H. Yuan, O. Sheng, L. Zhang, C. Fang, W. Zhang, H. Huang, Y. Xia, C. Liang, J. Zhang, Y. Gan, X. Tao, *Nano Res.* **2018**, *11*, 477.

[236] Y. Zhao, Z. Liu, L. Sun, Y. Zhang, Y. Feng, X. Wang, I. Kurmanbayeva, Z. Bakenov, *Beilstein J. Nanotechnol.* **2018**, *9*, 1677.

[237] R. Yang, H. Du, Z. Lin, L. Yang, H. Zhu, H. Zhang, Z. Tang, X. Gui, *Carbon* **2019**, *141*, 258.

[238] M. Xiang, H. Wu, H. Liu, J. Huang, Y. Zheng, L. Yang, P. Jing, Y. Zhang, S. Dou, H. Liu, *Adv. Funct. Mater.* **2017**, *27*, 1702573.

[239] G. Ding, Y. Li, Y. Zhang, C. Huang, X. Yao, K. Lin, K. Shen, W. Yan, F. Sun, L. Zhou, *ACS Appl. Mater. Interfaces* **2019**, *11*, 19096.

[240] S. Rehman, S. Guo, Y. Hou, *Adv. Mater.* **2016**, *28*, 3167.

[241] T. Ma, T. Liu, T. Huang, A. Yu, *J. Power Sources* **2018**, *398*, 75.

[242] L. Chen, X. Li, Y. Xu, *Funct. Mater. Lett.* **2018**, *11*, 1840010.

[243] S.-J. Kim, K. Kim, J. Park, Y.-E. Sung, *ChemCatChem* **2019**, *11*, 2373.

[244] Q. Pang, D. Kundu, L. F. Nazar, *Mater. Horiz.* **2016**, *3*, 130.

[245] C. Dai, J.-M. Lim, M. Wang, L. Hu, Y. Chen, Z. Chen, H. Chen, S.-J. Bao, B. Shen, Y. Li, G. Henkelman, M. Xu, *Adv. Funct. Mater.* **2018**, *28*, 1704443.

[246] J. Zhou, N. Lin, W. l. Cai, C. Guo, K. Zhang, J. Zhou, Y. Zhu, Y. Qian, *Electrochim. Acta* **2016**, *218*, 243.

[247] J. Pu, Z. Shen, J. Zheng, W. Wu, C. Zhu, Q. Zhou, H. Zhang, F. Pan, *Nano Energy* **2017**, *37*, 7.

[248] H. Xu, A. Manthiram, *Nano Energy* **2017**, *33*, 124.

[249] S. D. Seo, D. Park, S. Park, D. W. Kim, *Adv. Funct. Mater.* **2019**, *29*, 1903712.

[250] Y. Zhang, Z. Mu, C. Yang, Z. Xu, S. Zhang, X. Zhang, Y. Li, J. Lai, Z. Sun, Y. Yang, Y. Chao, C. Li, X. Ge, W. Yang, S. Guo, *Adv. Funct. Mater.* **2018**, *28*, 1707578.

[251] M. Wang, L. Fan, D. Tian, X. Wu, Y. Qiu, C. Zhao, B. Guan, Y. Wang, N. Zhang, K. Sun, *ACS Energy Lett.* **2018**, *3*, 1627.

[252] J. He, G. Hartmann, M. Lee, G. S. Hwang, Y. Chen, A. Manthiram, *Energy Environ. Sci.* **2019**, *12*, 344.

[253] L. Luo, S.-H. Chung, A. Manthiram, *Adv. Energy Mater.* **2018**, *8*, 1801014.

[254] C. Ye, L. Zhang, C. Guo, D. Li, A. Vasileff, H. Wang, S.-Z. Qiao, *Adv. Funct. Mater.* **2017**, *27*, 1702524.

[255] L. Hu, C. Dai, J. M. Lim, Y. Chen, X. Lian, M. Wang, Y. Li, P. Xiao, G. Henkelman, M. Xu, *Chem. Sci.* **2018**, *9*, 666.

[256] Z. Liu, X. Zheng, S.-l. Luo, S.-q. Xu, N.-y. Yuan, J.-n. Ding, *J. Mater. Chem. A* **2016**, *4*, 13395.

[257] Y. Tian, H. Huang, G. Liu, R. Bi, L. Zhang, *Chem. Commun.* **2019**, *55*, 3243.

[258] Z. Li, S. Zhang, J. Zhang, M. Xu, R. Tatara, K. Dokko, M. Watanabe, *ACS Appl. Mater. Interfaces* **2017**, *9*, 38477.

[259] Z. Zeng, W. Li, Q. Wang, X. Liu, *Adv. Sci.* **2019**, *6*, 1900711.

[260] K. Sun, Q. Zhang, D. C. Bock, X. Tong, D. Su, A. C. Marschilok, K. J. Takeuchi, E. S. Takeuchi, H. Gan, *J. Electrochem. Soc.* **2017**, *164*, A1291.

[261] Y. Zhao, W. Cai, Y. Fang, H. Ao, Y. Zhu, Y. Qian, *ChemElectroChem* **2019**, *6*, 2231.

[262] X. Huang, J. Tang, B. Luo, R. Knibbe, T. Lin, H. Hu, M. Rana, Y. Hu, X. Zhu, Q. Gu, D. Wang, L. Wang, *Adv. Energy Mater.* **2019**, *9*, 1901872.

[263] Z. Cheng, Z. Xiao, H. Pan, S. Wang, R. Wang, *Adv. Energy Mater.* **2018**, *8*, 1702337.

[264] X. Zhu, W. Zhao, Y. Song, Q. Li, F. Ding, J. Sun, L. Zhang, Z. Liu, *Adv. Energy Mater.* **2018**, *8*, 1800201.

[265] H. Wu, Y. Huan, D. Wang, M. Li, X. Cheng, Z. Bai, P. Wu, W. Peng, R. Zhang, Z. Ji, M. Zou, X. Yan, *J. Electrochem. Soc.* **2019**, *166*, A188.

[266] J. Xu, W. Zhang, H. Fan, F. Cheng, D. Su, G. Wang, *Nano Energy* **2018**, *51*, 73.

[267] S. S. Zhang, D. T. Tran, *J. Mater. Chem. A* **2016**, *4*, 4371.

[268] S. Majumder, M. Shao, Y. Deng, G. Chen, *J. Electrochem. Soc.* **2019**, *166*, A5386.

[269] X. Li, Z. Pan, Z. Li, X. Wang, B. Saravanakumar, Y. Zhong, L. Xing, M. Xu, C. Guo, W. Li, *J. Power Sources* **2019**, *420*, 22.

[270] C. Dai, L. Hu, X. Li, Q. Xu, R. Wang, H. Liu, H. Chen, S.-J. Bao, Y. Chen, G. Henkelman, C. M. Li, M. Xu, *Nano Energy* **2018**, *53*, 354.

[271] X. Tan, X. Wang, X. Wang, Y. Wang, C. Li, D. Xia, *Ionics* **2019**, *25*, 4047.

[272] T. Lei, W. Chen, J. Huang, C. Yan, H. Sun, C. Wang, W. Zhang, Y. Li, J. Xiong, *Adv. Energy Mater.* **2017**, *7*, 1601843.

[273] X. Lu, Q. Zhang, J. Wang, S. Chen, J. Ge, Z. Liu, L. Wang, H. Ding, D. Gong, H. Yang, X. Yu, J. Zhu, B. Lu, *Chem. Eng. J.* **2019**, *358*, 955.

[274] J. Jiang, J. Zhu, W. Ai, X. Wang, Y. Wang, C. Zou, W. Huang, T. Yu, *Nat. Commun.* **2015**, *6*, 8622.

[275] C. Dai, L. Hu, M.-Q. Wang, Y. Chen, J. Han, J. Jiang, Y. Zhang, B. Shen, Y. Niu, S.-J. Bao, M. Xu, *Energy Storage Mater.* **2017**, *8*, 202.

[276] H. Wu, Y. Li, J. Ren, D. Rao, Q. Zheng, L. Zhou, D. Lin, *Nano Energy* **2019**, *55*, 82.

[277] Y. Xia, H. Zhong, R. Fang, C. Liang, Z. Xiao, H. Huang, Y. Gan, J. Zhang, X. Tao, W. Zhang, *J. Power Sources* **2018**, *378*, 73.

[278] Z. Y. Wang, L. Wang, S. Liu, G. R. Li, X. P. Gao, *Adv. Funct. Mater.* **2019**, *29*, 1901051.

[279] Z. Meng, S. Zhang, J. Wang, X. Yan, H. Ying, X. Xu, W. Zhang, X. Hou, W.-Q. Han, *ACS Appl. Mater. Interfaces* **2018**, *1*, 1594.

[280] J. Zhang, H. Hu, Z. Li, X. W. Lou, *Angew. Chem., Int. Ed.* **2016**, *55*, 3982.

[281] J.-Y. Hwang, H. M. Kim, S. Shin, Y.-K. Sun, *Adv. Funct. Mater.* **2018**, *28*, 1704294.

[282] L. Zhang, Z. Chen, N. Dongfang, M. Li, C. Diao, Q. Wu, X. Chi, P. Jiang, Z. Zhao, L. Dong, R. Che, K. P. Loh, H. Lu, *Adv. Energy Mater.* **2018**, *8*, 1802431.

[283] S. Chen, Z. Wu, J. Luo, X. Han, J. Wang, Q. Deng, Z. Zeng, S. Deng, *Electrochim. Acta* **2019**, *312*, 109.

[284] X.-Q. Niu, X.-L. Wang, D.-H. Wang, Y. Li, Y.-J. Zhang, Y.-D. Zhang, T. Yang, T. Yu, J.-P. Tu, *J. Mater. Chem. A* **2015**, *3*, 17106.

[285] H. J. Peng, G. Zhang, X. Chen, Z. W. Zhang, W. T. Xu, J. Q. Huang, Q. Zhang, *Angew. Chem., Int. Ed.* **2016**, *55*, 12990.

[286] Y. Wang, M. Li, L. Xu, T. Tang, Z. Ali, X. Huang, Y. Hou, S. Zhang, *Chem. Eng. J.* **2019**, *358*, 962.

[287] F. Zhou, L.-T. Song, L.-L. Lu, H.-B. Yao, S.-H. Yu, *ChemNanoMat* **2016**, *2*, 937.

[288] B. Cao, Y. Chen, Li, L. Y , Y. Mo, *ChemSusChem* **2016**, *9*, 3338.

[289] H. Huang, J. Liu, Y. Xia, C. Cheng, C. Liang, Y. Gan, J. Zhang, X. Tao, W. Zhang, *J. Alloys Compd.* **2017**, *706*, 227.

[290] X. Lang, Y. Zhao, K. Cai, L. Li, D. Chen, Q. Zhang, *Energy Technol.* **2019**, *7*, 1900543.

[291] Z. Cui, J. Yao, T. Mei, S. Zhou, B. Hou, J. Li, J. Li, J. Wang, J. Qian, X. Wang, *Electrochim. Acta* **2019**, *298*, 43.

[292] Z. Gao, Y. Schwab, Y. Zhang, N. Song, X. Li, *Adv. Funct. Mater.* **2018**, *28*, 1800563.

[293] Y.-S. Liu, C. Ma, Y.-L. Bai, X.-Y. Wu, Q.-C. Zhu, X. Liu, X.-H. Liang, X. Wei, K.-X. Wang, J.-S. Chen, *J. Mater. Chem. A* **2018**, *6*, 17473.

[294] H. Li, S. Ma, H. Cai, H. Zhou, Z. Huang, Z. Hou, J. Wu, W. Yang, H. Yi, C. Fu, Y. Kuang, *Energy Storage Mater.* **2019**, *18*, 338.

[295] H. Wei, E. F. Rodriguez, A. S. Best, A. F. Hollenkamp, D. Chen, R. A. Caruso, *ACS Appl. Mater. Interfaces* **2019**, *11*, 13194.

[296] L. Luo, S. H. Chung, H. Yaghoobnejad Asl, A. Manthiram, *Adv. Mater.* **2018**, *30*, 1804149.

[297] N. Song, Z. Gao, Y. Zhang, X. Li, *Nano Energy* **2019**, *58*, 30.

[298] R. Razaq, D. Sun, Y. Xin, Q. Li, T. Huang, L. Zheng, Z. Zhang, Y. Huang, *Nanotechnology* **2018**, *29*, 295401.

[299] Z. Wang, J. Liu, L. Sun, Y. Zhang, Q. Fu, H. Xie, H. Sun, *Chem. Eur. J.* **2018**, *24*, 14154.

[300] X. Zeng, X. Gao, G. Li, M. Sun, Z. Lin, M. Ling, J. Zheng, C. Liang, *J. Mater. Chem. A* **2018**, *6*, 17142.

[301] R. Fang, S. Zhao, Z. Sun, D.-W. Wang, R. Amal, S. Wang, H.-M. Cheng, F. Li, *Energy Storage Mater.* **2018**, *10*, 56.

[302] H. Shi, Z. Sun, W. Lv, S. Wang, Y. Shi, Y. Zhang, S. Xiao, H. Yang, Q.-H. Yang, F. Li, *J. Mater. Chem. A* **2019**, *7*, 11298.

[303] W. Cai, G. Li, K. Zhang, G. Xiao, C. Wang, K. Ye, Z. Chen, Y. Zhu, Y. Qian, *Adv. Funct. Mater.* **2018**, *28*, 1704865.

[304] H. Al Salem, V. R. Chitturi, G. Babu, J. A. Santana, D. Gopalakrishnan, L. M. Reddy Arava, *RSC Adv.* **2016**, *6*, 110301.

[305] B. Gao, X. Li, K. Ding, C. Huang, Q. Li, P. K. Chu, K. Huo, *J. Mater. Chem. A* **2019**, *7*, 14.

[306] Z. Cui, C. Zu, W. Zhou, A. Manthiram, J. B. Goodenough, *Adv. Mater.* **2016**, *28*, 6926.

[307] Z. Li, Q. He, X. Xu, Y. Zhao, X. Liu, C. Zhou, D. Ai, L. Xia, L. Mai, *Adv. Mater.* **2018**, *30*, 1804089.

[308] W. G. Lim, C. Jo, A. Cho, J. Hwang, S. Kim, J. W. Han, J. Lee, *Adv. Mater.* **2019**, *31*, 1806547.

[309] C. Li, J. Shi, L. Zhu, Y. Zhao, J. Lu, L. Xu, *Nano Res.* **2018**, *11*, 4302.

[310] R. Luo, Q. Yu, Y. Lu, M. Zhang, T. Peng, H. Yan, X. Liu, J.-K. Kim, Y. Luo, *Nanoscale Horiz.* **2019**, *4*, 531.

[311] D.-R. Deng, T.-H. An, Y.-J. Li, Q.-H. Wu, M.-S. Zheng, Q.-F. Dong, *J. Mater. Chem. A* **2016**, *4*, 16184.

[312] W. Ren, L. Xu, L. Zhu, X. Wang, X. Ma, D. Wang, *ACS Appl. Mater. Interfaces* **2018**, *10*, 11642.

[313] X. Li, K. Ding, B. Gao, Q. Li, Y. Li, J. Fu, X. Zhang, P. K. Chu, K. Huo, *Nano Energy* **2017**, *40*, 655.

[314] L. Ma, H. Yuan, W. Zhang, G. Zhu, Y. Wang, Y. Hu, P. Zhao, R. Chen, T. Chen, J. Liu, Z. Hu, Z. Jin, *Nano Lett.* **2017**, *17*, 7839.

[315] D. R. Deng, F. Xue, Y. J. Jia, J. C. Ye, C. D. Bai, M. S. Zheng, Q. F. Dong, *ACS Nano* **2017**, *11*, 6031.

[316] H. Zhang, D. Tian, Z. Zhao, X. Liu, Y.-N. Hou, Y. Tang, J. Liang, Z. Zhang, X. Wang, J. Qiu, *Energy Storage Mater.* **2019**, *21*, 210.

[317] Z. D. Huang, Y. Fang, M. Yang, J. Yang, Y. Wang, Z. Wu, Q. Du, T. Masese, R. Liu, X. Yang, C. Qian, S. Jin, Y. Ma, *ACS Appl. Mater. Interfaces* **2019**, *11*, 20013.

[318] H. Liu, H. Shen, R. Li, S. Liu, A. Turak, M. Yang, *ChemElectroChem* **2019**, *6*, 2074.

[319] X. Li, B. Gao, X. Huang, Z. Guo, Q. Li, X. Zhang, P. K. Chu, K. Huo, *ACS Appl. Mater. Interfaces* **2019**, *11*, 2961.

[320] B. He, W.-C. Li, Y. Zhang, X.-F. Yu, B. Zhang, F. Li, A.-H. Lu, *J. Mater. Chem. A* **2018**, *6*, 24194.

[321] C. Ye, Y. Jiao, H. Jin, A. D. Slattery, K. Davey, H. Wang, S.-Z. Qiao, *Angew. Chem., Int. Ed.* **2018**, *57*, 16703.

[322] J. N. Coleman, M. Lotya, A. O'Neill, S. D. Bergin, P. J. King, U. Khan, K. Young, A. Gaucher, S. De, R. J. Smith, I. V. Shvets, S. K. Arora, G. Stanton, H.-Y. Kim, K. Lee, G. T. Kim, G. S. Duesberg, T. Hallam, J. J. Boland, J. J. Wang, J. F. Donegan, J. C. Grunlan, G. Moriarty, A. Shmeliov, R. J. Nicholls, J. M. Perkins, E. M. Grieveson, K. Theuwissen, D. W. McComb, P. D. Nellist, V. Nicolosi, *Science* **2011**, *331*, 568.

[323] B. Anasori, M. R. Lukatskaya, Y. Gogotsi, *Nat. Rev. Mater.* **2017**, *2*, 16098.

[324] Z. Xiao, Z. Li, X. Meng, R. Wang, *J. Mater. Chem. A* **2019**, *7*, 22730.

[325] X. Tang, X. Guo, W. Wu, G. Wang, *Adv. Energy Mater.* **2018**, *8*, 1801897.

[326] J. Pang, R. G. Mendes, A. Bachmatiuk, L. Zhao, H. Q. Ta, T. Gemming, H. Liu, Z. Liu, M. H. Rummeli, *Chem. Soc. Rev.* **2019**, *48*, 72.

[327] X. Zhao, M. Liu, Y. Chen, B. Hou, N. Zhang, B. Chen, N. Yang, K. Chen, J. Li, L. An, *J. Mater. Chem. A* **2015**, *3*, 7870.

[328] Y. Dong, S. Zheng, J. Qin, X. Zhao, H. Shi, X. Wang, J. Chen, Z. S. Wu, *ACS Nano* **2018**, *12*, 2381.

[329] L. P. Lv, C. F. Guo, W. Sun, Y. Wang, *Small* **2019**, *15*, 1804338.

[330] H. Tang, W. Li, L. Pan, C. P. Cullen, Y. Liu, A. Pakdel, D. Long, J. Yang, N. McEvoy, G. S. Duesberg, V. Nicolosi, C. J. Zhang, *Adv. Sci.* **2018**, *5*, 1800502.

[331] J. Song, X. Guo, J. Zhang, Y. Chen, C. Zhang, L. Luo, F. Wang, G. Wang, *J. Mater. Chem. A* **2019**, *7*, 6507.

[332] E. S. Sim, G. S. Yi, M. Je, Y. Lee, Y.-C. Chung, *J. Power Sources* **2017**, *342*, 64.

[333] H. Lin, D.-D. Yang, N. Lou, S.-G. Zhu, H.-Z. Li, *Ceram. Int.* **2019**, *45*, 1588.

[334] Y. Zhao, J. Zhao, *Appl. Surf. Sci.* **2017**, *412*, 591.

[335] H. Tang, W. Li, L. Pan, K. Tu, F. Du, T. Qiu, J. Yang, C. P. Cullen, N. McEvoy, C. Zhang, *Adv. Funct. Mater.* **2019**, *29*, 1901907.

[336] Y. Wang, J. Shen, L. C. Xu, Z. Yang, R. Li, R. Liu, X. Li, *Phys. Chem. Chem. Phys.* **2019**, *21*, 18559.

[337] Y. Yao, W. Feng, M. Chen, X. Zhong, X. Wu, H. Zhang, Y. Yu, *Small* **2018**, *14*, 1802516.

[338] H. Zhang, Q. Qi, P. Zhang, W. Zheng, J. Chen, A. Zhou, W. Tian, W. Zhang, Z. Sun, *ACS Appl. Energy Mater.* **2019**, *2*, 705.

[339] X. T. Gao, Y. Xie, X. D. Zhu, K. N. Sun, X. M. Xie, Y. T. Liu, J. Y. Yu, B. Ding, *Small* **2018**, *14*, 1802443.

[340] L. Jiao, C. Zhang, C. Geng, S. Wu, H. Li, W. Lv, Y. Tao, Z. Chen, G. Zhou, J. Li, G. Ling, Y. Wan, Q. H. Yang, *Adv. Energy Mater.* **2019**, *9*, 1900219.

[341] H. Pan, X. Huang, R. Zhang, D. Wang, Y. Chen, X. Duan, G. Wen, *Chem. Eng. J.* **2019**, *358*, 1253.

[342] W. Bao, D. Su, W. Zhang, X. Guo, G. Wang, *Adv. Funct. Mater.* **2016**, *26*, 8746.

[343] W. Bao, X. Xie, J. Xu, X. Guo, J. Song, W. Wu, D. Su, G. Wang, *Chem. - Eur. J.* **2017**, *23*, 12613.

[344] R. Demir-Cakan, M. Morcrette, F. Nouar, C. Davoisne, T. Devic, D. Gonbeau, R. Dominko, C. Serre, G. Ferey, J. M. Tarascon, *J. Am. Chem. Soc.* **2011**, *133*, 16154.

[345] H. Park, D. J. Siegel, *Chem. Mater.* **2017**, *29*, 4932.

[346] F. Li, X. Zhang, X. Liu, M. Zhao, *ACS Appl. Mater. Interfaces* **2018**, *10*, 15012.

[347] J. Zhou, R. Li, X. Fan, Y. Chen, R. Han, W. Li, J. Zheng, B. Wang, X. Li, *Energy Environ. Sci.* **2014**, *7*, 2715.

[348] A. E. Baumann, G. E. Aversa, A. Roy, M. L. Falk, N. M. Bedford, V. S. Thoi, *J. Mater. Chem. A* **2018**, *6*, 4811.

[349] X. J. Hong, T. X. Tan, Y. K. Guo, X. Y. Tang, J. Y. Wang, W. Qin, Y. P. Cai, *Nanoscale* **2018**, *10*, 2774.

[350] X.-F. Liu, X.-Q. Guo, R. Wang, Q.-C. Liu, Z.-J. Li, S.-Q. Zang, T. C. W. Mak, *J. Mater. Chem. A* **2019**, *7*, 2838.

[351] D. Cai, M. Lu, Li, J. C , D. Chen, H. Tu, J. Li, W. Han, *Small* **2019**, *15*, 1902605.

[352] Y. Mao, G. Li, Y. Guo, Z. Li, C. Liang, X. Peng, Z. Lin, *Nat. Commun.* **2017**, *8*, 14628.

[353] H. Zhang, W. Zhao, M. Zou, Y. Wang, Y. Chen, L. Xu, H. Wu, A. Cao, *Adv. Energy Mater.* **2018**, *8*, 1800013.

[354] H. Zhang, W. Zhao, Y. Wu, Y. Wang, M. Zou, A. Cao, *J. Mater. Chem. A* **2019**, *7*, 9195.

[355] Y. Wu, H. Jiang, F. S. Ke, H. Deng, *Chem. Asian J.* **2019**, *14*, 3577.

[356] D. Su, M. Cortie, H. Fan, G. Wang, *Adv. Mater.* **2017**, *29*, 1700587.

[357] Y. Yang, Z. Wang, T. Jiang, C. Dong, Z. Mao, C. Lu, W. Sun, K. Sun, *J. Mater. Chem. A* **2018**, *6*, 13593.

[358] H. Jiang, X. C. Liu, Y. Wu, Y. Shu, X. Gong, F. S. Ke, H. Deng, *Angew. Chem., Int. Ed.* **2018**, *57*, 3916.

[359] B. Liu, R. Bo, M. Taheri, I. Di Bernardo, N. Motta, H. Chen, T. Tsuzuki, G. Yu, A. Tricoli, *Nano Lett.* **2019**, *19*, 4391.

[360] P. Geng, S. Cao, X. Guo, J. Ding, S. Zhang, M. Zheng, H. Pang, *J. Mater. Chem. A* **2019**, *7*, 19465.